Preparation and Characterisation
of Flexographic Inks

By

Manal Hamroush

Submitted in accordance with the requirements for the degree
of Doctor of Philosophy

The University of Leeds

School of Chemistry

Department of Colour Science

April 2012

The candidate confirms that the work submitted is her own
and that appropriate credit has been given where reference has been made
to the work of others.

Acknowledgements

I would like to thank professor Long Lin my supervisor for his ultimate help, besides his humane and scientific support throughout my PhD studies at Leeds university.

I would like to thank Professor Jim Guthrie for his assistance and support with inverse gas chromatography and his useful advices along my study.

Many thanks to Mr. Algy Kazlauciunas for his help and assistance in thermal analysis, particle sizing and zeta potential measurements besides, SEM-EDX analysis. most of all his kindness and appreciation of my tight timescale in carrying out some much needed analysis.

Special thanks to Mr. Riad kalioundji for his extreme support along my practical way in the ink industry, besides, his help in deciding the topic of my thesis, and his support in all the necessary practical experiments in his developed print house.

My appreciation to Haldun Filiz for his contribution in formatting my thesis and his wide experience in calculations related to my IGC figures.

Many thanks to Dr. Fadi Alrouh from the Organic Chemistry Department, Faculty of Science, Aleppo University-Syria, for his contribution in illustrating my results relating to organic chemistry in my thesis.

Thank you a lot my mother for your endless care and for the love that I can see in your eyes which motivates me to go ahead when frustrations prevails.

Particular thanks to my father, who brought up me in ethical basis, my appreciation for his hands which cared for me a lot, and his encouragement throughout to be at this level in life.

Thank you my sisters and brothers, Suzan, Majed, Husam and Kinda for all of your help and patience in all circumstances, and to everybody in my family and friends.

Thank you my children Saadallah and Shahed and my incoming baby for your patience and your awareness of the importance of my time and study inspite of your small ages.

Finally, I know it is not enough to say thank you Firas, you were the person who supported me a lot, you confirmed to me that you are really my gift in this life.

Abstract

This study focuses on the preparation of nitrocellulose-based flexographic inks suitable for printing on biaxially- oriented polypropylene (BOPP), for which the adhesion of the manufactured ink to the BOPP substrate is an essential property of importance. The choice of BOPP as the main substrate in this study follows from its position as one of the more commonly used substrates for printing worldwide.

The importance of using fumaric rosin UCH150H in preparation of flexographic inks resulted from the experience of using this resin in preparing flexographic polyamide inks, where the adhesion results were very good, when this resin was added to flexographic nitrocellulose inks, the adhesion was improved remarkebly.

Two polymers are used in this study: fumaric rosin (UCH150H) and a polyurethane (Surkopak 5323) and many formulations were tested. The use of fumaric rosin to form flexographic inks instead of polyurethane was novel. When used in combination with polyurethane as an additive in nitrocellulose flexographic inks rather than titanium acetyl-acetonates (TAA,) this offers benefits, as (TAA,) has many disadvantages when used to prepare flexographic inks for printing on BOPP.

Comparative tests of the adhesion of the inks to the substrate are carried out by tape test after printing the two prepared inks on BOPP and subjecting these to Corona treatment. The principal factor influencing the adhesion is found to be the polymer structure, and it is found that the inks prepared by using UCH150H exhibited better adhesion to the BOPP substrate than those prepared from Surkopak 5323.

Analytical techniques were employed to provide information as to why the adhesion was superior when using the ink prepared from UCH150H, including wetting

contact angle measurements, optical microscopy, scanning electron microscopy (SEM) and electron diffractive X-ray (EDX), atomic force microscopy (AFM), electronic scanning for chemical analysis (ESCA), Fourier Transform infrared (FTIR) spectroscopy, nuclear magnetic resonance (NMR) spectroscopy and inverse gas chromatography (IGC). The novelty in using IGC to study BOPP coated separately with UCH150H and Surkopak 5323 facilitates the comparison of physical properties associated with the polymer before and after printing on BOPP.

Furthermore, the substitution of Surkopak 5323 by UCH150H is better for the environment as the latter is derived primarily from natural products (*e.g.* colophony from pine trees), while Surkopak 5323 is based on an isocyanate precursor which is no longer used in the UK for health and safety considerations, although still used in other countries such as middle east (Leach and Pierce, 1999).

On this basis, polyurethanes were replaced by amine-cured epoxy systems in the UK, but both these and the polyurethanes are more expensive than UCH150H, which is another attraction of using UCH150H in flexographic inks.

The implementation of optical microscopy and scanning electron microscopy confirms that UCH150H had better adhesion on BOPP when incorporated in flexographic ink than Surkopak 5323. The results gained from EDX also confirm that the oxygen content increased by increasing the UCH150H and Surkopak 5323 composition in the flexographic ink printed on BOPP. Application of the tape test confirms that the remaining ink layer on the BOPP surface after applying the test, is the residue of adhered polymer layer which is greater in the case of UCH150H than Surkopak 5323.

AFM confirms that the surface of BOPP coated with UCH150H was positively charged and the surface of BOPP coated with Surkopak 5323 was negatively charged.

Other techniques such as IR, NMR and ESCA confirm the chemical structure of UCH150H and Surkopak 5323; the presence of un-reacted carboxylic acid in the UCH150H, is found to play an important role in adhesion according to IGC studies.

These data suggest that the superior adhesion is the result of interacting acidic groups with BOPP surface by hydrogen bonds, where the basicity increases after adhesion of UCH150H and Surkopak 5323 to BOPP substrate.

The flexographic inks prepared by using fumaric rosin UCH150H were tried in many print houses and the results of the print were acceptable, especially the adhesion. On the other hand, the ink was commercially competitive compared to the available flexographic inks in the market, besides, the safety of using fumaric rosin UCH150H for food substrates because of its natural source.

It should be noted that flexographic ink preparation, printing substrates, tape test, viscosity measurements, colour density of print, wetting measurements and optical microscopy were done in the lab of ink factory (TOPINKS) in Aleppo-Syria.

SEM, thermal analysis, FTIR, particle size testing were done in Leeds University, colour chemistry department. Atomic force microscopy (AFM) was done in Leeds University (Institute of practical science and engineering), ESCA) was done in Leeds University (Physical department), NMR was done in Homs university-Syria and IGC in Aleppo university-Syria.

ABBREVIATIONS

TAA	Titanium acetyl-acetonates
NC	Nitrocellulose
PU	Polyurethane
BOPP	Bi-axially oriented polypropylene
PP	Polypropylene
CDT	Corona discharge treatment
γ_s^d	Dispersive component of the surface free energy
γ_s^p	Polar component of the surface free energy
DSC	Differential scanning calorimetry
T_g	Temperature of glass transition
TGA	Thermogravimetric analysis studies
FTIR	Fourier transform infrared spectroscopy
NMR	Nuclear magnetic resonance spectroscopy
ESCA	Electron spectroscopy for chemical analysis
PU	Polyurethane
SK resin	Ketonic resin
AFM	Atomic force microscopy
TM-AFM	Tapping mode-Atomic force microscopy
C_5	n-pentane
C_6	n-hexane
C_7	*n*-heptane
C_8	*n*-octane
Acet	Acetone
THF	Tetrahydrofuran
EtAc	Ethyl acetate
DCM	dichloromethane
EtOH	Ethanol
SEM	Scanning electron microscopy
EDX	Electron diffractive X-ray
CMY	Cyan, Magenta, Yellow
sec	second

TABLE OF CONTENTS

LIST OF FIGURES

VIII

LIST OF TABLES

Chapter 1 Introduction

1.   Background to flexography printing

Flexography or flexo printing can be described as rotary relief printing process, in which the image carrier is a photopolymer plate or a flexible rubber with raised image areas. It was called 'aniline printing' since the inks were made of synthetic, organic aniline dyes. It is a versatile method of printing and many packaging products, such as tissues, foil, papers, paper board, plastic film, and corrugated board can be printed with flexo. In fact, the invention of cellophane was the main reason behind flexographic printing being widely accepted in the packaging industry. Flexo printing became extremely popular in the mid 1930's right after it proved to be acceptable for food packaging.

Despite its suitability for printing on cellophane food packaging, the flexo process took small steps in commercial printing mainly because aniline dyes were thought to be poisonous and might contaminate the food products (Oldring *et al.*, 2003). In 1946, the government of the United States of America allowed the aniline inks to be used for printing food packaging; although, aniline printing was still rejected by many package printers and food processors. In 1952, the name of the aniline printing industry was changed to its present name 'flexographic printing' and since that time, flexography has seriously grown to a level where it now represents approximately 17% of the printing market. (Adams and Dolin, 2002).

In this printing process (a typical flexographic printing process is graphically illustrated in Figure 1.1), the anilox roller, which is composed of a network of

engraved cells of a characteristic shape, size, and depth, meters the ink onto the surface of the printing plate. As the ink fills the cells, the additional ink is removed by a doctor blade system and the ink transferred to the printing plate. Following which, the ink film is transferred from the plate to the substrate (Frank and Rupp, 2000).
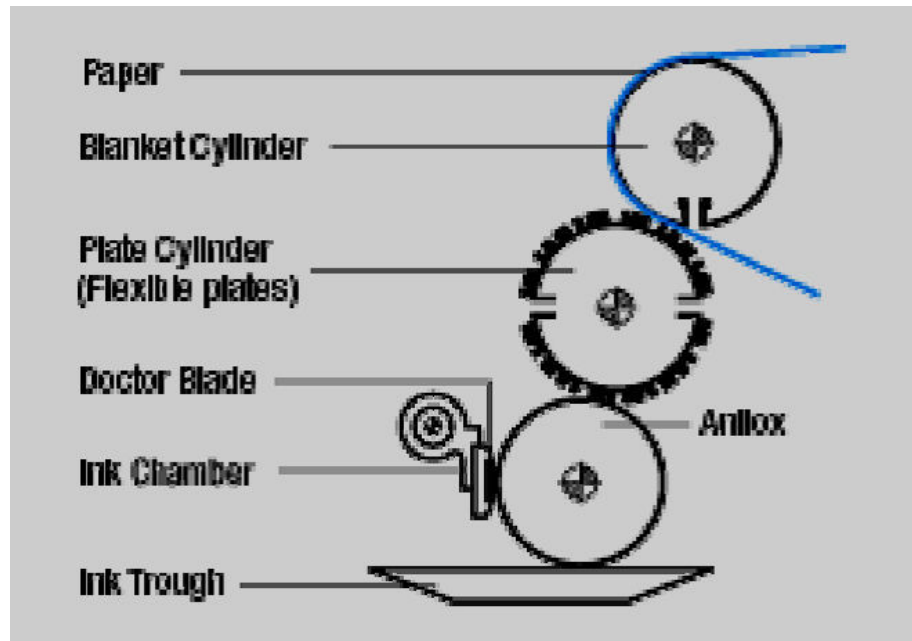
Figure 1.1 Schematic illustration of flexographic printing process (Kimya, 2003)

Recently, the quality of flexographic printing has improved dramatically as a result of improvements to printing plates, ink systems and especially inking units (such as anilox and doctor blade system) (Deganello *et al.*, 2012).

1.1 Flexographic ink systems

There are three flexographic ink systems, which differ in the method of drying and in the medium used for ink delivery.

- Solvent based inks, which dry by solvent evaporation.

- Water based inks, which also dry by evaporation, the delivery medium is water or solvent in addition to water.

- UV-cured inks, which do not require a medium, make use of liquid components in the inks and are chemically cured during the printing process (Laden, 1997).

The majority of printers are moving towards using water–based systems. It is, however, widely known that most of the properties of solvent–based inks are superior to those of water–based inks.

Many resins can be used in the formulation of flexographic printing inks depending on the substrate, resins include nitrocellulose, soluble acrylic polymers, polyurethanes, alcohol–soluble grades of ethyl cellulose, cellulose acetate propionate (CAP), polyamides, poly(vinyl butyral) – whose use has grown to replace CAP - and other resins such as ketone resins and PVC – PVA copolymers (Todd, 1994).

Whilst there are a variety of specific formulations, but a typical ink will contain the following ingredients (Williams, 2001).

Pigment (or dyestuff)	4-12%
Extender pigment	0-8%
Resin	10-30%
Solvents	40-60%
Plasticiser/wax/additives	2-10%

Briefly, the composition of solvent based inks can be summarised in Figure 1.2.
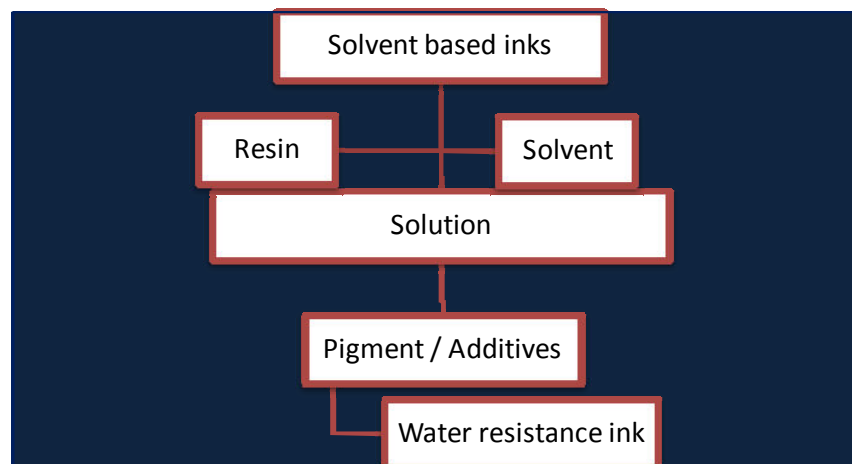
Figure 1.2 Composition of flexographic solvent based ink (Laden, 1997)

1.2   Flexography ink chemistry

In general, the three major constituents of an ink are the colourant, the binder and the solvent. Each component has a different task but at the same time is dependent on the other two. Many types of additives are used to give other properties, and to modify the basic components to obtain a wider range of properties available. For example, the properties of raw materials are affected by the other elements (constituents) in the ink. For instance, the fastness of a pigment might be improved by the presence of certain resins that are used in the formulation.

The ink formulation is related to the use of ink and the printed job, *e.g.* cost will be taken into consideration when it comes to ink manufacturing equipment (Leach and Pierce, 1999). The best formulation is the simplest one, based on using the minimum number of ingredients, especially additives, for two reasons:

- In case of facing any problem during the printing process, it will be easier to investigate the underlying reason.

- The use of many components can potentially contribute to some interactions between the ink components.

For coextruded films, nitrocellulose inks are modified with polyurethanes and titanium acetyl-acetonates (TAA) to facilitate their use in all purposes (surface, reverse and lamination).

TAA fulfills the role of adhesion promoter for the treated side of the film, but they also have a negative impact as TAA may react with pigments making the ink unstable.

The formulation of the white ink for the treatment of one side of coextruded polypropylene is as follows (Leach and Pierce, 1999).

Titanium dioxide (CI pigment white 6)	30.0%
Nitrocellulose resin	11.0%
Dioctyl phthalates	3.0%
Polyurethane	8.0%
Polyethylene wax*	1.0%
Eurcamide**	1.0%
Ethanol	27.0%
Ethyl Acetate	16.0%
TAA	3.0%

Polyethylene wax*: is an anti scratch additive, and Eurcamide** a friction reducer.These additives are very important for surface printing, but for lamination printing, one can exclude these additives from the formulation.

Another formulation of concentrated pigment for NC - printing ink was suggested by Evonik 2008 (Personal comunication).

Ethyl Acetat	17.1%
Ethanol	49.0%
Synthetic resin TC	2.5%
NC DLX 3/5*	13.3%
Printex 35	15.6%
Unimoll M66**	2.5%

NC DLX 3/5* is low viscosity grade of NC from Nobel NC company Ltd.

Unimoll M66** is a Dicyclohexyl phthalate (Plasticizer)

1.3   Ink components

A functional flexographic ink must possess a number of qualities: the ink confers colour to the printed substrate and there must be a degree of adherence between the ink and the materials being printed. Finally, it is extremely valuable to produce a consistent finish.

There are five ingredients that contribute to a successful ink: allowing it to adhere to a substrate and produce its visible effect (Kunjappu, 2001).

1.3.1   Solvents

Solvents are very important in delivering the ink to the substrate and helping the ink to flow through the printing mechanism. The evaporation of the solvent after printing serves to make the ink form a solid coating on the substrate. A number of factors influence the choice of solvent including volatility, but the specific solubility of the resin

is of over-riding importance. Where mixed resins with different solubilities are employed, the use of solvent mixtures compatible with the different solubility parameters may be preferred. Thus, commonly-used solvents in solvent – based flexography inks include ethanol, propanol and propyl acetate (Marrion, 2004).

In flexography printing, there is a further limitation on the kind of solvent that may be used which is imposed by the particular printer, as some manufacturers identify specific solvents and this might, in turn, limit the choice of the resin. For instance, food packaging inks place an additional constraint on this choice, because any traces of retained solvent in the print after drying might cause unacceptable risk of odour or taint (Leach and Pierce, 1999).

For liquid inks, the choice of solvent plays a big role in the ink composition as the main issue of the drying process (Thompson, 1998). In this context, the major solvent used in flexographic printing is ethanol, due to the beneficial drying properties that arise from the presence of its hydroxyl group and the shortness of its carbon chain. The hydroxyl group participates in hydrogen bonding, making the resulting ink formulation more viscous and less volatile than less polar organic compounds of similar molecular weight. Many ionic compounds may be dissolved because of the polar nature of the hydroxyl group, while the non-polar end hydrocarbon chain facilitates the dissolution of non-polar materials such as oils, numerous flavouring, colouring, and medicinal agents. Hydrogen bonding also causes pure ethanol to be hygroscopic to the extent that it readily absorbs water from the air.
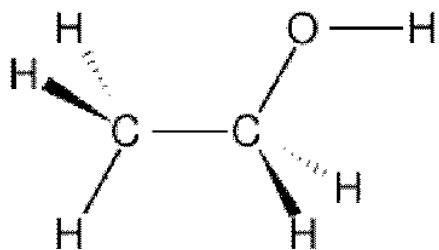
Figure 1.3 Ethanol 3-d structure

Ethanol is not used as pure anhydrous alcohol (100 %) in the commercial manufacture of printing inks, rather as a denaturation to which methanol (4 % v/v) has been added.

1.3.2   Colourants

The definition of a colourant is a material that reflects and absorbs specific wavelengths of light. Two categories of colorants used in printing: dyes and pigments. Dyes dissolve into the liquid solution and are transparent, although the colours of dyes are quite strong. However, dyes can be damaged easily by chemicals and water, moreover they can be toxic. Pigments are recognized as small, insoluble particles that are produced from a range of organic and inorganic compounds. The two major properties that can affect characteristics are the particle size and chemical stability. Inks that contain pigments are more resistant to chemicals, heat and tend to bleed less through the substrate than corresponding ink-based dyes (Parfitt and Sing, 1976).

Pigments are particularly appropriate for conventional printing inks due to their high colour strength and constant light - fastness, but when the pigment particles are big, the gloss of the printed ink film is reduced. Table 1.1 gives examples of typical pigments used in conventional printing inks (Lin *et al.*, 2004).

Table 1.1 Typical pigment choices for conventional printing inks

Ink Colour	Typical pigment used
Yellow	CI Pigment Yellow 13
Magenta	CI Pigment Red 57:1
Cyan	CI Pigment Blue 15:3
Black	Carbon Black

1.3.3   Resins

Resins cause the ink to adhere to the substrate, provide the gloss to the finished coating and in some cases aid the dispersion of the pigment. Resins offer flexibility, scuff resistance, cohesive strength, block resistance, and compatibility with the printing plates. Some commonly used resins in printing inks are nitrocellulose, polyamides, carboxylated acrylics, polyurethanes, fumaric resin and ketones (Leach and Pierce, 1999).

1.3.3.1 Fumaric resin

One synthetic resin that is used in printing inks is derived from the chemical reaction of fumaric acid and rosin (**Molecular Formula:** $C_{15}H_{20}O_6$)

http://pubchem.ncbi.nlm.nih.gov/summary/summary.cgi?cid=5280656   (accessed on June 2010).

The rosin is obtained from turpentine which is distilled from oleoresin, or crude turpentine, and obtained from the sap of coniferous trees, in particular the long leaf pine. Rosin is also called colophony and is the hard, resinous material that remains when the volatile contents of turpentine are boiled away.

Rosin is also used in the manufacture of printing ink vehicles, varnishes and lacquers (http://printwiki.org/Rosin), particularly in flexographic and gravure inks, in combination with other resins for non-absorbent substrates and with glycols for moisture-set inks where hardness and gloss are required (Leach and Pierce, 1999).

Although the fumaric rosin is used in flexographic inks, among all the reviewed references, no information was found regarding the usage of this polymer in flexographic NC inks, meaning that the use of fumaric rosin in combination with NC to manufacture flexographic inks for BOPP printing in the present work is novel.

Their chemical structure is thought to be:
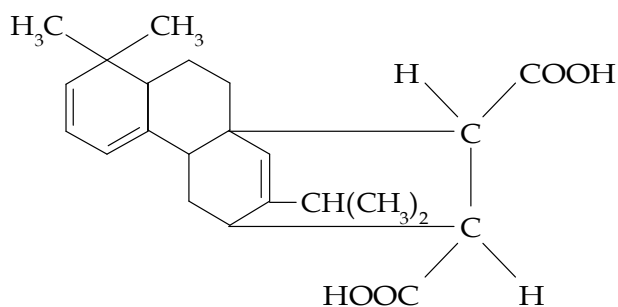
Figure 1.4 Chemical structure of fumaric resin in which the carboxyl groups are trans to one another (Leach and Pierce, 1999)

1.3.3.2 Polyurethane chemistry

Urethane polymers have received important attention in the ink, adhesive and coatings industries over the past 40 years.

Polyurethanes can be described as a polyol reacted with a diisocynate or polyfunctional isocyanate materials (Figure 1.5) (Arcurio *et al*, 2004).
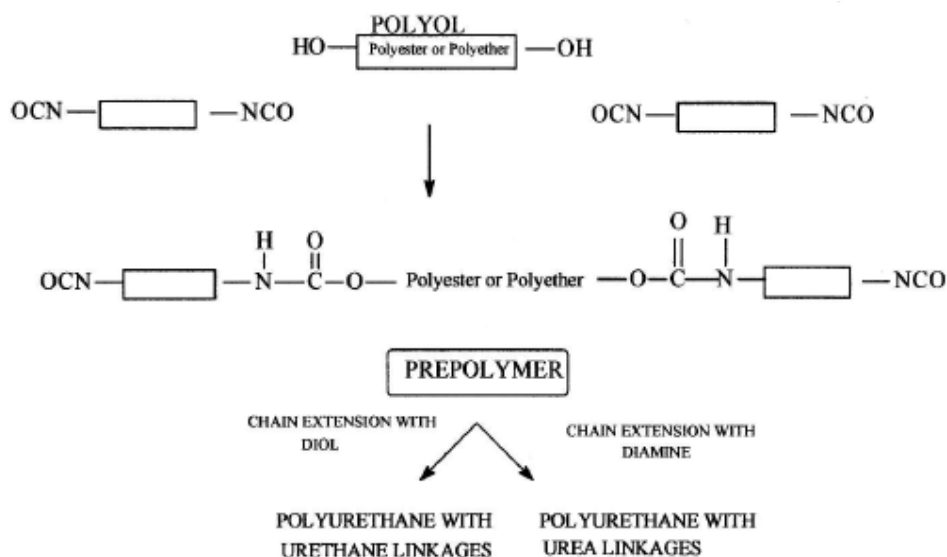
Figure 1.5 Polyurethane products (Frieden et al., 2010)

Properties of Urethane polymers

Urethanes can be classified as varying from very hard to soft through to tacky. Most of their mechanical properties are changed according to changes in the molecular weight of the polyurethane and the intermolecular forces within polyurethanes have an influence on such properties. The intermolecular forces are a result of hydrogen bonding, dipole moments and polarizability, they hold the polymer chains together in a similar way to that found in primary chemical bonds but these associations are weaker and easily influenced by the increase of temperature or stress. In addition to the intermolecular forces, the final properties of urethane polymer are determined by the nature of the basic building blocks.

Polyesters offer very good weathering, chemical resistance, abrasion resistance and toughness; while polyethers offer elasticity, flexibility, and stability. Plasticizing resins, especially those based on polyurethane chemistry, were introduced to the market during the early 1970's, and now form a significant part of the international ink industry. One of the most important features of polyurethanes is their low thermoplasticity, which offers significant release properties to inks printed in the heat sealing area of flexible packages. Thus, polyurethanes are not like other plasticizers because they impart respective heat seal resistance.

Adhesion promoters, such as titanium chelates (Figure 1.6), are generally used as additives in ink systems to improve adhesion properties by a complex cross-linking mechanism (Figure 1.7) which involves the hydroxyl groups present in the binder system of ink and the corona discharge treated surface of the substrate. Additionally, the adhesion promoter maximizes the heat seal properties up to 180 °C which is beneficial when packaging is carried out on high speed lines.
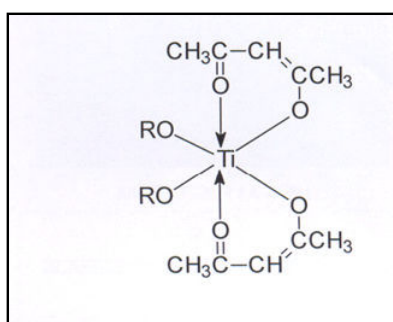
Figure 1.6 Bis(penta-2,4-dionato-o,o)bis(alkanolato)titanium)

(www.dupont.com/tyzor)
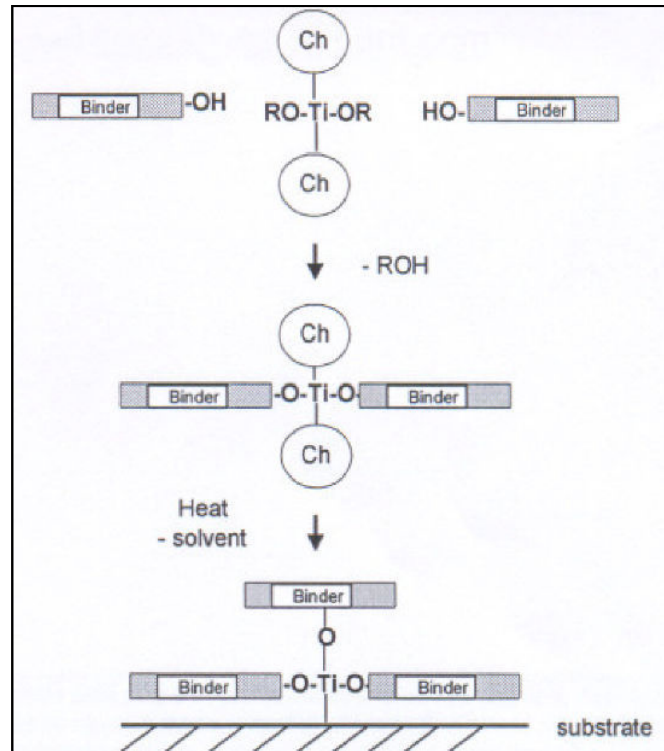
Figure 1.7 Cross linking mechanism of titanium chelates with substrate

Polyurethanes are mixed with other resins like nitrocellulose to confer heat resistance, and anti blocking, the reason being that these solvent borne polyurethane resins do not form a film. Polyurethanes are used primarily in ink formulations as modifiers especially when hard co-resins are used in the ink formulation.

Some other benefits of conventional systems include:

- low solvent retention, which results in reduced odour in the final packaging;

- the same ink could be used for both Flexo and Gravure applications;

- a single ink system for multiple structures;

- the print properties are good and are combined with easy clean up.

These elastomeric urethanes are considered as universal resins, which could be used by themselves or in combination with other resins in solvent based ink to meet all the requested needs of flexible packaging (Frieden *et al.*, 2010).

1.3.4   Additives

Additives are used in the final ink to improve its properties and some commonly used examples are plasticizers, which enhance the flexibility of resins; waxes, which improve the slip, scuff and rub resistance; wetting agents, that alter the surface tension of the ink to improve the adhesion properties of printed ink to substrates. (Laden, 1997).

Adhesion promoters are used in the formulation of inks for printing on to substrates with difficult adhesion such as treated polypropylene. Many adhesion promoters are used in inks and some may cause negative effects such as:

- an increase in ink viscosity due to reaction with the resin or pigment;

- loss of heat-sealing properties for some coated films;

- changes in colour with certain resins or coatings;

- Odour problems.

It is very important, therefore, to test these materials very well before using them in ink formulations (Leach and Pierce, 1999).

A typical press-ready ink composition would comprise:

Component	Solvent-based ink
Solvent	70%
Resin	15%
Pigment	10%
Additives	5%
Total	100%

1.4 Manufacturing of flexographic inks

Flexographic varnishes are mixtures of resins dissolved in solvent, whose use is limited in flexographic inks, because strong solvents attack the rubber of polymer plates. In spite of this, a small number of esters can be used (Todd, 1994).

The steps of ink manufacturing are as follows.

1. The solvent mixture is weighed into a known container of known weight.

2. A high-speed stirrer is immersed in the solvent mixture.

3. The resin is added gradually to the solvent mixture with stirring.

4. After complete dissolution of resin, the container is reweighed and solvent losses through evaporation are calculated.

5. The pigment is added to the prepared varnish in steps 1-2-3 and 4, then stirring for about 30 min by using a high-torque mixer to ensure that the pigment is properly dispersed.

6. The ink is passed through a grinding mill for few times on a loose setting, then the final pass on a tighter setting.

1.5   Fundamental concepts of adhesion

1.5.1   Introduction to adhesion

What is an adhesive and what are its key properties?

"An adhesive is a material which, when applied to the surfaces of materials, join them together and resist separation" (Petrie, 2000).   While the definition of "adhesion" is contradictory, therefore, "adhesion may be defined as the attraction between different bodies for one another". For the purposes of this work, adhesion was defined according to ASTM D 907 as "the state in which two surfaces are held together by interfacial forces which may consist of valence forces or interlocking action or both" (Koleske, 1995).

For the optimum bonding of surfaces, four aspects should be considered: stability, continuity, cleanliness and wetting of the surface by the adhesive or sealant (Figure 1.8). Cleanliness does not mean the removal of all the materials on the surface, but rather the removal of weakly attached materials. This is because some of the films surfaces are in close contact with the bulk substrate and offer a proper surface for adhesion.
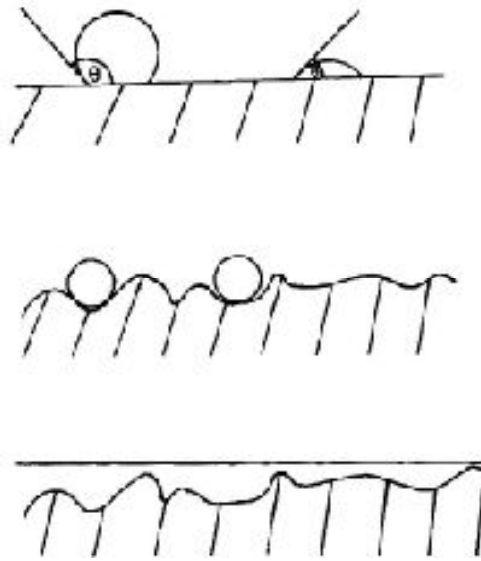
Figure 1.8 Liquid droplets making a high and low contact angle on a flat, solid surface. Centre: high contact angle leading to no spreading on a rough surface. Bottom: wetting on a rough surface

Discontinuities on the printed surface are related to fluctuations in manufacturing processes or chemical inconsistency in the substrate, thus the treatment of the surface is not homogenous. This affects negatively the strength of adhesion by creating localized regions of poor bonding and stress concentration within the joint. The strength of interaction is estimated by identifying the work of adhesion between two materials at interface (Calhoun *et al.*, 2006). The work of adhesion is defined as the "separation of two phases one is a solid and the other is a liquid which solidifies to form a thin film, these two phase are seen as the combination of two contiguous polymer phases".

$$W_a = Y_1 + Y_2 - Y_{12} \qquad\qquad (1.1)$$

W_a is the work of adhesion.

Y_1 and Y_2 are the surface tension of the two phases and Y_{12} is the surface tension of the contact layer of solid and liquid (Koleske, 1995).

The mechanism of adhesive attachment still not clearly defined, although many theories have been suggested to explain the phenomenon of adhesion. As one cannot rely on one theory to explain the adhesion, each theory explains specific concepts and information that are useful in understanding the basic demands for a good bond. The general theories of adhesion are based on (1) adsorption, (2) mechanical interlocking, (3) electrostatics, (4) diffusion, and (5) weak boundary layers (Comyn and Philippe, 2006).

1.5.1.1 Adsorption theory

This theory explains that adhesion results from molecular contact between two materials and the surface forces that develop are pointed out as secondary or van der Waals forces. For the latter to develop, the adhesive must be in close contact with the substrate surface. The limit of contact and resulting bond strength are functions of wetting energetics and the importance of wetting in adhesion is well known. The interfacial area of contact
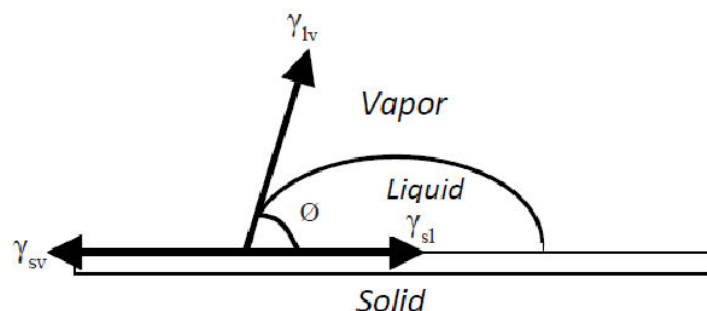
Figure 1.9 Schematic diagram of the contact angle and interfacial tension of the three surfaces at three-phase-boundary (Subedi, 2011)

solid–vapor interfacial energy is denoted by γ_{sv} , the solid–liquid interfacial energy

by γ_{sl} , the liquid–vapor interfacial energy (i.e. the surface tension) by γ_{lv} , and the

equilibrium contact angle θ .

The optimum wetting is obtained when the substrate's surface tension (critical

surface energy C) is higher than the surface tension of the liquid or adhesive.

Thus, substrates with low surface energies such as polyethylene will not be wetted

by other materials and are used for some applications that require inert surfaces

(Petrie, 2000).

1.5.1.2 Mechanical theory

When the roughness of a surface is increased, then the adhesion will be decreased

because of the availability of uncoated voids, and the contact between the adhesive

and the substrate is not good.   However, in mechanical adhesion substrate

roughness is thought to provide a mechanical locking of the adhesive to the

substrate (Koleske, 1995).   Mechanical adhesion only occurs with absorbent

materials: the polymeric adhesive molecules penetrate the voids of the adherent

surfaces, and interpenetration with both themselves (cohesion) and the solid surface

(adhesion). According to the mechanical theory the adhesive penetrates the gaps on

the surface, by displacing the trapped air at the interface serving to lock-on

mechanically to the substrate.

One way that surface roughness aids in adhesion is by strengthening the total

contact area between the adhesive and the surface.   If one considers that the

intermolecular attraction is the cause of adhesion, then by increasing the actual area

of contact, the total energy of surface interaction will increase proportionally. As a

result, the mechanical theory explains that roughening of surfaces is very useful because it:

(1) offers "teeth" to the substrate (mechanical interlocking).

(2) develops forces of adhesion by increasing the total effective area.

However, if the adhesive wets the surface well then roughening will be effective. (Wake, 1978).

1.5.1.3 Electrostatic and diffusion theories

As the concept of the capacitor is well understood, then one can explain the electrostatic theory simply, as when two dissimilar materials are brought into contact, a charge transfer takes place, and an electrical double layer is formed; to separate the two charged layers work is required. This is thought to be mainly applicable to metal-polymer bonds, yet this theory is not applicable to two non polymer systems (Koleske, 1995).

The diffusion theory, which is related to Voyutski, is a volume phenomenon. The proposition is that polymer adhesive molecules diffuse into the substrate and lock mechanically into the surface structure, after which no clearly defined interface exists. This theory is applicable only to high molar mass materials and it has been demonstrated to be applicable as a mechanism to additives and substrates which are mutually soluble. However, it is difficult to visualise the concept of polymer molecules diffusing through hard, impenetrable surfaces (Thompson, 1998).

1.5.1.4 Weak-boundary layer theory

The weak boundary layer theory suggested by several workers preserves that true interfacial fracture does not occur, and that fracture normally occurs cohesively in a

weak boundary layer (WBL), which could be near the interface between coating and substrate. Experimental evidence has perhaps rebutted the first point, that true interfacial failure can occur, but it has been proven that the second is valid in some cases.

Of practical importance to WBL investigations is the locus of fracture occurring in one or more of the zones in Figure 1.10. For a strong bond, the boundary layer (layers) must be chemically durable and rheologically sound.
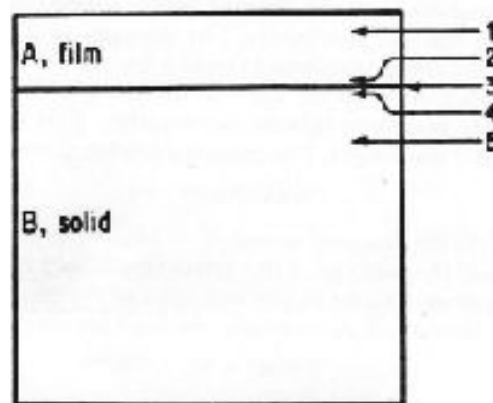
Figure 1.10 Weak boundary layer theory. Possible zones of failure

Regions 1 and 5 of figure 1.10 are within the respective bulk phases, and are distances from the interface.

Region 3 is the interface regions 2 and 4 are the regions near the interface with the same chemical composition as the bulk phase.

1.5.1.5 Chemical bonding theory

In chemical bonding theory of adhesion, the formation of covalent, ionic or hydrogen bonds along the interface is suggested (Petrie, 2000).

According to this theory, an adhesive molecule is attracted to a specific site on a solid surface and it is possible to react with the surface. The attraction is generated from van der Waals forces or specific donor-acceptor interactions (Toit and Sanderson, 1999).

There is no single theory of adhesion to demonstrate all possible interactions that take place between the adhesive and the adherend. The existing theories of adhesion presented in this chapter offer methods by which one can explain practical observations.

They are important in understanding why adhesives stick and why, at times, they fail. Adhesion theories offering a qualitative awareness of joint strength.

Each theory of adhesion is applicable in certain circumstances, but none are generally applicable. By being familiar with these theories, one can develop a knowledge base and an awareness of how adhesives and sealants work in practical situations (Petrie, 2000).

1.6   Surface treatment and the importance of the surface treatment

Careful surface preparation is required to achieve good adhesion and in the case of a typical surface treatment, failure at the interface might occur because of insufficient wetting or the existence of a weak boundary layer, which should be prevented or realistically minimised. However, the treatment of all substrates must be carried out in a suitable fashion prior of bonding to remove or prevent the formation of weak boundary layers and then to provide a coherent surface (Christine *et al.*, 1999).

The surface energy values for many polymeric films are typically lower than 30 mJ/m^2, which means that polymeric films generally have relatively low adhesion

properties. To solve this problem a range of surface treatments can be applied including chemical, thermal and electrical methods (Pascual *et al.*, 2008).

Recently, applications of polypropylene (PP) and its copolymers has grown remarkably; the necessity of surface pre-treatment of polyolefins results from their inherently poor adhesion and this is particularly pertinent as many industrial applications need good adhesion properties. In most cases, such treatments modify surfaces in one or more of the following ways:

a) by removing the weak boundary layer;

b) by changing the surface topography;

c) by changing the chemical nature of the surface;

d) by modifying the physical structure (Toit and Sanderson, 1999).

Polymers having both polar and non-polar regions in their molecular chain can present different chain segments at the surface depending on the polarity of the surroundings.

Wiping the surface with non-polar solvents, such as *n*-hexane, can orient the non polar components towards the surface. Exposure of the polymer surface to heat after surface treatment could cause untreated molecular species to deposit on the surface, accordingly the surface treatment would be lost.

In general, for good adhesion to be achieved the critical surface energy of the substrate must be equivalent to or greater than the surface energy of the adhesive; this applies equally to crystalline thermoplastics such as polyolefins, linear polyesters, and fluorocarbons. In their natural state many polymeric substrates are

not suitable for adhesive bonding and the methods used for improving the bonding characteristics of polymeric surfaces include:

1. oxidation by flame or chemical treatment;

2. corona discharge;

3. ionized inert gas treatment which activates the surface by a chemical change (*e.g.* crosslinking) or physical change;

4. metal-ion treatment by removing fluorine from the fluorocarbons surfaces;

5. applying primers, adhesion promoters, and other wettable chemical species (Petrie, 2000).

For instance, to improve the adhesion properties of polyolefins, corona treatment is applied. Isotactic polypropylene (PP) is one of the most commonly used synthetic polymers, which requires improvements when it is used in technical applications, and this could be achieved by corona treatment, the purpose of which is to produce polar chemical functional groups at the polymer surface. When activated, two important chemical processes are happening simultaneously at the surface:

1. cross-linking of the polymer chain;

2. degradation of polymer chain by oxidation, *i.e.* producing chemical degradation products on the surface area of the polymer (Overney *et al.*, 1993).

Corona treatment in air at room temperature is considered one of the most widespread methods for activating the polymer surface. Although the method is very simple, the physical mechanism of charging and discharging is still unclear, and the main purpose of such treatments is to improve the adhesion properties of the materials, where different ionic groups initiated by the corona, deposit on the

surface. As a result, air corona is characterized by high concentration of oxygen (Yovcheva *et al.*, 2007) and an increase in surface energy; the adhesion is enhanced along with the wetting properties. Oxidation plays an important role in corona discharge treatment under different working gases to get a better adhesion and it is the essential chemical mechanism for corona treatment. The surface energy of a solid is made up of two components: dispersion (apolar) and polar. When the surface polarity is high, the surface will be more active and reacts with polar interfaces. Surface wettability and adhesive bonding increase when the polarity is high; when the treatment is strong, the surface energy and polarity are high (Mesic *et al.*, 2006). Additionally, corona treatment of a film can increase its cohesive strength and regions of cross-linking at the surface (Christine *et al.*, 1999).

Many controversial opinions have been expressed about the reasons behind the poor adhesion of polyolefins. (Bikerman, 1967) discussed the weak boundary layer at the polymer surface, intimating that the main purpose of modification was to remove this fine layer of low molecular mass compounds from the surface. Brewis and Briggs, (1985) proposed that the incompatibility of the chemical functionality of polyolefins was the reason for poor adhesion. Levine *et al.*, (1964) suggested that the critical surface tension of a polymer is related to the strength of the adhesive bonds and found that the adhesion is increased when the critical surface tensions of wetting are increased. Levine also suggests that the polarity and surface energy increase as a result of most chemical changes. Blais *et al.*, (1974) investigated the correlation between the polymer surface roughness and adhesion. The mechanical anchoring of the adhesive in the irregular pores of the substrate is the reason behind increasing adhesive properties of polypropylene. According to Haller, (1988)

cohesion forces which hold the atoms or molecules in any solid would be possible only if the original state is restored. Reactivation of these cohesion forces would be possible only if the original intervals between the atoms could be re-established; the same applied to the joining of different materials. However, in practice such affinity is prevented by surface roughness and weak-boundary layers that originate from the adsorption of impurities from the surroundings (Toit and Sanderson, 1999).

Polymeric surfaces contains many low molecular weight fragments, and what could be seen in the surface region are oxidation products, plasticizers, processing aids, lubricants and slip aids, adsorbed water, and organic contaminants (Figure 1.11) and other surprises for the end-user. All of these will affect the resulting bond strength without changing the bulk properties of the material significantly. A migration of some components in the polymeric bulk materials to the surface could happen.
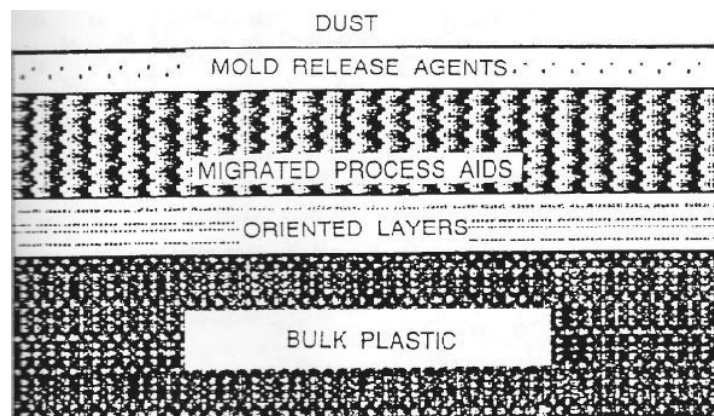
Figure 1.11 Schematic representation of polymer (substrate surface regions)

1.6.1 Choosing the surface treatment

Surface preparation is carried out in many ways such as solvent wiping, which is a simple way, mechanical scraping, chemical cleaning, and acid etching. The following considerations should be taken into account when selecting a surface preparation:

1. the ultimate bond strength required;

2. the degree of continuity necessary and the service environment;

3. the degree of and type of contamination originally on the adherend;

4. the quality of adherend and nature of its surface;

5. production considerations such as cost, cycle time, safety environmental compliance, training, monitoring and control.

Any surface treatment used to achieve good bonding (or sealing) requires the completion of one or more of the following operations: *mechanical abrasion, cleaning, or active surface modification*. Passive surface treatment processes clean and remove weakly attached surface layers (*e.g.*, solvent washing, mechanical abrasion) and do not change the chemistry of the surface; while active surface treatment processes change the surface chemically (*e.g.*, anodizing, etching, plasma treatment).

When PP is extruded high temperatures and pressures in atmospheric gases are applied, oxidation happens by a free radical mechanism including initiation, propagation and termination as shown in Figure 1.12; besides this, branching reactions also can occur. These steps lead to the insertion of oxygen into the polymer but none of these reactions can cause a remarkable decrease in the molecular weight of oxidized polypropylene during processing. This occurs by different chain-scission reactions; β-scission, illustrated in figure 1.13 is the most common:

a) Initiation of oxidation

RH + energy ⟶ R• + H•

b) Propagation of Oxidation

R• + O₂ ⟶ ROO•

ROO• + RH ⟶ ROOH + R•

H• + RH ⟶ R• + H₂

ROOH ⟶ RO• + •OH

c) Termination of Oxidation

RO• + •H ⟶ ROH

ROO• + •H ⟶ ROOH

R• + •R′ ⟶ R—R′

RO• + •R ⟶ ROR

2RO• ⟶ ROOR

2ROO• ⟶ ROOR + O₂
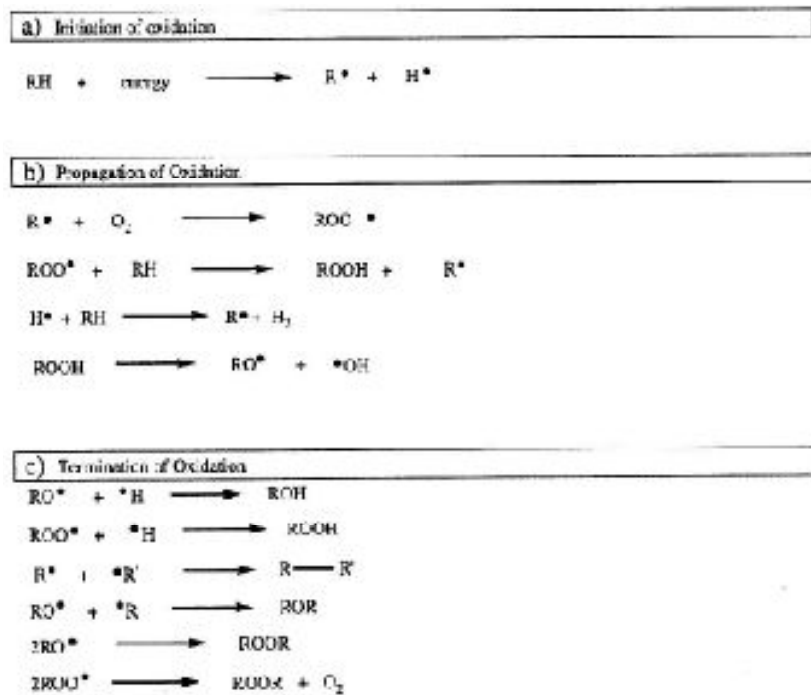
Figure 1.12 General mechanisms for the oxidation of polypropylene
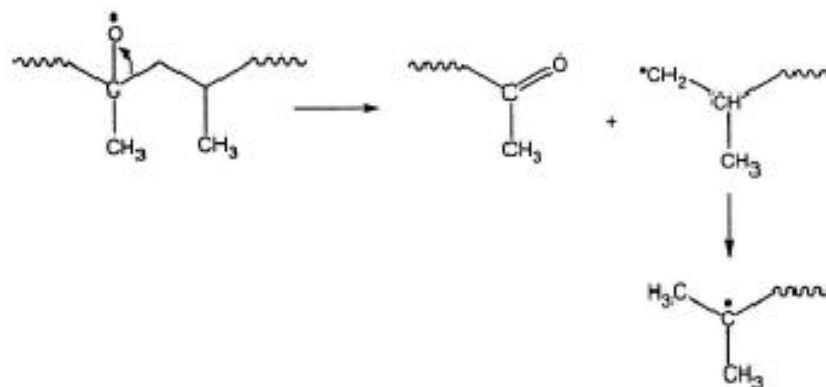
Figure 1.13 Mechanism of β-scission in polypropylene oxidation

Owing to the low price and attractive balance of mechanical properties, PP is obtaining more attention as a new construction material. The latter involves the long-term stability in sunlight, and a wide knowledge of the oxidation behavior is needed when it comes to stabilising and predicting the useful life time of PP (Erikson *et al.*, 2002).

Polyethylene (PE) and PP are two of the three most widely-used synthetic polymers worldwide, thus, most of the research on corona treatments of polyolefins films is based on PE and PP films and data concerning corona treatment have been generated within the last thirty years (Christine *et al.*, 1999). For a PP film, the spectrum showed carbon to be the major element present at the surface of the untreated film. This confirms that the polar groups obtained by Corona discharge treatment (CDT) contain oxygen and with increasing corona energy the amount of oxygen incorporated increased. Applying CDT to BOPP yields functional groups such as hydroxyl, carbonyl, peroxy, ester, carboxylic acid and anhydride groups (Figure 1.15). It is suggested that the energy delivered to the surface by CDT is controlling the type of functional groups introduced to the surface of PP films, and their relative concentrations. Fig 1.14. represents the changes in the relative concentrations of the species introduced as a function of the energy of corona (O'Hare *et al.*, 2001).
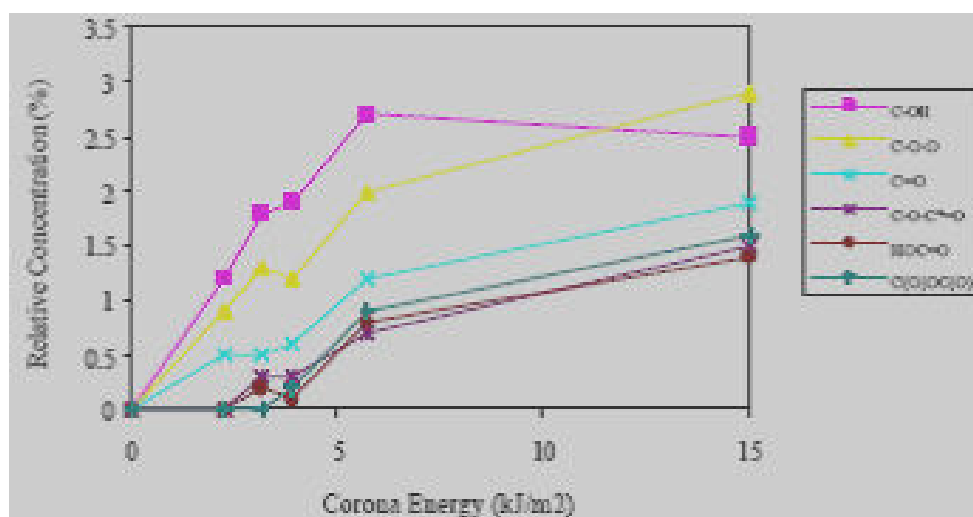
Figure 1.14 The functionalities introduced by Corona Discharge Treatment as a

function of Corona energy

Hydroxyl, peroxy and carbonyl groups are generated at all levels of CDT, but the more highly oxidised species are not introduced until more aggressive energy levels have been applied. More surprisingly, at energy levels where the atomic concentration of oxygen is decreased slightly, the carboxylic acid, ester and anhydride groups are increased in concentration. This suggests that until the energy level of ~4 kJm^{-2} is exceeded, oxidation and cross linking are the main mechanisms of CDT; above this energy level, a chain scission mechanism also occurs (O'Hare *et al.*, 2001). The processing of unmodified commercial PP films is extremely difficult because these films have essentially hydrophobic surfaces, thus further surface modification like introduction of polar functional groups is carried out. Corona treatment is widely used for plastics and particularly for polyolefins to generate these groups through surface modification (Gourianova *et al.*, 2005) *via* a free process of the following type (Briggs *et al.*, 1983).

Figure 1.15 Radical process during discharge treatment of surface oxidation

1.6.2 Polarity of corona-treated films

The surface free energy of a solid material, γ_s consists of two constituents, dispersive (nonpolar) and polar; each demonstrating the type of molecular interactions between two phases:

$$\gamma_s = \gamma_s^d + \gamma_s^p$$

Where γ_s^d is the dispersive component and γ_s^p is the polar component.

The activity of the surface increases when the polar component is high, then the surface tends to interact with different polar interfaces and high polarity improves surface wettability and adhesive bonding. The polarity of polymers used in making films, PE and PP is near-zero, thus these polymers show poor wettability and ink adhesion, when applying electrical discharge, such as corona treatment to polymer, the surface polarity increases. The stronger the treatment, the higher the polarity (M.Blitshteyn, 1995). Both the dispersive contribution to surface energy and the acidic character of the surface increases when applying the corona treatment, while the basicity is increase slightly. At a high corona current some chemical degradation of the surface occurs (Belgacem *et al.*, 1995).

1.7 Polypropylene (PP) properties

PP films are replacing other materials such as PE, poly(vinyl chloride), polyester and cellophane, because of its low density. There are three types of PP: unoriented film, cast film, or biaxially-oriented film. Biaxially oriented polypropylene film (BOPP), which is the used film in this study, is stretched in both the machine and transverse directions, producing molecular chain orientation in two directions. PP can be

isotactic, syndiotactic, or atactic depending on the orientation of the pendant methyl groups attached to alternate carbon atoms. In isotactic PP (Figure 1.16 top), the pendant methyl groups branching off from the polymer backbone are all on the same side of the polymer backbone, with identical configurations relative to the main chain.
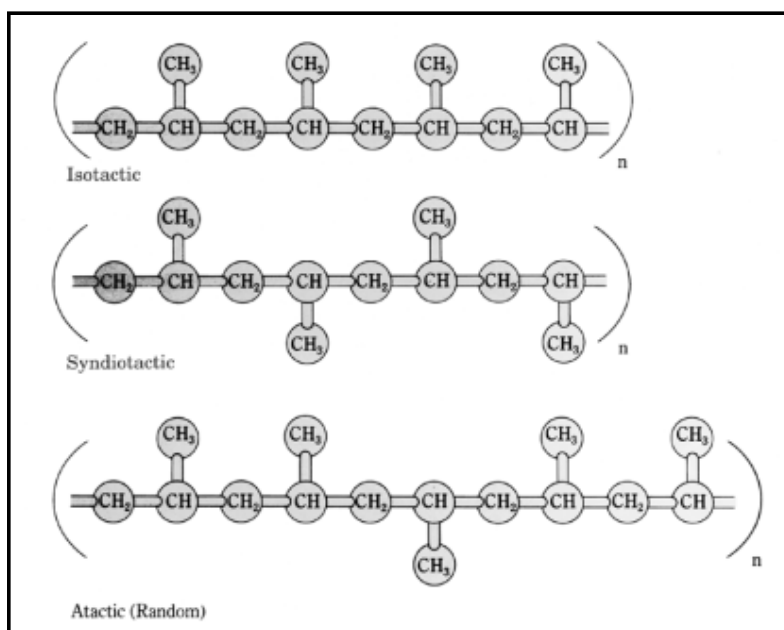
Figure 1.16 Stereochemical configurations of polypropylene (Maier and Calafut, 1998)

In syndiotactic PP (Figure 1.16 middle), consecutive pendant methyl groups are on opposite sides of the polymer backbone chain. In atactic PP (Figure 1.16 bottom), pendant methyl groups are oriented randomly with respect to the polymer backbone. The portion of the chain shown is repeated n number of times to form the polymer (Maier and Calafut, 1998). There is a link between stereo regularity and the existence of regular chains. The infrared spectra of the isotactic, syndiotactic and atactic forms of PP show distinctive differences, as shown in Figure 1.17.

The absorbance values at 970 and 1460 cm^{-1} do not rely upon tacticity, whereas the absorbances at 840, 1000 and 1170 cm^{-1} are feature of isotactic PP, and the absorbance at 870 cm^{-1} is mark of syndiotactic PP.
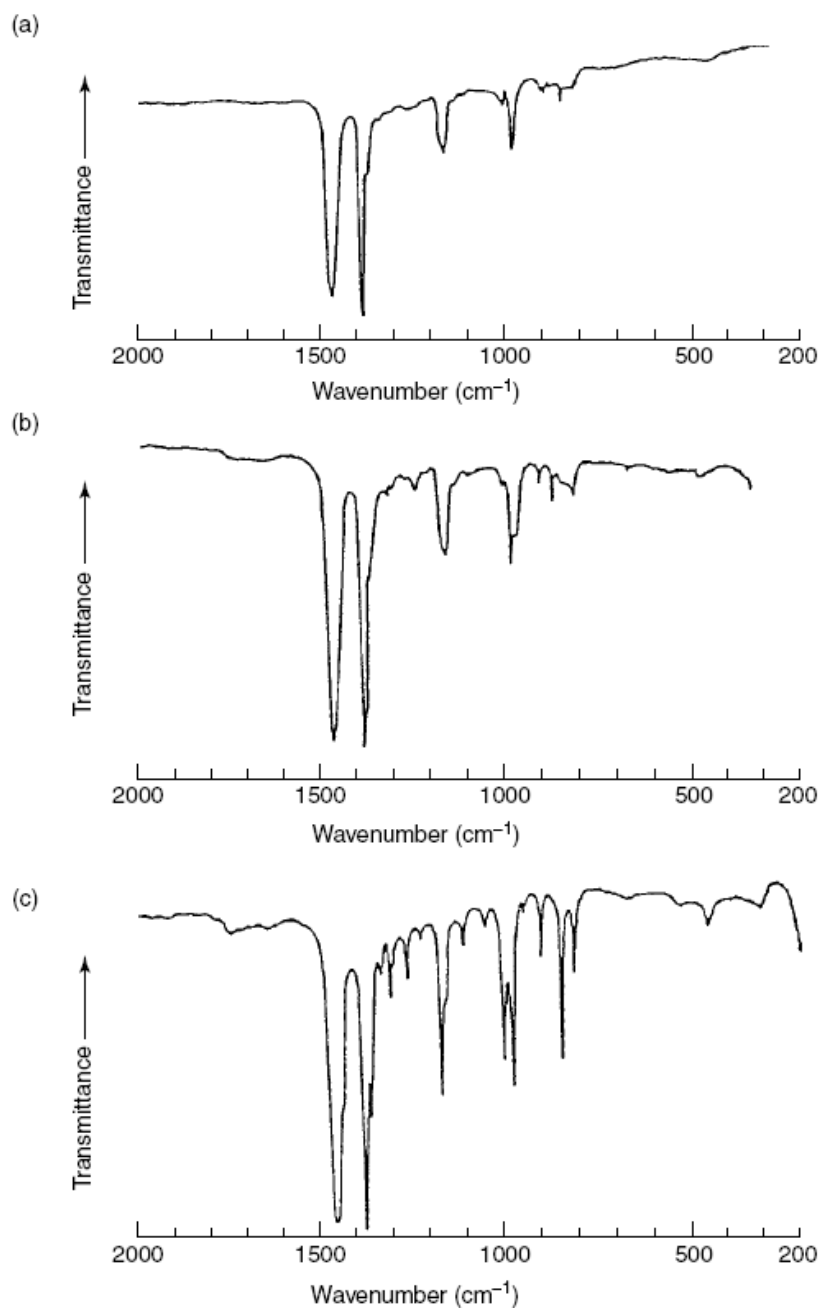
Figure 1.17 Transmission infrared spectra of polypropylene stereoisomers: (a) atactic; (b) syndiotactic; (c) isotactic.
From Klopffer, W., Introduction to Polymer Spectroscopy (Stuart, 2004).

Such differences are related to the different helical structures present in the isomers and can be used to evaluate the fractions of isotactic and syndiotactic sequences in samples, Branching in polymers can be tested by using infrared spectroscopy (Stuart, 2004).

The crystalline structure of a solid semi crystalline polymer declines at the melting point, T_m, when the material goes through a phase change from solid to liquid. At the melting point, physical characteristics of the material, such as density, refractive index, heat capacity, and transparency, change suddenly as the material becomes a viscous liquid. Melting points are usually measured using differential scanning calorimetry (DSC). The melting point of a polymer differs with the degree of crystallinity. A typical isotactic PP has a theoretical melting point of about 171°C while the melting points of commercial isotactic PP can vary from 160-166°C (Maier and Calafut, 1998).

1.7.1 Polypropylene glass transition

Amorphous regions of PP display a glass transition, T_g, at a temperature around

-11°C (Rajan et al., 2004)., depending on the measurement method, heating rate, thermal history, and microstructure. The T_g is related to the amount of free volume in a polymer. Above the T_g molecules and segments of polymer chains vibrate and move in noncrystalline polymer regions. Motions investigated include those due to diffusion, rotation about bond axes, and translation under mechanical stress. At the T_g, free volume is limited and only low amplitude vibrations can happen. This movement lasts down to absolute zero, to a point where all movement stops. Resins with lower molecular weight normally have lower T_g related to increased free volume

at the ends of the polymer chain and lower degrees of chain complexity. General use temperatures of PP are normally between the T_g and melting temperatures, so that strength and stiffness from the crystalline region are combined with toughness of the amorphous "tie points". The low temperature ($\leq 5°C$) brittleness of PP is related to its proportionally high T_g; as the temperature falls, approaching the, T_g, the resin becomes increasingly brittle, and impact resistance becomes negligible (Maier and Calafut, 1998).

1.8 Aim of the research

In this introduction a discussion is presented of selected ink components, mainly the fumaric rosin polymer (UCH 150H) and polyurethane (Surkopak 5323), with a brief mention of adhesion theories. The mechanism of polyolefins surface pretreatment also discussed, as well as the properties of biaxially oriented polypropylene which is the surface used in this study.

This study is divided into three parts: the first addresses many formulations related to the preparation of concentrated pigment paste, the sizes of pigment particle sizes in the concentrated paste were tested and the approved formulation of the obtained paste was used for further comparisons.

The second part involves the preparation of a number of varnish formulations incorporating UCH150H and Surkopak 5323, either separately or combined (with UCH150H in the minority as an additive). By mixing the prepared concentrated pigment with the prepared varnishes, three formulations of flexographic inks were obtained.

The final part evaluates the adhesion difference of these three flexographic inks by tape test after printing them on to biaxially oriented polypropylene (having exposed one side to corona treatment); all the components of the studied inks are similar apart from the polymeric component.

In order to describe the physical and chemical nature of the interactions between the BOPP surface and the polymers under study (Surkopak 5323 and UCH150H), it was necessary to ascertain their surface properties such as the dispersive interaction parameter and acid-base character by inverse gas chromatography (IGC). The contact angle of the prepared flexographic ink and polymer solutions will be measured and scanning electron microscopy (SEM) will be conducted to evaluate the difference existing in the surface properties.

Recently, a number of advanced surface-active analytical techniques have emerged which now permit sophisticated characterization of polymer surfaces. The chemical composition of polymer will be analyzed by Fourier Transform infrared (FTIR) spectroscopy, electron spectroscopy for chemical analysis (ESCA) and NMR spectroscopy. A similar approach will be used to determine the chemical composition of the surface after applying the polymers to the BOPP. AFM will be applied so as to investigate the adhesion of polymer materials on the BOPP surface and examining the true surface morphology of the polymer film fine structure.

The novelty of this research is the use of fumaric rosin as a polymer in the formulation of NC Flexography inks, whereas PU is the commonly used polymer in such kind of formulations. The benefits beyond the use of fumaric rosin are associated with its derivation from natural sources (coniferous trees), which reduces its impact on the environment. From the viewpoint of cost, the fumaric rosin is less

expensive than other polymers commonly used in manufacturing NC Flexographic inks. The other novel point involves the study of the printed BOPP substrate using the IGC technique. The BOPP was printed once from the fumaric rosin solution and on the second occasion from the PU solution, then a comparison of these two printed BOPP samples was made. Finally another comparison was carried out in which the properties of the polymer before and after printing on the BOPP surface (treated side) were determined.

Chapter 2   Surface science

2.1   Inverse gas chromatography (IGC)

This technique is defined as the reverse of a conventional gas chromatographic (GC) experiment, but the principles of IGC are simple. The technique is based on the physical adsorption of a well-known probe at different concentrations by a solid interface. In IGC, characterization of the surface and properties of packing materials is studied by injecting probes of known physico – chemical properties at infinite dilution and consequently behave independently.   As the GC instruments are available, besides, the accuracy rapidity and simplicity of this way, IGC was considered a good supplementary way for determination of surface properties (Belgacem *et al.*, 1995). IGC is an economical and suitable operation, which are some of the reasons explaining the widespread use this technique in the technical literature. It has become a common tool in research and used for routine laboratory applications. IGC data can be collected quite rapidly over a wide temperature range and many probes can be used in the mobile phase to explain the stationary phase characteristics.

Practically, an empty column should be packed regularly with the solid material under study, normally a powder, film, or fibre. A solute (at low concentration) is introduced into the mobile phase, an inert gas of known flow rate, and travels down the packed column, the retention behaviour of the solute is measured by a detector. The main feature, which is measured by IGC, is the retention volume V_n and all the other properties are derived from this value. This is a measure of interaction of gas probe molecules with the solid sample. From many measurements of V_n a number of kinetic and thermodynamic parameters can be measured (Thielmann *et al.*, 2001).

Information related to adsorption process is derived from the retention time and the peak shape. Examination of the interfacial interactions in polymer systems is of high importance and the characteristics of the surface, interface and inter-phase are determined by physical forces, when the materials at interface are not bonded chemically caused by fluctuating dipoles, and into specific or non-dispersive forces. This can be of high importance and include acid/base interactions, hydrogen bond forces, etc. Present approaches favour the summing of all non-dispersion forces into acid / base terms, making it necessary to characterize the components of polymer systems as electron donors and / or acceptors (Mukhopadhyay *et al.*, 1993).

The IGC technique can be executed over a wide temperature range at different moisture contents of the non-mobile phase with corrosive substances (Kamdem *et al.*, 1993). In this way, the surface properties and thermodynamics of adsorption of organic and inorganic materials, were studied in the last 40 years by IGC (Conder *et al.*, 1979).

IGC is commonly used to characterize films, particulates, and fibres. When the retention time is long, the interaction of stationary phases with the probe is more powerful and the surface is more energetic. This is the reason behind a range of thermodynamic parameters being derived from the retention attitude (Burnett *et al.*, 2007). Now many technical problems rely on interface interactions, particularly when it comes to reinforcement – matrix interaction control, IGC plays an important role when the good understanding of surface is very important in all types of composite materials, or the coatings compatibility with substrate when protective layers must be applied to any sensitive materials, or in case of the effectiveness of

adhesion, *etc.* (Gutierrez *et al.*, 1999). IGC has also been used as a procedure for the identification of acid / base parameters for polymers fibres, and fillers, among other constituents of polymer systems (Chen, 1988).

Nowadays, the effectiveness and importance of IGC in the investigation of polymer – probe and polymer – polymer interaction is widely recognized (Olabisi *et al.*, 1997). A thermodynamic evaluation of polymer - interaction of polymer can assist understanding the resulting blends, miscibility and the choosing of compatible systems of polymer (Di Paola *et al.*, 1982). However, when comes to amorphous or semi-crystalline polymers below the temperature of glass transition T_g, retention would be controlled only by adsorption (Chehimi *et al.*, 1997). The wide applications of IGC technique became the most important element in the growth pattern of IGC.

Apart from offering thermodynamic information, IGC remains an important source for deciding phase transitions, for estimating adsorption properties, and for measuring dispersive and non-dispersive forces acting at surfaces and interfaces.

Having given this series of applications and the continued growth of materials science, it is feasible to conclude that IGC methodology will last to play an important role in explaining the materials attitude, and in forming multi-component systems that would achieve requested goals of durability and performance (Schreiber and Lloyd, 1989).

2.1.1 The importance of the T_g in IGC for polymer surface characterization

The pertinence of IGC measurements to the measurement of bulk properties relies on whether the vapour molecules can penetrate into the bulk to a crucial extent in the

course of the experiment. Temperature becomes an important issue: it has been proved that IGC data that are gathered above the T_g of the stationary phase result from a combination of surface and bulk sorption. The thermodynamic interaction of polymers above their glass transition was studied extensively by IGC with low molecular weight probes (Lavoie *et al.*, 1969). Below T_g, it is supposed that the surface effects prevail sufficiently when the contribution from bulk sorption is neglected. Different terms for diffusion variables and for their temperature reliance have been suggested (Mukhopadhyay *et al.*, 1993). However, some old IGC literature advises that IGC measurements of thermodynamic properties should be undertaken at a temperature of not less than 50°C higher than T_g to avoid problems with a slow achievement of the equilibrium on the column (Lavoie *et al.*, 1996).

2.1.2 The use of IGC to study adhesion of polymers

When it comes to balancing the advantages of the IGC technique, several difficulties arise; some of which have not yet been resolved. Which is focused on the point of surface *vs.* bulk characterization of interaction properties, which has been discussed for several years (Lichtenthaler *et al.*, 1974.) with the conclusion that polymer – solvent interactions measured by IGC experiments report on the character of the surface, considering the large surface / volume ratio in placed column. On the other hand, (Courval *et al.*, 1975) argued that film thicknesses in packed columns are sufficiently large to permit the diffusion of vapour probe molecules, so that bulk properties contribute to measurements made by the packed column technique. The properties of particulates – the characteristics of its components, compositions, structure and interfacial interaction determine the filled polymers. The effect of this factor is related to the size of the interface and to the strength of the interaction

proportional to the reversible work of adhesion (Fowkes *et al.*, 1981). IGC determines mainly the electron acceptor and donor characteristics of the surface, additionally the work of adhesion which can be derived from surface tension (Fekete *et al.*, 2004).

The increased understanding of the concept of solid surfaces, interfaces and inter-phases in defining the useful characteristics of polymeric system, has contributed to the advancing of IGC as an efficient technique for estimating the probability for interaction of various components of polymer mixtures, composites, and many component polymeric systems in general. The capability of the IGC technique to present information related to the acid-base interaction potentials of polymer surfaces is widely discussed in the literature. The data obtained from IGC experiments maybe linked directly with observed performance criteria such as gloss, colour development, adhesion, rheological properties, and mechanical properties (Mukhopadhyay *et al.*, 1993).

The methods used in this study were based on work conducted by previous workers of the department, Acklam (2006) and Santos (2003), who have in their theses a broad review on the theory and application of IGC. In fact, many publications have presented the theory of IGC at infinite dilution, only the relevant theoretical details are mentioned here.

2.1.3   Retention time determination

The characteristic of interaction with solid stationary phase material is determined by the retention time and hence the retention volume. The retention time is specified

by the time taken for the probe molecule to elute from the column. This time is governed by the flow rate of the carrier gas through the column.

Therefore, the retention time t_r is usually converted into a net retention volume, V_n, which may be specified as the volume of carrier gas which is needed to elute a given probe, as follows:

$$V_n = (t_r - t_0) F C J \tag{2.2}$$

t_0 is the retention time of the non-interacting probe species, methane. F is the carrier gas flow rate in cm³/s. J is the James-Martin correction factor, correcting for the compressibility of the carrier gas:

$$J = 1.5 \; \frac{\left(\dfrac{P_i}{P_o}\right)^2 - 1}{\left(\dfrac{P_i}{P_o}\right)^3 - 1} \tag{2.3}$$

P_i and P_0 are the inlet and outlet pressures of the carrier gas respectively. C is a correction factor, allowing for the vapour pressure of the water at the temperature of the bubble flow meter used to determine the flow rate. Thus:

$$C = 1 - \frac{P_{H_2 0}}{P_o} \tag{2.4}$$

P_{H_2O} is the vapour pressure of the water in the flow meter (kPa), at the temperature of measurement.

The net retention volume V_g can be normalized by gramme of the interacting support material which is present in the stationary phase.

$$V_g = \frac{V_n}{m} \tag{2.5}$$

Here, m is the mass of interacting stationary phase.

The net retention volume can be split into two functions, one relates to bulk adsorption and the other relates to surface adsorption.

2.1.4 The dispersive component of the surface free energy of solid surfaces

The Fowkes approach is used to determine the free energy of adsorption and the dispersive component of the surface free energy of solid surfaces. This approach has become the most widely realized mathematical approach and has been amended as obstacles have been encountered.

The Fowkes approach relies on the determination of the work of adhesion W_a between species that interact only *via* dispersive forces, and is identified by the equation:

$$W_a = 2\,(\gamma_s^d \gamma_\ell^d)^{0.5} \tag{2.6}$$

Here, γ_s^d and γ_ℓ^d are the dispersive components of the surface energies of the stationary phase and the probe, respectively.

The work of adhesion is related to the free energy of adsorption of the probe by the equation:

$$-\Delta G_a = N_A \, a \, W_a + K' \tag{2.7}$$

Here, N_A is Avogadro's constant; "a" is the molecular surface area of the probe and K' is a constant.

The sum of the work of adhesion for a surface area of one mole of the molecules is equal to the negative Gibbs free energy of adsorption of that molecule.

The free energy of adsorption ΔG_a may defined in terms of the retention volume of the probes:

$$\Delta G_a = -RT \ln(V_n) + K \tag{2.8}$$

R is the Universal gas constant, T is the column temperature and K is a constant for a given column.

Accordingly, Equations 2.6, 2.7 and 2.8 can be combined to give:

$$-\Delta G_a = RT \ln(V_n) = 2N_A \, a \, (\gamma_s^d)^{0.5} (\gamma_\ell^d)^{0.5} + K'' \tag{2.9}$$

The values of $(\gamma_l^d)^{0.5}$ have been pre-determined for several non polar (*n*-alkane) probes and several polar probes. Thus, a plot of $RT \ln(V_n)$ against a function of $(\gamma_l^d)^{0.5}$ gives a slope of $2N_A (\gamma_s^d)^{0.5}$ and an intercept of K''.

The values used in this study are presented in Table 2.1.

Table 2.1 Values of $a\sqrt{(\gamma_l^d)}$ for selected n-alkane probes (Kamdem *et al.*, 1993);

(Baoli *et al.*, 2007)

Probes	a [x10^{-10}m^2]	(γ_l^d) [mJ/m^2]	$a\sqrt{(\gamma_l^d)}$ [cm^2(mJ/m^2)$^{0.5}$]
n-Pentane*	46.1	16.0	1.84 x 10^{-16}
n-Hexane*	51.1	18.4	2.21 x 10^{-16}
n-heptane*	57.0	20.3	2.57 x 10^{-16}
n-octane*	62.8	21.3	2.90 x 10^{-16}

The problem with the Fowkes approach is that it does not always generate precise values of (γ_s^d) due to the doubt of the molecular surface area value of the adsorbed non polar species. The problem is that the alkane molecule might be arranged in a flat profile or in head to tail arrangement on the surface. Therefore, different interactions may happen. The Fowkes approach has become the most widely used model owing to its graphically simple nature and the capacity to decide the disperse component of the surface tension from the relationship (Czeremuskin *et al.*, 1997).

When polar probes are involved, specific interaction with the polymer surface is probable; thus, there shall be a specific component to the total surface free energy, besides the dispersive component.

The total free energy of adsorption, ΔG_a^{tot}, can be defined as:

$$\Delta G_a^{tot} = \Delta G_a^d + \Delta G_a^s \tag{2.10}$$

The term ΔG_a^d is related to the dispersive component of the interactions for the total Gibbs free energy of adsorption. ΔG_a^s relates to the specific component of interactions for the total Gibbs free energy of adsorption. This specific function happens because of Lewis acidic interactions and to Lewis basic interactions.

The specific component of the free energy is specified from the *n*-alkane plot of $RT\ln(V_n)$ against $a\sqrt{(\gamma_l^d)}$.

Generally, the polar probes are classified into three groups. These are the Lewis acidic probes, *e.g.* dichloromethane (DCM), the Lewis basic probes, *e.g.* tetrahydrofuran (THF) and the Lewis amphoteric probes, *e.g.* diethyl ether (DEE), acetone (ACE) and ethyl acetate (EAA). when polar probes are eluted through the column, specific interaction

happens with the material being analysed. The ΔG_a^s value can be identified from the distance between the ordinate values of the polar probe data point and the *n*-alkane reference line, as explained in Figure 2.1.
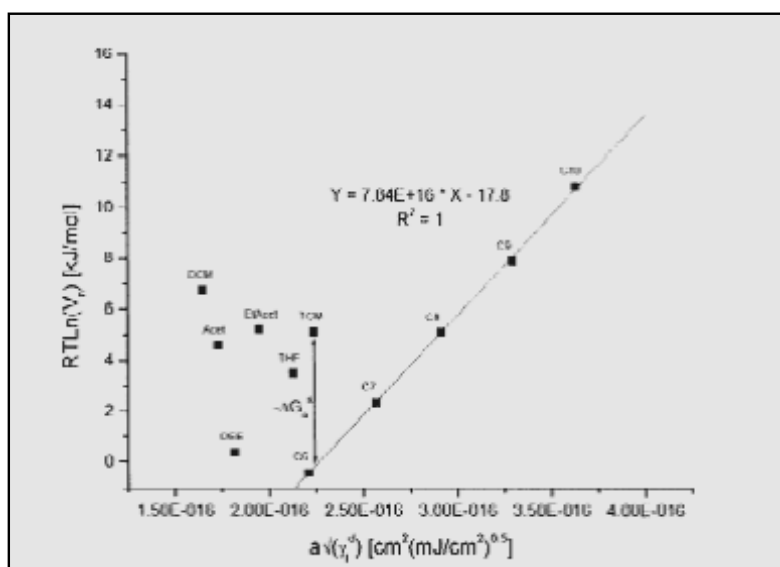
Figure 2.1 A Diagram illustrating the Fowkes Plot

An equation could be written for this procedure as,

$$-\Delta G_a^s = RT \ln \left[\frac{V_n^{tot}}{V_{n,ref}^d} \right]$$ (2.11)

Where V_n^{tot} and $V_{n,ref}^{tot}$ are the retention volume for the polar probe and the retention volume for the *n*-alkanes reference line respectively.

2.1.5 Determination of Lewis acid and Lewis basic values K_a and K_b

The major interest of IGC analysis are the determination of Lewis acidic property and the Lewis basic character of a material. A Lewis acid is a molecule or ion whose

incomplete electronic configuration allows it to bond to another species to accept an electron pair from that species. A Lewis base is a molecule or ion that is capable of donating a pair of electrons to a species, resulting in the formation of a coordinate bond (Atkins, 1999).

The second law of thermodynamics is related to the processes that are spontaneous or non-spontaneous. A definition by Kelvin of the second law is "No process is possible in which the sole result is the adsorption of heat from a reservoir and its complete conversion into work" (Atkins, 1999).

The spontaneity of a process can be identified by the Gibbs' free energy for that process. In case of an adsorption process, as in IGC,

$$\Delta G_a = \Delta H_a - T\Delta S_a \qquad (2.12)$$

The polar probe adsorption on the polymer surface causes a change in the enthalpy and entropy of the system. These factors are related to the Gibbs' free energy of adsorption by equation 2.12.

ΔH_a and ΔS_a relate to the enthalpy of adsorption and to the entropy of adsorption respectively and T is the column temperature. A plot of $\Delta G_a / T$ against $1/T$ offers the values of the enthalpy of adsorption and the entropy of adsorption. The values of ΔH_a and ΔS_a are derived from the gradient and the intercept respectively.

The Gutmann approach (Riddle and Fowkes, 1990) permits the determination of the Lewis acidity value and of the Lewis basicity value from ΔH_a, by using equation 2.13.

$$-\Delta H_a = K_a xDN + K_b xAN* \qquad (2.13)$$

Here DN and AN* are defined as the donor number and modified acceptor number, respectively, corresponding to the polar probes.

These numbers are defined as the donor number DN, expressing the bacisity or electron donor ability, is the molar enthalpy value for the reaction of the electron donor with a reference acceptor $SbCl_s$.

The acceptor number AN expressing the acidity or electron-acceptor ability, is defined on basis of ^{13}P NMR chemical shift observed when $(C_2H_5)_3PO$ reacts with the acceptor (Planinšek et $al.$, 2001).

Plotting $-\Delta H_a / AN^*$ against DN / AN^* gives K_a as the slope and K_b as the intercept.

Values of a $(\gamma_\ell^d)^{0.5}$ and DN and AN* of the surface area for the polar probes used in this study are summarised in Table 2.2.

Table 2.2 Values of $a\sqrt{(\gamma_l^d)}$, DN and AN* for the selected polar probes (Santos et $al.$, 2002)

Probes	$a\sqrt{(\gamma_l^d)}$	AN*	DN
Tetrahydrofuran (THF)	2.13 x 10⁻¹⁶	2.1	84.4
Dichloromethane (DCM)	1.73 x 10⁻¹⁶	16.38	0.0
Ethyl acetate (EtAc)	1.95 x 10⁻¹⁶	6.3	71.8
Acetone (Ace)	1.765 x 10⁻¹⁶	10.5	71.4

Acid-base forces contribute effectively to surface interactions in polymer composite systems; the demand to quantitatively describe acid-base properties brought the technique of IGC to light. When Gutmann and Fowkes' donor and acceptor parameters are introduced, the surface acid-base characteristics of polymers can be easily identified by the IGC method (Baoli *et al.*, 2007).

2.2   Wetting

In coating applications, it is very important that the liquid coating wets the substrate; the steps to acheive this are substrate cleaning and the use of surfactants to lower the liquid coating surface tension and decrease the contact angle to zero. Good wetting of the substrate leads to a good adhesion of the coating to the substrate (Koleske, 1995). Because of the difficulties involved in direct measurement of the surface tension of a solid phase, indirect approaches have been suggested, of which the simplest method is thought to be contact angle measurements.

Contact angle measurements are performed simply by determining the tangent (angle) of a liquid drop with a solid surface of the base. The probability of evaluating solid surface tension from contact angles relies on a relationship that was identified by Young in 1805. The contact angle of a liquid drop on an ideal solid surface is specified by the mechanical equilibrium of the drop under the effect of three interfacial tensions: solid-vapour, γ_{sv}, solid-liquid, γ_{sl}, and liquid-vapour, γ_{lv}. This equilibrium relation is known as Young's equation:

$$\gamma_{lv} . \cos\theta_y = \gamma_{sv} - \gamma_{sl} \qquad\qquad (2.14)$$
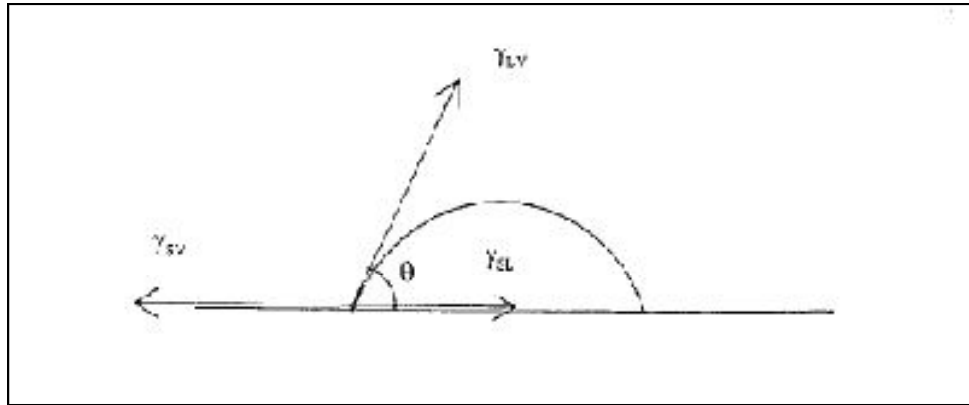
Figure 2.2 Forces acting at the circumference of a liquid drop on a solid surface

Where θ_y is the Young contact angle, *i.e.* a contact angle which can be inserted into Young's equation (Mittal, 2003).

All adhesive bonds are formed by placing an adhesive, which is a liquid at the time of wetting, on a solid substrate when a contact angle θ will be made with the surface; the liquid will wet the surface completely when the contact angle is zero. To minimize the distortion due to the gravity, only small droplets (a few μl) are used.

The contact angle can be identified by many ways including:

(i) direct measurement by viewing through a microscope eye piece;

(ii) measuring the height (h) and radius (r) of the base of the drop, using a microscope or by projecting an image on a screen, followed by use of equation:

$$\tan \theta/2 = h/r \qquad\qquad (2.15)$$

(iii) the Wilhemly plate method in which a plate of the test solid is suspended from a microbalance, and partially immersed in the liquid (Comyn, 1997).

The wetting tension theory is part of a broader picture of the interaction between solid surfaces (plastic films) and fluids (inks, coatings, adhesives). Adhesive bond formation begins with interfacial molecular contact by wetting. To measure the degree of wetting, we use the concepts of surface tension of a fluid and surface energy of a solid.

The surface tension of a liquid is described as the tendency of the fluid to "stick together". The surface tension units of measurements are: Force/length = mN/m = dyne/cm.

The surface energy (tension) of a solid is expressed by molecular forces of its interaction with other surfaces. It is measured as free energy per unit area:

$$\text{Energy/area} = \text{force/length} = mJ/m^2 = mN/m = dyne/cm$$

The dyne/cm unit of measurement, which is common in the industry.

The surface energy of a solid material, such as flexible films, cannot be measured directly because solids do not change shape measurably in reaction to surface energy forces (Blitshteyn, 1995). The wetting tension of a specific solid is evaluated from its surface energy. Although the wetting tension value is normally less than the surface energy, it is mostly equated with it and is a favorable measure for the purpose of evaluating corona treated films. The wetting tension of a polymer film is related to a group of physical parameters where no measurements of accuracy exist. It is normally very difficult to know the real test results, what is really known is what is measured. In such cases, measurement precision, rather than accuracy, is the most important issue. For that reason there is a need for a test which will offer the desired level of precision (Blitshteyn, 1995).

Chapter 3   Microscopic studies

3.1 Atomic force microscopy (AFM)

One of the most common tools in nanotechnology is atomic force microscopy (AFM), which was invented by Binning, Quate, and Gerber.   It is one of the most widespread methods of imagining nanoscale structures (Abramovitch *et al.*, 2007). The (Figure 3.1) shows the standard plan of an atomic force microscope.
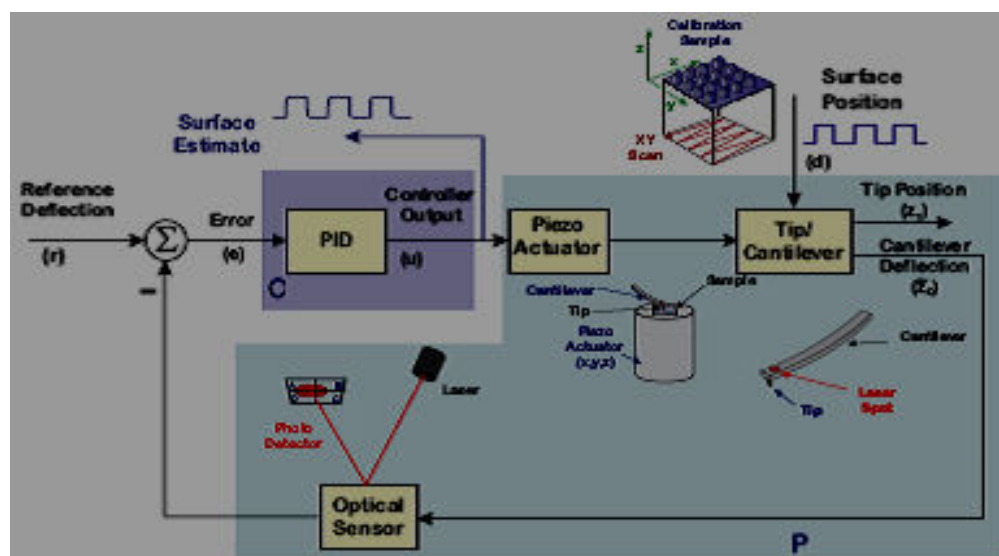
Figure 3.1 Standard plan of atomic force microscope

The above AFM Control Block diagram shows a scanned sample model, wherein the tip and cantilever are fastened and the sample is moved under the tip by the piezo stimulator.

In this way, the controller tries to guarantee a constant level of contact force. The measured quantity which is the surface profile, is expressed by an unknown perturbation of the control loop and the deflection of the cantilever is verified with optical detection.

The task of an AFM is to distinguish a sample by bringing a sharp probe in close proximity to the sample's surface; the probe tip is influenced by two types of forces on the surface, attractive and repulsive. These forces produce a deflection of the cantilever on which the tip resides and this deflection is investigated (Abramovitch *et al.*, 2007). Louey *et al.*, 2001 used AFM to calculate pull off forces between a model colloidal silica probe and lactose particles suitable for use as carriers in dry powder inhaler (DPI) formulations. Sindel and Zimmermann, 2001 applied AFM both quantitatively to study forces of interaction between lactose substrates. This invention measured the influence of the morphology of contacting asperities and surface roughness. These characteristics are connected directly to the force of adhesion. In summary, AFM offers a very flexible stand, adjustable to a number of experimental geometries (Roberts, 2005).

3.1.1 Modes of operation

In order to measure adhesion forces by AFM, two systems are used for such a purpose.

3.1.1.1 Contact mode AFM

In contact mode, the tip is dragged across the surface with a feedback loop to minimize the deflection of the cantilever away from its nominal position. The force of the interaction with the surface is controlled through controlling the deflection of the cantilever. Thus, this mode is also known as constant force mode. This mode is used when visualising materials that are not adversely affected by being in shear with a sharp tip (Abramovitch *et al.*, 2007).

3.1.1.2 Dynamic force mode AFM

This mode is used to determine the soft features. An oscillating cantilever is used to image surface features in dynamic force mode. There are two major kinds of dynamic mode:

1. In tapping mode (TM-AFM), using an electrical oscillator, the cantilever is purposely excited to amplitudes of up to nearly 100 nm so that the cantilever effectively bounces up and down as it moves over the sample. The oscillation amplitude is measured by rms (root mean square) value of the deflection detector signal. The feedback system is adjusted to sense the perturbation on the oscillation amplitude caused by remittent contact with the surface. In liquids, the tip of the cantilever taps the sample slightly during the part of the force curve; this mode is similar to the tapping mode operating in air, except that the sample is tapped against the tip instead of the cantilever being driven at resonance to tap the sample.

2. In non-contact tapping mode (NC-AFM), the oscillating cantilever does not touch the surface of the sample. The space between the tip and the sample is on the scale of tens to hundreds of Angströms, with oscillation amplitude only about 5 nm. In this mode, a sinusoidal excitation of the cantilever with a frequency close to its main resonant frequency is used. In some applications, in order to motivate the vibration of the probe, it is convenient to externally modulate the long-range attractive forces, that cover changes in the amplitude, frequency, and phase of the cantilever and keep a durable distance during scanning. These changes in amplitude or in state can be detected and used by the feedback loop to yield topographical data (Khulbe *et al.*, 2008). The next figure describes a schematic diagram of AFM with a colloid probe.
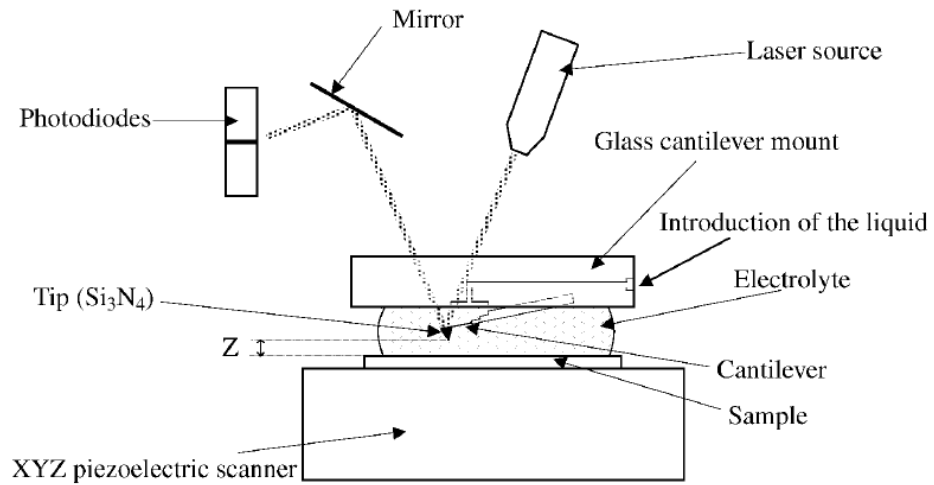
Figure 3.2 Schematic representation of the AFM operating principle. (Jacquot and

Takadoum, 2001)

A typical force-distance plot of an individual adhesion is presented in Figure 3.3, which shows the cantilever deflection as a function of z-piezo position. At first, the probe - sample distance is large with no probe-surface interaction. As the probe approaches the sample's surface (shown by the extension curve), this non-contact region is known as the "Zero-deflection" line or baseline. At close proximity (less than 5 ηm), the short-range van der Waals' forces produce an attraction, which causes a small descending deflection and contact between the probe and the sample. During sample contact, the AFM stage movement and cantilever deflection, become coupled. As a result, this causes an upward deflection of the cantilever and this linear region represents the zero separation distance and is known as the "hard wall" or constant compliance region.

The adhesion between the probe and the sample produces a hysteresis observed as a downward deflection past the initial contact point as the probe retracts from the sample's surface to its original non-contact position (shown by the retraction curve). The probe and sample separate and the cantilever returns to the baseline when the retraction force overcomes the adhesion force. The magnitude of the adhesion force is determined from the vertical cantilever deflection prior to detachment from the sample. Larger adhesion forces produced larger vertical cantilever deflections (Louey *et al.*, 2001).
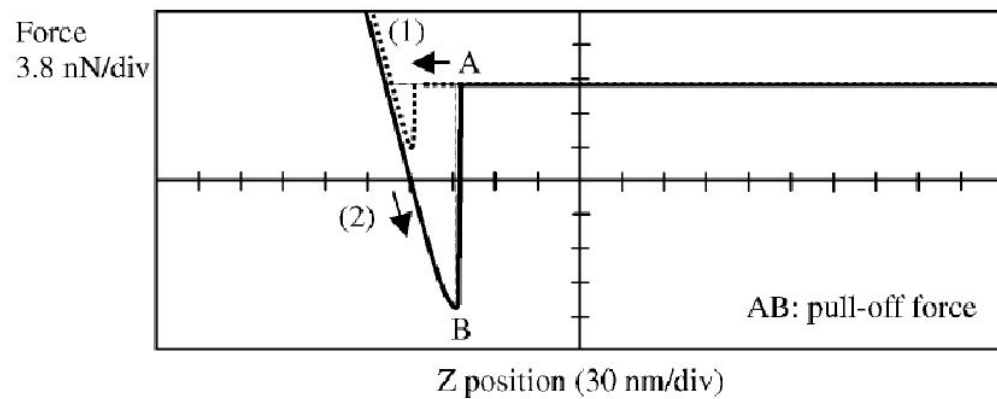
Figure 3.3 Experimental force versus displacement. Curve (1): Piezoelectric extension; curve (2): retraction (Jacquot and Takodoum, 2001)

In many fields such as printing, painting, lamination to other films, adhesive bonding, and other coating applications, contact of the adhesion properties of polymer surfaces is of great importance. The performance of the final product relies on the surface properties of the polymeric material. Extensively used commercial polypropylene (PP) films have predominantly hydrophobic surfaces, and their processing is nearly impossible without further surface modification like introduction of polar functional groups. Corona treatment is a widespread surface modification method used for plastics and particularly for polyolefins to produce

these groups (Gourianova *et al.*, 2005). PP is widely used in several areas, ranging from packaging to film capacitors. There have been examples of spherulitic structures on PP studied with scanning electron microscopy and transmission electron microscopy. AFM has been used to evaluate crystalline PP and nanometre-scale fibre formation on shear-deformed isotactic and hard elastic PP surfaces. The morphology of a biaxially-oriented PP (BOPP) film has been extinsively studied using AFM. The surface morphology of the BOPP film is represented by a fibre-like network structure (Figure 3.4).
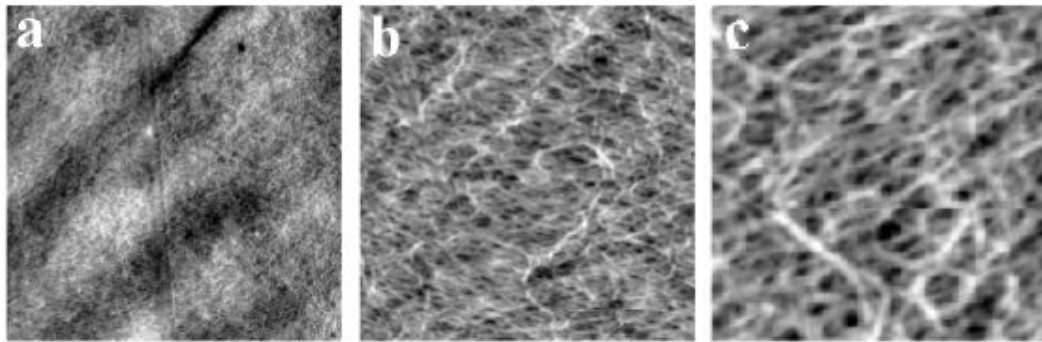
Figure 3.4 A typical AFM images of BOPP films in a scan area of

(a) 20 µm x 20 µm, (b) 4 µm x 4 µm and (c) 1 µm x 1 µm.

Chapter 4   Experimental

This chapter presents the analytical methods and sample preparations used in the study covering the flexographic ink preparation and comparing the adhesion of polymers Surkopak 5323 and Fumaric rosin (UCH150H) within each ink composition after applying the ink over bi-axially oriented polypropylene (BOPP) substrate (corona treated).

4.1   Materials

4.1.1 Solvents

The solvents (ethanol and isopropanol, analytical grade) used in the flexographic inks have low boiling points and are compatible with the polymers used: ethanol was used to adjust the viscosity of the flexographic inks.
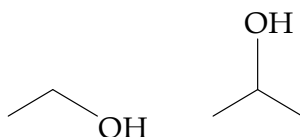
Figure 4.1 Chemical structures of ethanol and isopropanol

Ethyl acetate was also used as a solvent for nitrocellulose, and methoxypropanol was used in small amount as a retarder.

4.1.2 Polymers

4.1.2.1 Bi-axially oriented polypropylene film

The substrate used in this research is a BOPP film from Dubai Poly Film Co. LLC, it is white opaque milky, both side heat sealable, one side corona treated, with a thickness of 35 micron and treatment level is 40 dyne/cm. This polymer was used as a substrate for printing two kinds of ink with two different polymer structures, and the adhesion was tested to compare the adhesion difference of the inks used on BOPP.

4.1.2.2 Fumaric rosin

An alcohol soluble polymer (ACE, China), produced in light yellow flakes or irregular lumps, from the reaction of fumaric acid modified rosin through esterification with glycerol or pentaerythritol. The softening range is 125-155°C.

Acid value mg.KOH/g is 160-210.
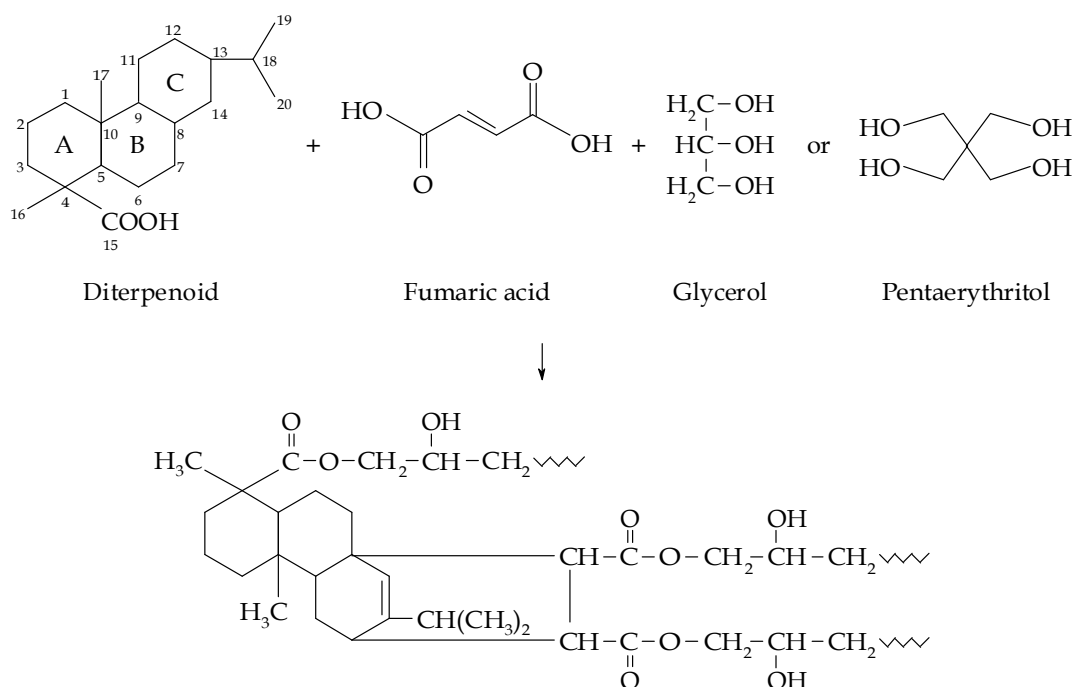
Figure 4.2 Fumaric rosin (UCH150H) from ACE China

4.1.2.3 Polyurethane

A plasticising polyurethane resin, Surkopak 5323 (BIP Oldbury Limited, UK), of weight average molecular weight 5000-7000 g/mol. and designed for nitrocellulose based inks and coating systems, was used. The polyurethane is based on ethyl acetate/isopropanol (40%) and is a polymer of polypropylene glycol and diphenyl methane diisocyanate.
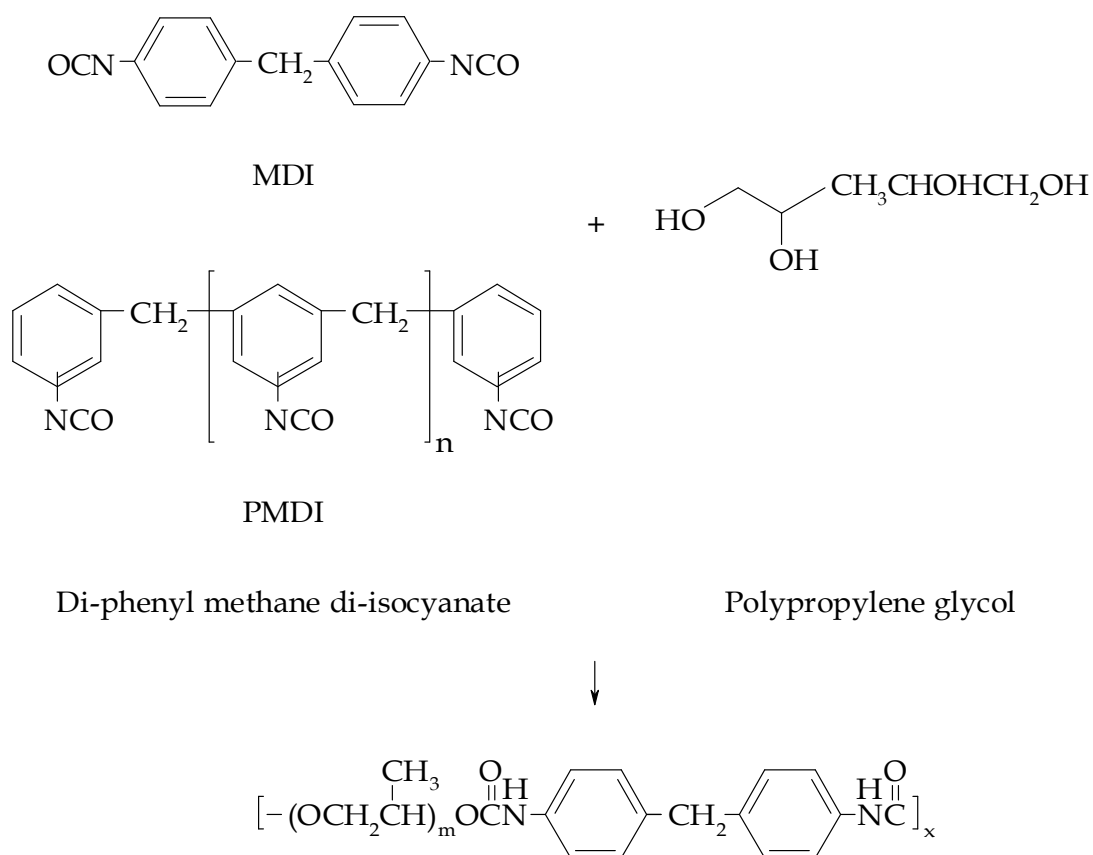
Figure 4.3 Chemical structure of Surkopak 5323

4.1.2.4 Nitrocellulose

Nitrocellulose (grade 18/25 and 1/2 from Nitro Quimica – Brazil) of viscosity 18-25 cP, nitrogen content 10.8-11.2 %, and ethanol moisturised 35%. Nitrocellulose (NC)

has versatile applications in flexographic inks and is a very commonly used resin in solvent-based flexographic inks, normally in combination with other polymers such as maleic, polyamide or acrylic resins. Nitrocellulose is a white fibrous material with favourable thermal stability at room temperature. At increased temperatures, it decomposes strongly with the development of brown nitrous oxide fumes – the ignition point is 180 ^{0}C (Leach and Pierce, 1999). Nitrocellulose, was accidentally discovered by Dr. Friedrich Schönbein, in Basiléia, in 1846, when making experiments using mixtures of sulfuric acid and nitric acid (Figure 4.4) in his own house. Nitrocelluloses are obtained by the nitration (Figure 4.4) using sulfuric-nitric mixtures of a great variety of different cellulose substrata, such as those originating from the cotton linen, of purified wood pulp – soluble cellulose. The nitration process, depending on the water content of sulfuric-nitric mixture, may lead to the formation of nitrocelluloses of different nitrogen contents: from 10.5% to 12.2%, which are used for the manufacture of paints and varnishes, and from 12.5% to 13.6%, which are used for manufacture of military and civil explosives, rocket propellants and gunpowder of single and double base.
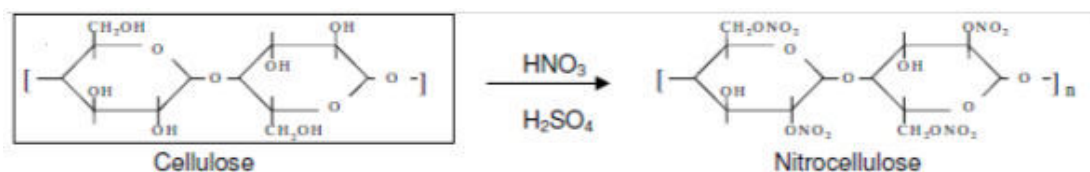
Figure 4.4 Eq. 1: Nitration reaction

After the nitration process, nitrocellulose is produced in very high molecular weight and is unsuitable for use in some applications, such as, for example, resin base for paints and varnishes, as it makes solutions with extremely high viscosity, when

dissolved in proper solvents. A process for the reduction of the molecular weight of nitrocellulose is used, hydrolyzing the glycoside bonds (Eq. 2) of the cellulose structure in a controlled way. In this fashion, a great range of products of different viscosities may be produced industrially, with low, medium, and high viscosities (Todd, 1994).
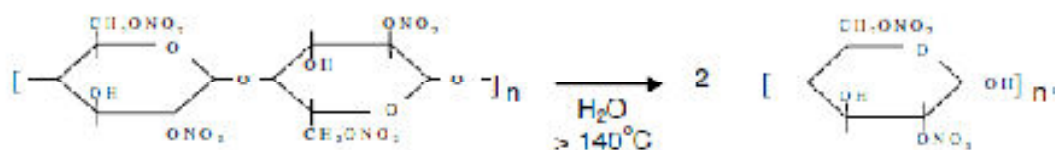
Figure 4.5 Eq. 2: Nitrocellulose Hydrolysis

For its use in paints and varnishes, the nitrocellulose must be dehydrated and moistened with some damping agent compatible with the system of solvents used in the subsequent formulation. Typical damping agents include ethyl, isopropyl or butyl alcohol, depending on the demands of the market and the availability and price of the inputs.

For the industrial fields of paints and varnishes, a great variety of nitrocellulose resins are produced, according to the applications, printing paints for packing (flexographic paints and for rotogravure), sealer varnishes and for wood finishings, automobile re-paintings and varnishes for leather, *etc.* Inks based on nitrocellulose have excellent scratch and rub resistance, besides, other desirable features including good solvent release, low odour, good pigment wetting, heat resistance and very wide compatibility. This compatibility allows the possibility of making inks for nearly all substrates in combination with other resins and plasticisers.

Nitrocellulose inks can thus vary widely, based on the particular modification. In these formulations, NC will normally improve pigment wetting, drying, heat resistance and film forming characteristics, while the modification alter positively gloss and adhesion, inks composed from pigmented nitrocellulose chips give further improvements in gloss which is important for film and foil printing (Thompson, 1998).

4.1.2.5 Ketonic resin

The ketone resin (SK resin from Evonik Industries) is 100% solid resin with a melting temperature of 110-120 ^{0}C, glass transition temperature, T_g ~ 90 ^{0}C, and OH number ~ 325 mg KOH/g.
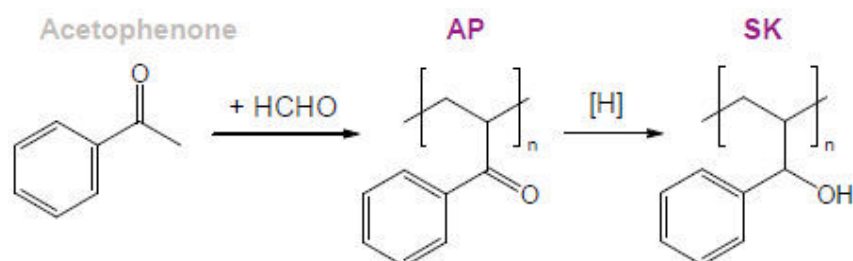
Figure 4.6 SK resin

The use of SK resin in flexographic inks improves hardness and gloss, offers excellent pigment wetting, and improves wetting of substrate and adhesion. The benefits of SK resin in pigment grind are the development of higher colour strength and gloss, higher colorant stability, and the possibility of a higher pigment load (meaning that less solvent is needed). This also renders the inks suitable for a variety of let-down binders (Evonik Industries, 2008).

4.1.3 Pigments

Pigment Yellow 13 and Pigment Red 57:1 (Hangzhou Riwa Import & Export Co., LTD, China) and Pigment blue 15:4 M4D7-X (Mallak pigments, India) were used in this work.

4.1.4 Adhesion promoter

TAA75 from Dupont was used to improve adhesion properties of NC-PU flexographic inks.

4.2 Methods and instruments

4.2.1 Flexographic ink preparation

Pigment concentrated paste preparation

The PS horizontal mill is used for the grinding and dispersion of pre-dispersed mixture of pigment and binder or other materials (www.profarb.com.pl/eng/machines.htm). The prepared concentrated ink is passed into the milling chamber of the grinding machine; this chamber is filled with milling media (Zirconium beads of 0.8 – 1.2 mm) which occupy a third of the volume of the grinding chamber. The grinding medium is a zirconia polycrystal ceramic with a high density (6.20 gm/cm^3), which is cost effective for speedy milling, which typically lasts around 160 times longer than glass, 8-9 times than ZTA, 6-8 times than zirconium silicate and 15 times than MgO stabilised zirconia milling beads (www.jyoticeramic.com/zirconox1.html).

The temperature is controlled to be no higher than 40°C by applying a cooling system during grinding, and the pressure is 1 bar. While the disks are rotating, the shear stress between beads grinds the substance to the required fineness, about 50-80 nm (Rentzhog, 2004).

The ink was milled for 8 hours during which time six ink samples were collected at various different milling times: 1 hour, 2 hours, 4 hours, 6 hours, 8 hours and 10 hours (until the optimum particle size for each pigment was reached, where although increasing the grinding time the particle size of pigment will not be changed).
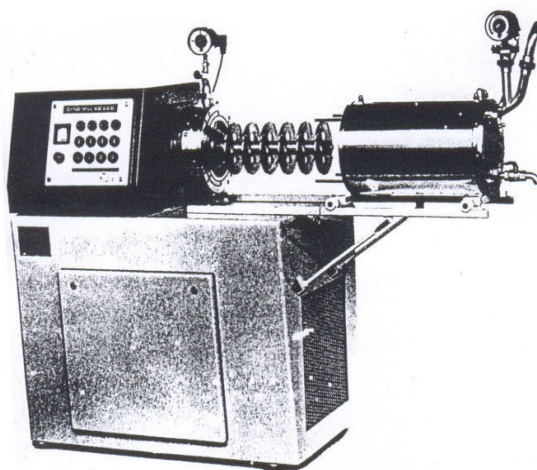
Figure 4.7 Dyno mill. (Grinding mill), Todd (1994)

4.2.1.1 Preparation of grinding media

The pigment concentrate mixture is prepared according to the mentioned steps in Section 1.4 and then grinding the pigment until an average particle size of about 500 nm to 800 nm is reached, thus, the grinding time of each colour is different from the other according to the quality of the pigment used. In this research, the grinding time for all colours was identical at 8 hours as explained in section 4.2.1.

The formulations of the suggested grinding base were selected to contain as few raw materials that are used in flexographic inks as possible. Following discussions with pigment suppliers such as Clariant, the initial ratio of pigment : binder was set as 1:0.5, the resin used for grinding the pigment was nitrocellulose (low nitrogen content, 35% ethanol) as the main component of solvent based flexographic inks to ensure proper wetting of the pigment.

SK resin was also used (at 5 %) according to the suggestion of Evonik Industries, to improve the wetting behavior, besides the other advantages such as improving adhesion and the possibility of achieving a higher pigment loading (as the viscosity is reduced by using this resin).

Table 4.1 Suggested % formulation for grinding media

	Formula A	Formula B	Formula C
Pigment	23	23	23
NC 18/25 (35% Ethanol)	11.5	17.5	22.5
Methoxy propanol	5	3.23	3.23
Ethanol	55.5	51.26	51.26
SK Resin	5	5	0

The grinding base according to Formula A shown in table 4.1 started to precipitate rapidly after a week so it was excluded from further tests. As the NC percentage was gradually increased the precipitation time was monitored until Formula B was reached, which resulted in no precipitation of the pigment. In the next step, SK resin

was excluded in order to minimize the number of components and for further studies in comparing the influence of Surkopak 5323 and Fumaric rosin (UCH150H) on the adhesion on BOPP substrate. Ethanol was used as the main solvent in the previous formulation as its rate of evaporation is lower than ethyl acetate, and it was found that grinding with ethyl acetate resulted in weak colour strength compared with ethanol, due to the comparatively high viscosity of the concentrated pigment base.

It should be noted that mentioned formulation in table 4.1 was made for CMY colours.

4.2.1.2 Preparation of extender

Table 4.2 Suggested % formulation for extender

	Varnish I	**Varnish II**	**Varnish III**	**Varnish IV**
Ethyl acetate	18.86	18.86	18.86	18.86
NC 18/25	8	8	8	8
UCH150H	11	5	0	0
Methoxy propanol	7.34	7.34	7.34	7.34
Ethanol	14.98	14.98	14.98	14.98
Isopropanol	39.82	39.82	39.82	39.62
Tyzor AA 75	0	0	0	0.2
Surkopak 5323	0	6	11	11

4.2.1.3 Preparation of the ink samples

The final ink is a mix of 60% of grinding media and 40% of Varnish and only Magenta colour is presented as the result of Cyan and Yellow were similar to Magenta.

Ink No. 01 consists of 60% Grinding media C + 40% Varnish I

Ink No. 02 consists of 60 % Grinding media C + 40 % Varnish II

Ink No. 03 consists of 60% Grinding media C + 40 % Varnish III

Ink No. 04 consists of 60% Grinding media C + 40% Varnish IV

4.2.2   Particles sizing and Zeta potential evaluation of concentrated pigment base B and C

4.2.2.1 Particle sizing testing

The particle size analysis and the determination of particle size distribution were determined using a Malvern Zetasizer-Nano Series, Nano-ZS (Malvern Instruments Ltd, Malvern, Worcestershire, UK). The DLS technique was used for PR 57:1, PB 15:4 and PY:13 in both formulations of concentrated base B and C. The samples were pre-mixed with ethyl acetate to aid dispersion and the dispersions were immersed in an ultrasonic bath for 15 minutes prior to measurement. A small amount of the sample was injected into a Zetasizer capillary curvette (DTS1060) for analysis (the Zetasizer averages the results from three scans of the sample). The attenuator was selected by the instrument and relates to the concentration of the sample being analysed. The dielectric constant and viscosity were set at 79 and 0.89 mPa s respectively (Malvern, 2005).

4.2.3   Tape test for adhesion

The principal method for measuring coatings adhesion is the peel test, which has and most importantly, after decades of use, people feel comfortable with it. Unfortunately, the often distinct functional requirements of coatings on plastic substrates dictate that the tape test as written may not be a suitable measure of practical adhesion performance (Koleske, 1995). Printing and peel tests were used according to the following procedure. The ink was applied to BOPP by using RK printing proofer from RK with flexo head, anilox 150 lines/inch.

Figure 4.8 RK printing proofer machine with Flexographic head

The printed inks have approximately the same composition according to the prepared inks in section 4.2.1.3, and the only difference is the polymer contained in each one. The inks were printed after diluting with 30% ethanol, and then printed on the BOPP substrate, while viscosity of each ink was adjusted on a 20 sec/Zhan cup No.2 at 25°C. After printing a flexible adhesive tape is applied to a coated substrate surface and then removed, the removal process has been described in terms of the "peel phenomenon".

4.2.4 Viscosity monitoring

Viscosity assessments were made using a Zahn Cup No.02, an efflux viscometer consisting of a small cup with a hole in the bottom and a handle, so that the cup can be dipped into the liquid to be measured. The flow is measured as the number of seconds it takes for a measured amount of ink to flow out of a Zahn cup. Zahn cups are graded by the size of the hole (Zahn cup No.02 from RK is suitable for making flow measurements on flexographic inks). In order to obtain accurate results, the same cup was used for all measurements and the cup was always cleaned after each use and was dry without dents. Sometimes the ink is too viscous, and in these cases an accurate amount of suitable solvent is added and mixed with the ink then the viscosity is measured by Zahn cup. In this way the flow properties of the inks are compared easily. The measurement were completed three times at 25°C for each ink and the average was calculated. A viscosity comparison of base B and base C for CMY colours was done, along with a viscosity comparison of the inks prepared in section 4.2.1.3.

4.2.5 Measurement of colour density of print

Colour density readings were carried out on prints that displayed the inks prepared in section 4.2.1.3. The print was done using RK-printing proofer/flexo head, and an anilox of 150 line/inch. The viscosity of the ink was controlled at 20 sec/Zahn cup No. 02 and the average of three readings was calculated for each system for CMY colours. As the reproducibility of the readings was excellent, further readings were not considered necessary. The measurements were done on the solid part of the print (step wedge 100%) by using Xrite portable Spectrophotometer-Model SP-62 with 0/45 optical geometry, circular illumination at 45°, measurement at 0° according to DIN 5033.

4.2.6   Thermal analysis studies

The thermal analysis was achieved for polyurethane (Surkopak 5323) and fumaric rosin (UCH150H) polymers to examine the physical performance of these polymers over a given temperature range.

4.2.6.1 Differential scanning calorimeter (DSC)

This method measures the difference in energy inputs between the sample and a reference. This difference is measured as a function of temperature or time over a set heating programme. DSC was performed on polyurethane Surkopak 5323 and fumaric rosin (UCH150H) polymers using the TA instrument DSC 2010 differential scanning calorimeter. The samples were weighed (2.0-2.5mg) and placed onto the aluminium plate. The vessel and sample were heated at a rate of 10°C min^{-1} in case of fumaric rosin (UCH150H) and for Surkopak 5323 liquid nitrogen was used on the cell to get the temperature down, under a nitrogen flow of 200 cm^3 min^{-1}, over a temperature range of 70-95 °C for UCH150H and -14 to -4°C for Surkopak 532.

The technique analyses exothermic relaxation processes and the endothermic relaxation process.

4.2.6.2 Thermogravimetric analysis studies (TGA)

TGA was conducted on a TA instruments TGA 2050 model, at a heating rate of 10°C min^{-1} over a temperature range of 0-500 C°, the gas flow rate for the balance chamber was 30 cm^3 min^{-1} and 150 cm^3 min^{-1} for the furnace. A plot of weight percentage against temperature was obtained, showing the weight loss of polyurethane and fumaric rosin as temperature was increased.

Figure 4.9 Photograph of the TGA instrument used

The technique was used to monitor the weight loss against temperature and to determine any significant changes in the slope of the plots. The data were used to compare any differences between the studied polymers samples fumaric rosin (UCH150H) and polyurethane (Surkopak 5323).

4.2.7   Microscopy studies

4.2.7.1 Optical Microscopy

Optical microscopy was performed to compare the adhesion of PU inks against fumaric rosin inks. The analysis was carried out after applying the tape test on the BOPP film printed with flexographic inks prepared according to the formulations mentioned in section 4.2.1.3. All the samples were printed by using RK printing Proofer from RK-Print UK, flexographic head, the screen is 150 line/inch.

4.2.7.2 Scanning electron microscopy (SEM) studies

SEM was utilized to visually assess destruction and physical changes to the surface of BOPP after printing the extender of two different polymers (polyurethane and fumaric rosin) and applying the adhesive tape. The surface images produced using a scanning electron microscope (SEM) at magnifications ranging from 10x to 200,000x. SEM is typically used at high magnifications (above 10,000x), but the great advantage of the technique is not solely its resolving power but the enormous depth of field, which is available when viewing a specimen (Goodhew, 1975). This makes it possible to image the rough surfaces, accordingly. The collection of data from secondary electrons (SE), backscatter electrons (BE), and characteristic X-rays enables a dot-mapping process on a cathode ray tube (CRT) to produce the image of a sample in the SEM. The signal from each spot is gathered after scanning the sample by the stream of electrons and the signal displayed on the CRT is a magnified image of the scanned area (Koleske, 1995).

The samples were prepared according to the following procedure. Two extenders containing the selected polymer (10%) and isopropanol (90%) were prepared, the first containing the polyurethane Surkopak 5323 and the second one fumaric rosin (UCH150H). Each extender was applied on BOPP (treated side) by using yellow bar, as a 6μm wet film deposit. Following exposure to air to effect drying, a 'Scotch' transparent tape was applied and peeled off, then the surfaces of the samples were analysed by SEM to assess the adhesion of each polymer on BOPP surface and surface appearance.

Using a specialist adhesive tape, Specimens of each sample were mounted on SEM stubs. The samples were gold coated to a thickness of around 300 Å using a Bio-Rad

conductive. A Jeol JSM-820 scanning electron microscope with integrated EDX capabilities was used to obtain images of the samples.

Figure 4.10 Bio-Rad Diode Sputter Coating unit

Figure 4.11 Jeol JSM-820 Scanning Electron Microscope with image analyser

Four sets of samples were subjected to SEM analysis: the first set comprises the printed BOPP samples coated with fumaric rosin (UCH150H) extender one time and

Surkopak 5323 extender on the next time (polymer extender is 10% polymer + 90% Isopropanol); the second set comprises the printed BOPP samples according to the prepared inks in section 4.2.1.3; the third set comprises the printed BOPP samples according to the scale of UCH150H shown in table 4.3.

Table 4.3 Printed BOPP samples in different scale of UCH150H

Paste C	66.66	66.66	66.66	66.66	66.66	66.66	66.66	66.66	66.66
UCH150H	0	0.4	0.83	1.25	1.66	3.33	5	6.66	8.33
Isopropanol	0	0.85	1.67	2.5	3.33	6.66	10	13.32	16.66
Ethanol	33.33	32.09	30.84	29.59	28.35	23.35	18.34	13.36	8.35

The final set is the printed BOPP samples according to the scale of Surkopak 5323 shown in table 4.4.

Table 4.4 Printed BOPP samples in different scale of Surkopak 5323

Paste C	66.66	66.66	66.66	66.66	66.66	66.66	66.66	66.66	66.66
Surkopak 5323	0	0.4	0.83	1.25	1.66	3.33	5	6.66	8.33
Isopropanol	0	0.85	1.67	2.5	3.33	6.66	10	13.32	16.66
Ethanol	33.3	32.09	30.84	29.59	28.35	23.35	18.34	13.36	8.35

4.2.7.3 Fourier transform infrared (FTIR) spectroscopy

Infrared (IR) Spectroscopy is a general experimental technique and it is proportionally easy to obtain spectra from samples in all physical states (Stuart, 2004). IR Spectroscopy is particularly useful in the coatings laboratory as it allows investigation of materials in almost any physical form, liquid, cast film, ground powder, solvent solution, and even dried paint are subjected to this technique (Koleske, 1995).

4.2.7.3.1 Fourier-Transform Infrared Spectrometers

(FTIR) spectroscopy is based on the idea of the interference of radiation between two beams to give an interferogram.

The last one is a signal produced as a task of the change of pathlength between the two beams. The two fields of distance and frequency are interconvertible by the mathematical approach of Fourier – Transformation. The basic components of an FTIR spectrometer are shown schematically in Figure (4.12).
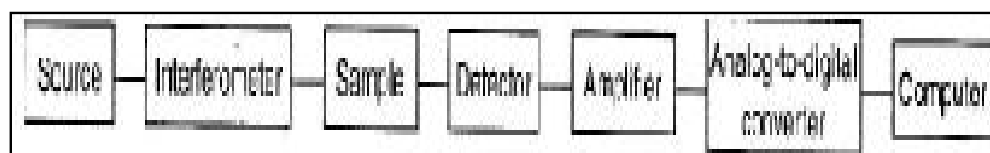
Figure 4.12 Basic components of an FTIR spectrometer

The radiation emerging from the source is passed through an interferometer to the sample before reaching a detector. After amplification of the signal, in which high-frequency contributions have been isolated by a filter, the data are transferred to

digital form by an analog-to-digital converter and converted to the computer for Fourier-transformation (Stuart, 2004).

The attenuated total reflection spectroscopy was depended on to study the nature and location of chemical changes which are generated by corona discharge treatment of polypropylene in different atmospheres (Carlsson and Wiles, 1970).

4.2.7.3.2 Transmission methods

Transmission spectroscopy is the oldest and most straighforward IR method and depends on the absorption of IR radiation at particular wavelengths as it is transmitted through a sample. It is possible to analyze samples in the liquid, solid or gaseous forms when using this mode (Stuart, 2004).

Reflectance methods

Reflectance techniques may be used for samples that are difficult to analyze by the classical transmittance mode. Reflectance methods can be divided into two types: internal reflectance measurements can be undertaken using an attenuated total reflectance cell attached to the sample. There is also a number of external reflectance measurements which involve an IR beam reflected directly from the sample's surface (Stuart, 2004).

4.2.7.3.3 Spectral analysis

The next step after an IR spectrum has been recorded is interpretation. Fortunately, spectrum interpretation is simplified by the fact that the bands that appear can

generally be attributed to particular parts of a molecule, giving what are known as group frequencies (Stuart, 2004).

Carbonyl stretching is one of the easiest absorptions to investigate in an infrared spectrum. It is normaly the most intense band in the spectrum, and depending on the type of C=O bond, occurs in the 1830–1650 cm^{-1} region.

N–H stretching is usually observed between 3400 and 3300 cm^{-1} (Stuart, 2004).

The main infrared bands of alkanes are summarized in Table 4.5.

Table 4.5 Characteristic infrared bands of aliphatic hydrocarbons (Stuart, 2004).

Wavenumber (cm^{-1})	Assignment
	Alkanes
2960	Methyl symmetric C–H stretching
2930	Methylene asymmetric C–H stretching
2870	Methyl asymmetric C–H stretching
2850	Methylene symmetric C–H stretching
1470	Methyl asymmetrical C–H bending
1465	Methylene scissoring
1380	Methyl symmetrical C–H bending
1305	Methylene wagging
1300	Methylene twisting
720	Methylene rocking
	Alkenes
3100 3000	=C–H stretching
1680 1600	C=C stretching
1400	=C–H in-plane bending
1000–600	–C H out of plane bending
	Alkynes
3300 3250	=C–H stretching
2260 2100	C=C stretching
700–660	–C H bending

The main IR bands of oxygenated compounds are summarized in Table 4.6.

Table 4.6 Characteristic infrared bands of oxygenated compounds (Stuart, 2004).

Wavenumber (cm^{-1})	Assignment
Alcohol and phenols	
3600	Alcohol O–H stretching
3550–3500	Phenol O–H stretching
1300–1000	C–O stretching
Ethers	
1100	C–O–C stretching
Aldehydes and ketones	
2900–2700	Aldehyde C–H stretching
1740–1720	Aliphatic aldehyde C=O stretching
1730–1700	Aliphatic ketone C=O stretching
1720–1680	Aromatic aldehyde C=O stretching
1700–1680	Aromatic ketone C–O stretching
Esters	
1750–1730	Aliphatic C–O stretching
1730–1705	Aromatic C–O stretching
1310–1250	Aromatic C–O stretching
1300–1100	Aliphatic C–O stretching
Carboxylic acids	
3300–2500	O–H stretching
1700	C=O stretching
1430	C–O–H in-plane bending
1240	C–O stretching
930	C–O–H out-of-plane bending
Anhydrides	
1840–1800	C=O stretching
1780–1740	C–O stretching
1300–1100	C–O stretching

Table 4.7 Characteristic infrared bands of amines

Wavenumber (cm^{-1})	Assignment
3335	N–H stretching (doublet for primary amines; singlet for secondary amines)
2780	N–CH_2 stretching
1615	NH_2 scissoring, N–H bending
1360–1250	Aromatic C–N stretching
1220–1020	Aliphatic C–N stretching
850–750	NH_2 wagging and twisting
715	N–H wagging

IR spectroscopy was carried out on samples of BOPP, BOPP printed with the fumaric rosin (UCH150H) extender (10% Fumaric rosin (UCH150H) + 90% isopropanol), and BOPP printed with Surkopak 5323 (10% Surkopak + 90% isopropanol). All samples were printed by yellow bar, 6 μm wet film deposit. Besides the FTIR of fumaric rosin and Surkopak 5323. An examination was carried out to evaluate the chemical structure of the surface by using a Perkin Elmer Spectrum one FT-IR spectrometer in Leeds University, Colour Chemistry Department, defining the changes of BOPP surface after printing with different polymers. Samples were located on the diamond of the golden gate ATR (attenuated total reflectance) apparatus, in case of printed BOPP samples, the samples were held in place during analysis.

4.2.7.4 Atomic force microscopy (AFM)

Atomic force microscopy (AFM) is a convenient and dependable way for studying adhesion phenomena. AFM combines excellent lateral resolution and immediate

measurement of interaction between AFM probe and sample (Gourianova *et al.*, 2005). The principle of AFM is based on the measurement of atomic forces between a very sharp tip and the sample surface. This technique can be used for two purposes: to obtain topographical information with a resolution approaching the diameter of single atoms, and to get physical information such as difference in elastic modules and chemical forces across a surface at the molecular scale.

The AFM equipment used was a Veeco Multimode AFM (Institute of Practical Science and Engineering, University of Leeds) with a Nanoscope IV controller. The probe used to collect the images was a stiff tapping probe of the TESPA (negatively charged) variety from Veeco, with a spring stiffness of about 40 N/m. The radius of curvature of the tip of the probe was about 10 nm.
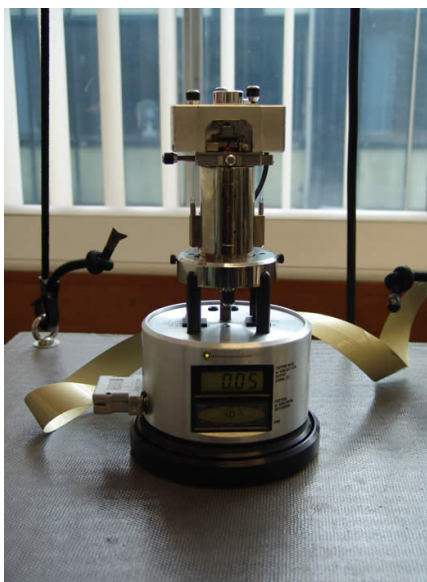
Figure 4.13 Veeco Multimode AFM

The samples examined by AFM were a BOPP sample without coating on the treated side, BOPP printed with Surkopak extender (10 % Surkopak + 90% isopropanol) and

BOPP printed with fumaric rosin (UCH150H) extender (10% fumaric rosin (UCH150H) + 90% isopropanol). All BOPP samples were printed by using Yellow bar, 6 μm wet film deposit. The force - distance plot for each sample was presented besides the surface morphology of studied samples and by studying the force *versus* displacement curves, the pull off force between the tip and the sample surface in air was measured.

4.2.7.5 Nuclear magnetic resonance (NMR) spectroscopy

Over the last three decades, NMR spectroscopy has become one of the most widely used and helpful methods for polymer characterization (Bovely and Mirau, 1996). In its simplest mode, nuclear magnetic resonance (NMR) is the study of the characteristics of molecules containing magnetic nuclei through the application of a magnetic field and monitoring the frequency at which they come into resonance with a radiofrequency electromagnetic field. When implemented to proton spins, the technique is sometimes called proton magnetic resonance (^{1}H-NMR). In the early days of this technique the only nuclei that could be investigated were protons (which act like relatively strong magnets), but now a many kinds of nuclei (especially ^{13}C and ^{31}P) are studied routinely.

The Chemical shift of a nucleus is the variation between its resonance frequency and that of a reference standard (Atkins, 1996) and some typical chemical shifts are given in Figure 4.14.
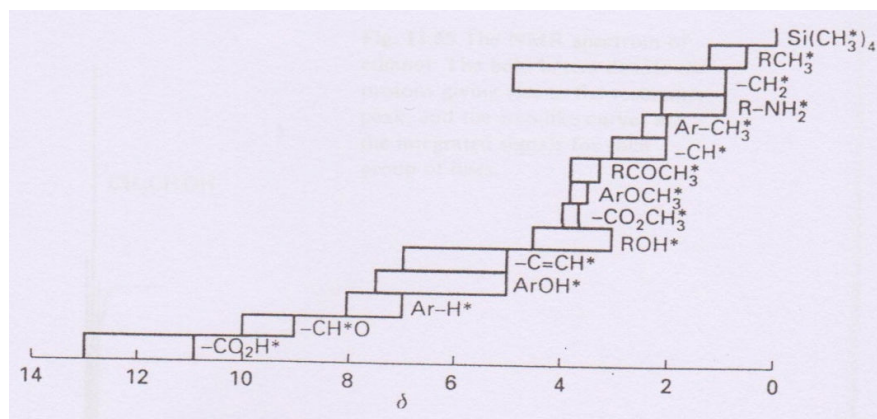
Figure 4.14 Typical chemical shifts in NMR (Atkins, 1996)

4.2.7.6   Electron spectroscopy for chemical analysis (ESCA)

Fundamentals of Electron Spectroscopy

In recent years, many developed surface-active analytical techniques have been involved in analysis permitting complicated identification of polymer surfaces such as ESCA (Toit and Sanderson, 1999).

In an ESCA experiment, the sample placed under high vacuum (8-10 Torr) is irradiated by a source of low-energy x rays, generally Al Kα(1486.6 eV) or Mg Kα (1253.6 eV), and the kinetic energy of the ejected electrons is measured under conditions of high resolution and precision. A photoelectron spectrum is a plot of the number of electrons detected versus their kinetic energy. The kinetic energy of a photoelectron depends on the energy of exciting radiation and the energy with which the electron is bound to its nucleus. The core electrons are those that are generally monitored in an ESCA measurement. Even though they are not directly involved in chemical bonding, their energies are influenced by the chemistry involved in bond formation. The binding energy of the electrons is calculated from

the energy of the exciting X radiation and the kinetic energy of the electrons, which escape from the sample without significant energy loss, using Einstein's photoelectric equation:
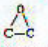
$$E(\text{binding}) = E(\text{X- ray}) - E(\text{Kinetic energy})$$

Although the x-ray photons penetrate deeply into the sample, the electrons that escape without energy loss come from the outermost surface layers since low-energy electrons have very short mean free paths in solids. It is estimated that these electrons escape depths range from about 1nm in metals to about 10 nm in organic polymers. Thus, the electrons detected in an ESCA experiment are representative of a very small amount of material, material which is present on the surface of the sample. Extreme care must therefore be taken in applying ESCA results to bulk properties of materials (Carlson, 1978).

There are several properties of ESCA which make it important for chemical

analysis. First, it is sensitive to approximately all elements in the periodic table. Second, chemical shifts offer some information of the nature of a species available. Third, ESCA is able of testing surfaces and surface reactions, and fourth, it has high absolute sensitivity (Hercules and David, 1974). Many investigations on the surface structures of block copolymers have been done using ESCA (Mochizuki *et al.*, 2000) and the work of Clark and co-workers has shown that ESCA is essential in the explanation of structure and bonding in polymer surfaces. This technique has been carried out successfully to a number of systems which cover plasma modification, polymer photooxidation, and plasma polymerization (Munro and Till, 1984). It has become clear that ESCA has the unique capability of offering accurate quantitative

depth profiling in the outermost ~50 Å of a number of polymeric materials (Clark and Peeling, 1976).

APPENDIX 3.1 O 1s BINDING ENERGIES (eV) IN CHO POLYMERS RELATIVE TO SATURATED HYDROCARBON (C 1s = 285.00 eV)

Functional group		Binding energy			Number of examples	Functional group		Binding energy			Number of examples
		Min.	Max.	Mean				Min.	Max.	Mean	
C—O—C (aliphatic)		532.47	532.83	532.64	8	Aromatic		531.62	531.70	531.65	3
(aromatic)		532.98	533.45	533.25	3	O²—C—Ar		533.06	533.22	533.14	
C—OH (aliphatic)		532.74	533.09	532.89	4	O¹					
(aromatic)				533.64	1						
C—C				533.13	1	—C—O²—C—		532.52	532.81	532.64	3
O—C—O		532.94	533.51	533.15	5	O¹ O¹		533.86	534.02	533.91	
O—C—O		532.95	533.07	532.99	2						
O						O²—C—O²		532.33	532.44	532.38	2
C=O (aliphatic)		532.30	532.37	532.33	3	O¹		533.88	533.97	533.93	
(aromatic)				531.25	1						
Aliphatic	1	531.96	532.43	532.21	20						
O¹—C—C	2	533.24	533.86	533.59							
O²											

ᵃ One or both carbon atoms in phenyl ring (PMS, PDMPO, PEEK).
ᵇ Carbon atom in phenyl ring (PHB).
ᶜ Carbonyl group bonded to phenyl ring (PEEK).

For PEEK and PET BE are referenced to aromatic CH C 1s = 284.70 eV.

Figure 4.15   O 1s Binding energies (eV) in CHO Polymers (Clark and Peeling, 1976).

APPENDIX 4 N 1s BINDING ENERGIES (eV) RELATIVE TO SATURATED HYDROCARBON (C 1s = 285.00 eV)

Polymer	Functional group	N 1s BE (eV)	Polymer	Functional group	N 1s BE (eV)
PPP[a]	P=N—P	397.93	N12	—C—N ‖ O	399.84
PEI	C—N	399.07			
PEOx	C—N	399.87	PU	O—C—N ‖ O	400.32
PA	C—N	399.92			
P9VC	C—N	400.22	PUa	N—C—N ‖ O	399.89
P2VP	Aromatic N	399.30			
P4VP	Aromatic N	399.34	KAP[a]	—C—N—C— ‖ ‖ O O	400.60
PAN[b]	C≡N	399.57			
PMAN	C≡N	399.57	ULTEM	—C—N—C— ‖ ‖ O O	400.40
PAM	—C—N ‖ O	399.83			
PMAM	—C—N ‖ O	399.96			
			PAAHC	—NH$_3^+$	401.46
PNVP	—C—N ‖ O	399.88	PVBTMAC	—N(CH$_3$)$_3^+$	402.14
			PNS	—NO$_2$	405.45
N66	—C—N ‖ O	399.81	CTN	—ONO$_2$	408.15
N6	—C—N ‖ O	399.77			

[a] Referenced to aromatic CH C 1s = 284.70 eV.
[b] Referenced to N 1s of PMAN.

Figure 4.16 N 1s Binding energies (eV) relative to saturated hydrocarbon (Clark and

Peeling, 1976).

Samples Preparation

The surface chemical composition of three samples were studied by ESCA:

1. the BOPP substrate alone

2. the BOPP substrate printed with PU extender (10 % PU + 90% isopropanol)

3. the BOPP substrate printed with fumaric rosin extender (10% fumaric rosin + 90% isopropanol).

The printing process was carried out using yellow bar, 6 μm wet film deposit.

The measurement information is given below:

Spectra were obtained using a Thermo Electron Corporation ESCA Lab 250 with the chamber pressure maintained below 1 x 10^{-9} mbar during data acquisition. A monochromated Al Kα x-ray source (15 kV 150 W) irradiated the samples, with a spot diameter of 500 μm. The spectrometer was operated in Large Area XL magnetic lens mode using pass energies of 150 eV and 20 eV for survey and detailed scans respectively. The spectra were obtained with a takeoff angle of 90°.

Using Avantage (Thermo VG software package) peak fitting algorithms, high resolution spectra were fitted. All spectra have been corrected for charge shifting by taking the standard C 1s binding energy to be 284.5 eV.

Figure 4.17 Thermo scientific ESCALab 250

4.2.8   Surface studies

4.2.8.1 Wetting

It is well known that the wetting phenomenon is part of our daily life as, *e.g.* rain drops on a window or ink on a paper. The wettability of a solid substrate by a liquid material is usually characterised by the contact angle of the liquid drop formed on the solid substrate. However, an accurate and unambiguous determination of the contact angle is not always straightforward, as it is influenced by many factors, especially when evaporation of the liquid drop is involved. In fact, as long as the atmosphere in the immediate vicinity of the drop is not saturated with the vapour of the liquid, liquid evaporation is not inevitable. Thus, a complete understanding of how evaporation influences the wetting behavior of the drop is very important in the research of fundamental aspects of wetting (Shi *et al.*, 2009).

The method used is the Pendant drop method by using a contact angle analyzer Phoenix 150/300. Drops of each liquid 5 μL in size were deposited on the film with a syringe. Measurement of the contact angle was carried out by observing the drops through a catherometer fitted with a protractor as shown in figure 4.18.

All experiments were performed at room temperature of 24°C, Every experiment was repeated at least three times (three runs) to confirm the reproducibility and no remarkable variation in the contact angle measurements was noticed; four liquids were used:

Solution of 50% ethanol + 50% fumaric rosin (UCH150H)

Solution of 50% ethanol + 50% Surkopak 5323

Ink No.01

Ink No.03
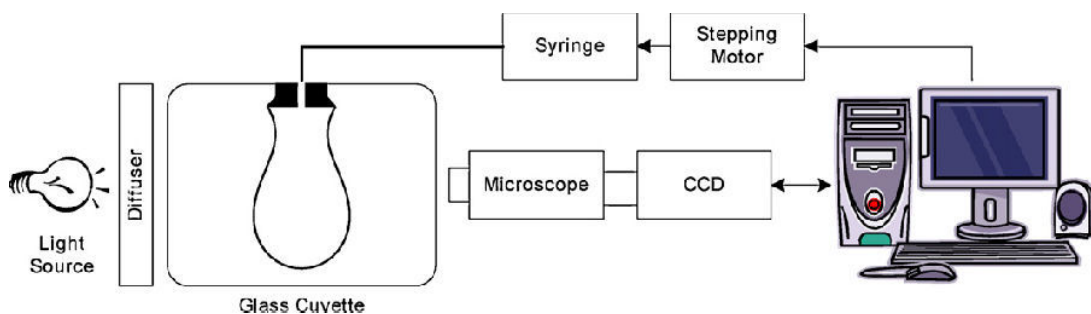
Figure 4.18 Schematic diagram of pendant drop method experimental setup

Furthermore, the surface tension of Surkopak 5323 solution and fumaric rosin (UCH150H) solution was measured by PG-X instrument (Colour Chemistry Department, Leeds University). A sufficiently big pendant droplet of about 8 μl is pumped out at the dispensing tip and the surface tension is determined from the droplet shape. This function is initially calibrated with a measurement of distilled pure water.

The polymer solution was 50% ethanol + 50% polymer.

Figure 4.19 PGX measuring head

4.2.8.2 Inverse gas chromatography (IGC)

4.2.8.2.1 Materials

The materials which are analysed for the study of interaction of polymer were polyurethane (Surkopak 5323), fumaric rosin (UCH150H), biaxially oriented polypropylene (BOPP), isopropanol and Chromosorb W/AW-DMCS. The nonpolar probes that were used were n-pentane (C_5), n-hexane (C_6), n-heptane (C_7) and n-octane (C_8). The polar probes which were used were acetone (Acet), tetrahydrofuran (THF), ethyl acetate (ETAC) and dichloromethane (DCM).

The analytical grade solvents that were used as probe molecules were obtained from Prolabo, with no further purification carried out on them before use.

Methane was used as a non interacting reference probe and the carrier gas utilised was helium (99.99% purity), Chromosorb W/AW-DMCS, an inert support supplied by Fluka, was used as the column stationary phase support for the polymer.

The support material is used to avoid undesirable pressure drop in the fumaric rosin (UCH150H), BOPP printed with Surkopak 5323 and BOPP printed with fumaric rosin (UCH150H) columns, and as a carrier polymer for polyurethane Surkopak 5323 polymer which is a thermoplastic polymer in liquid form.

Each experiment was repeated 3 times and method developed over 1 year until the values obtained were repeated.

4.2.8.2.2 Samples studied

- ✓ Polyurethane polymer Surkopak 5323

- ✓ Fumaric rosin (UCH150H)

- ✓ BOPP printed with polyurethane extender (10 % Surkopak 5323 + 90% isopropanol) by yellow bar, 6 μm wet film deposit.

- ✓ BOPP printed with fumaric rosin (UCH150H) extender (10% fumaric rosin (UCH150H) + 90% isopropanol) by yellow bar, 6 μm wet film deposit.

All the studied samples were supported with Chromosorb W/AW-DMCS (calcined, acid washed, treated with dimethyldichlorosilane) from Fluka prior to study.

The polymers under study (polyurethane Surkopak 5323 and fumaric rosin (UCH150H)) were diluted with isopropanol and then supported with Chromosorb (according to the soaking method) to achieve a better control of the amount of polymer on support and into the column, in this method the polymer is dissolved in isopropanol, the support (Chromosorb) was piled on a watch glass or a similar dish and a small amount of the solution was applied on the top of the support pile. Care was taken to wet the pile as much as possible without letting the solution touch the surface of the dish, either around or under the pile.

The solvent was allowed to evaporate and the pile was thoroughly mixed. Then a next portion of the solution was applied and the whole procedure was repeated until all the solution (including several rinsing of the solution flask) was used up. It took typically 10-20 applications and required only a few hours. No polymer was left on the surface of the dish. Then the support polymer was dried in the oven and quantitatively transferred into the column taking standard precautions of quantitative analytical chemistry. The method is fast, the amount of polymer is precisely known, and the analysis of the column material is avoided (Al-Saigh and Munk, 1984).

4.2.8.2.3 Apparatus and procedures

Measurements were made on a Shimadzu GC-9A equipped with a flame ionization detector (FID) system. Dried helium was used as a carrier gas and the flow rate was controlled using a needle valve pressure regulator and determined using a bubble flow meter that was equipped with a helium trap and thermometer.

The probe was injected manually using a 1.0 μl Hamilton syringe. The syringe was filled with 0.1 μl of probe. The injector was heated to 423 K and the FID detector to 453 K. The inlet pressure, P_{in}, was measured using a pressure gauge and the atmospheric pressure, P_0, was obtained through the internet;

(http://www.esyria.sy/eweather/todayforecast.php?city=01)

Figure 4.20 Shimadzu GC-9A

The columns were cut from copper tubing and shaped in a smooth spiral shape to fit the detector/injector geometry of the instrument. The dimensions of the columns were (52 cm), with outer and inner diameters of 8 mm and 5 mm respectively.

The columns were cleaned with a hot water-detergent solution followed by acetone and drying in a vacuum oven at 423 K for 6 hours.

Prior to packing, the columns were weighed. The stationary phase was introduced via a funnel; the column was then tapped gently for several minutes to allow the support to achieve even packing, following each addition of the stationary phase.

This procedure was continued until the column was filled to within ≈ 6 mm of the ends. The stationary phase was then retained in the column by the introduction of small plugs of silanised wool. The column was then re-weighed and the mass of support contained in the column was obtained by difference.

For IGC characterisation of studied surfaces, and bearing in mind the T_g of each material studied, the temperature range used was as follows in 10 K increments.

40-70°C for the Surkopak 5323

40-80°C for the fumaric rosin (UCH150H)

100-115°C for BOPP printed with Surkopak 5323 extender

40-70°C for BOPP printed with fumaric rosin (UCH150H) extender

Bearing in mind the T_g of the Surkopak 5323 is -11.98°C, the T_g of the fumaric rosin is 87.07°C and the T_g of BOPP is -11°C. Thus, the temperature range considered in this study was not below the T_g of the studied systems as explained in section 2.1.1. This

consideration is related to the physical nature of studied polymers at room temperature, in the solid state for fumaric rosin and liquid state for Surkopak 5323.

The applied flow rates were 50 ml/min for Surkopak 5323, and 20 ml / min for fumaric rosin (UCH150H), BOPP printed with Surkopak 5323 extender and BOPP printed with fumaric rosin (UCH150H) extender.

Prior to measurement, each column was conditioned for 2 hours at a temperature that was identical to the highest temperature of the IGC studies, under a helium flow rate of ≈ 20 ml/min. This was to ensure the removal of any residual volatiles, which could otherwise have affected the retention of the probes on the material being studied.

IGC data processing was carried out according to customary methods, well described in the literature (Section 2.1), the retention time of probe molecules was determined using the geometric technique outlined by Condor and Young. Background theory and experimental details have been provided in Sections 2.1.1, 2.1.2, 2.1.3, 2.1.4 and 2.1.5 respectively.

Chapter 5   Results and discussion

This chapter provides details of results and discussion relevant to the experimental studies carried out as detailed in Chapters 2-4.

5.1   Concentrated pigment paste preparation

A significant number of trials to prepare the ink were carried out according to the aforementioned formulations in Section 1.2. The preparation process was divided into two steps: the first step was the preparation of the concentrated pigment paste and the second the preparation of the extender. This method had several benefits.

1. This method saved time (the grinding process was time consuming) allowing preparation of the desired quantity of the concentrated pigment paste, which could then be mixed with different types of extender.

2. By carrying out such experimental trials, it was found that minimising the quantity of solvent during the grinding process gave better colour strength. This was achieved by yielding more efficient grinding and finer particle size as friction generated between the pigment particles became more significant when the viscosity was higher.

3. A high concentration of pigment was achieved, which facilitated the preparation of different concentrations of flexographic inks according to the desired pigment percentage. After a significant number of trials, it was possible to achieve a good colour strength according to Formula A shown in

Table 4.1, Section 4.2.1.1, but it was found that colour strength became weaker as a result of pigment settling. Consequently, it was not possible to use this formulation to obtain a pigment paste that was stable over a period of time of storage.

In the second step, the NC concentration was increased by 1% each time, until a percentage of 17.5% NC was reached according to formulation B shown in Table 4.1, Section 4.2.1.1. Then, the precipitation was monitored as a function of time. The intended aim of increasing NC percentage and avoiding the use of a dispersing agent was to minimise the number of flexographic ink formulation components, enabling the extension to further studies related to adhesion as discussed in Section 4.2.1.1.

Finally, the use of SK resin was suggested by Evonik industries, to achieve lower viscosity and higher pigment loading according to formulation C shown in Table 4.1, Section 4.2.1.1.

5.1.1 Evaluation of concentrated pigment pastes B and C

5.1.1.1 Viscosity comparison of concentrated pigment bases B and C

Viscosity testing of the obtained pigment concentrate was carried out according to formulations B and C for CMY colours by using Zahn Cup No. 02 after first diluting the concentrated pigment paste with ethanol to a ratio of 20:10 paste:ethanol as discussed in Section 4.2.4. According to the results obtained (see Table 5.1), it is apparent that no significant viscosity difference was obtained.

Table 5.1 Viscosity comparison of CMY concentrated pigment pastes derived from

formulation bases B and C

	Viscosity /sec	
Base	**Formula B**	**Formula C**
Cyan	32	32
Magenta	31	31
Yellow	38	40

5.1.1.2 Particle size testing of concentrated pigment bases B and C

The particle size and size distribution of CMY flexographic inks based on formulations B and C were measured according to the method discussed in Section 4.2.2.1. Table 5.2 and Figures 5.1 - 5.6 illustrate the average particle size and size distribution of pigments present in the various ink dispersion formulations.

Table 5.2 Average particle size (nm) of CMY concentrates according to formulations

B and C of concentrated pigment paste

	Average particle size /nm	
	Base B	**Base C**
Cyan	332.5	137.2
Magenta	1721	1642
Yellow	227.7	161.6
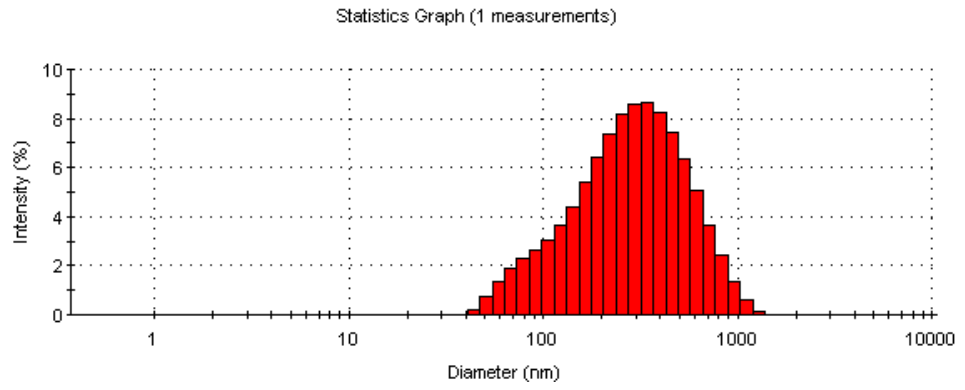
Figure 5.1 Particle size and size distribution of Cyan concentrate derived from
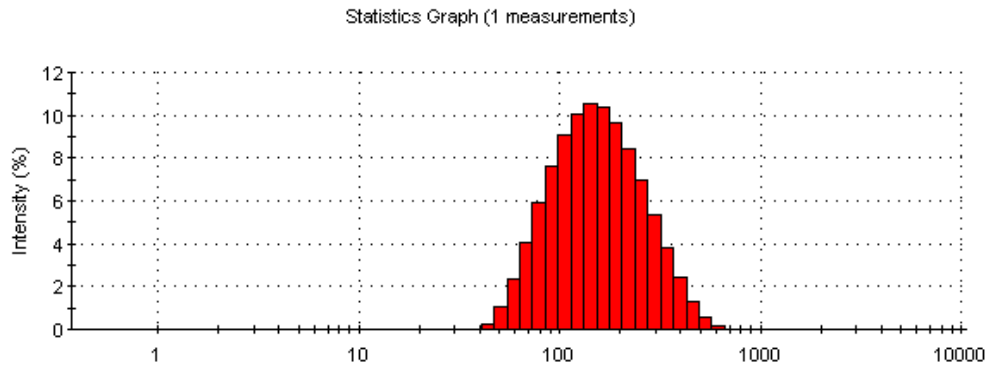
grinding base B

Figure 5.2 Particle size and size distribution of Cyan concentrate derived from
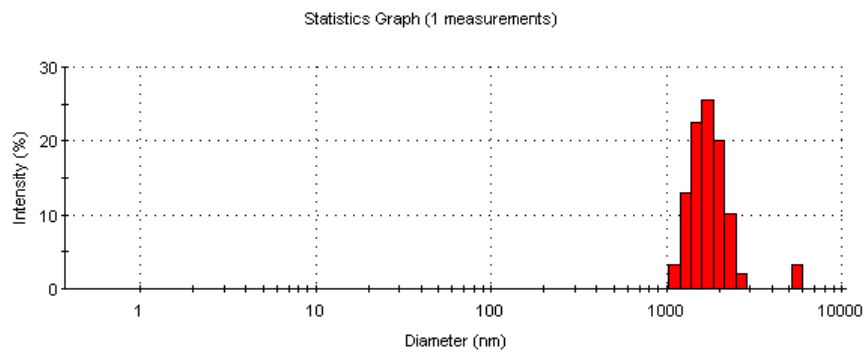
grinding base C

Figure 5.3 Particle size and size distribution of Magenta concentrate derived from
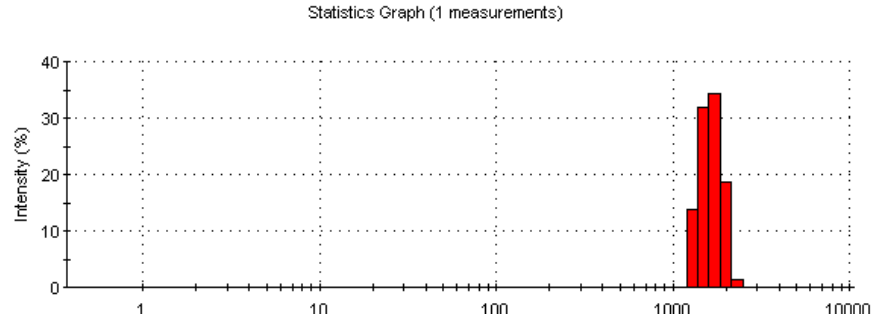
grinding base B

Figure 5.4 Particle size and size distribution of Magenta concentrate derived from
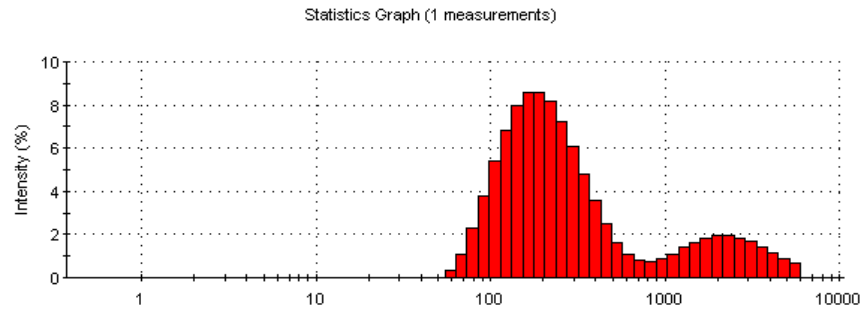
grinding base C

Figure 5.5 Particle size and size distribution of Yellow concentrate derived from
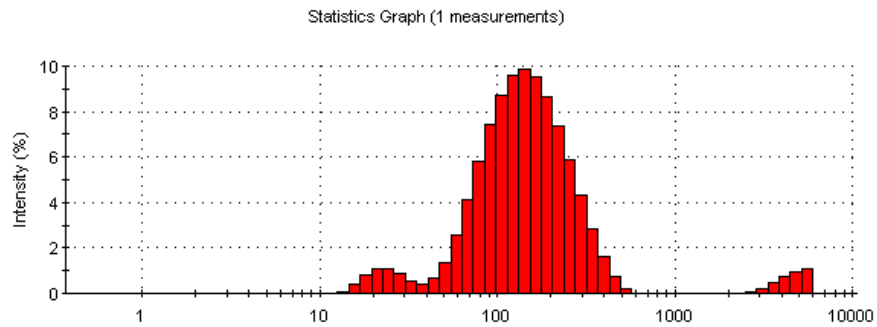
grinding base B

Figure 5.6 Particle size and size distribution of Yellow concentrate derived from

grinding base C

From the particle size measurement, it was found that the presence of the ketone resin in the grinding formulation of the base had no effect on the particle size of pigment achieved. Thus, Formulation C was considered in this study because the pigment particle size was not improved by using SK resin during grinding process and the preferred formulation contains the minimum number of ingredients.

5.2   Preparation of extender

According to Table 4.2 in Section 4.2.1.2, four formulations of the extender were suggested for use in preparing the final flexographic inks. In Section 1.2, the suggested formulation of white ink for the treatment of one side of coextruded polypropylene contains the polyurethane in combination with nitrocellulose (the reasons behind using polyurethane in flexographic inks were discussed in Section 1.3.3.2). Surkopak 5323 polymer was chosen from other polyurethane grades based on BIP advice. Adhesion promoters (discussed in Sections 1.3.4 and 1.3.3.2) are used in NC-PU flexographic inks to improve adhesion. Fumaric rosin is used in suggested extender formulation as a sole polymer and in combination with polyurethane, because it was found by trial that this resin offering better adhesion to the printed flexographic NC ink on BOPP substrate in comparison with NC-PU flexographic ink. Moreover, the solubility of fumaric rosin (UCH150H) in alcohol is another reason for choosing this resin in this study for the preparation of flexographic NC inks. Based on the above, four extender formulations were suggested: (a) using fumaric rosin (UCH150H) as a sole resin in combination with NC in the extender formulation (designated ink No. 01); (b) using fumaric rosin (UCH150H) in combination with Surkopak 5323 in NC extender formulation (ink No. 02); (c) using Surkopak 5323 as

sole polymer in combination with NC in the extender formulation (ink No. 03); (d) using adhesion promoter (TAA75) as an additive in NC-PU extender formulation (ink No. 04).

Depending on pigment concentrate C in this study, four ink formulations were obtained by mixing the concentrated pigment paste C with each of the suggested extender formulations. The suggested ratio of flexographic NC inks in this study was 60% concentrated pigment paste and 40% extender. The choice of 60% concentrated pigment paste ensured a ratio of about 13.8% pigment in the final ink from the suggestion in Section 1.1 that the pigment concentration is about 12%. By setting the ratio of NC% at 17% and the whole resin % as 23.6% these fall within the suggested range of resin in flexographic ink as mentioned in Section 1.1.

5.2.1 Tape test of prints for adhesion

The adhesion of inks No.01, No.02, No.03 and No.04 were tested based on the procedure mentioned in Section 4.2.3 and the visual results were as follows:
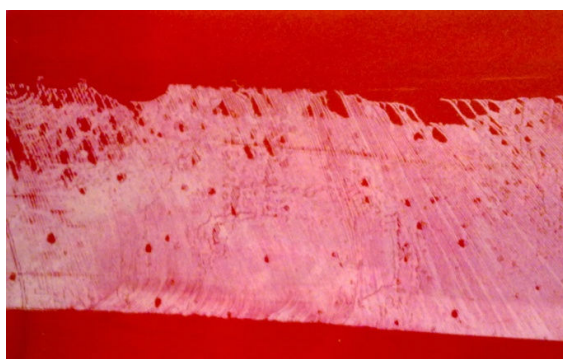
Figure 5.7 Tape test result of ink No.01
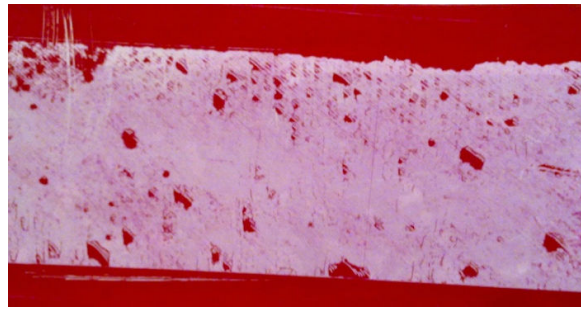
Figure 5.8 Tape test result of ink No.02
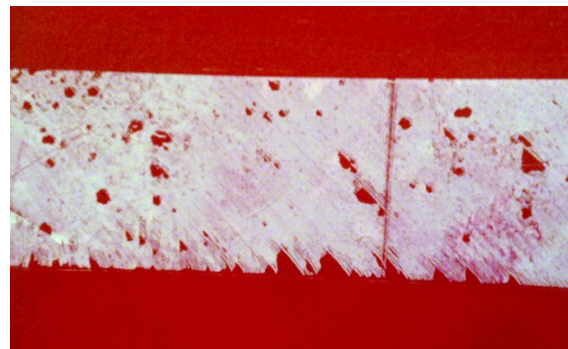
Figure 5.9 Tape test result of ink No.03
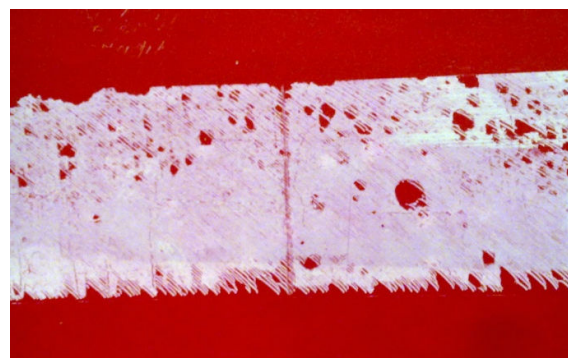
Figure 5.10 Tape test result of ink No.04

5.2.2   Measurement of the viscosity of the inks prepared

Table 5.3 Viscosity comparison of four prepared inks in section 4.2.1.3

Viscosity (sec), Zahn cup 2, 20:10 - ink:ethanol, 25°C				
	Ink No. 01	**Ink No. 02**	**Ink No. 03**	**Ink No. 04**
t = 0	21	21	20	22
t = 4 hours	27	24	20	22
t = 24 hours	37	28	21	23
t = 48 hours	37	27	20	22

As can be seen from the Table 5.3, the viscosity of inks containing the fumaric rosin (UCH150H) increased, but this increase is still acceptable for flexographic inks, whereas the viscosity of inks containing Surkopak 5323 remained almost constant.

5.2.3 Measurement of colour density of print

The results of measured density for the prepared inks (Magenta colour) are summarised in Table 5.4, relying on the procedure mentioned in Section 4.2.5.

The measurements were repeated 3 times and the results remained almost constant.

Table 5.4 Comparison of the colour density of prepared flexographic inks

Measurement on step Wedge 100% (Solid data)	Ink No.01	Ink No.02	Ink No.03	Ink No.04
Ink density after preparation	2.22	2.25	2.20	2.23
Ink density after 48 hours of preparation	2.33	2.36	2.37	2.30

From the tape test for adhesion, viscosity measurement and colour density measurement of the prepared inks, the following conclusions can be reached:

1. The viscosity of the inks prepared by using the fumaric rosin (UCH150H) are similar to those inks prepared using Surkopak 5323 up to 4 hours only.

2. The colour densities of all the prepared inks are almost identical.

3. The principal difference is that the adhesion of the inks 01 an 02 prepared using the fumaric rosin (UCH150H) are superior to the adhesion of the inks prepared using Surkopak 5323 only, 03 and 04.

4. When all components in the prepared inks are identical, then it can be concluded that the polymer used has the greatest effect on the adhesion of the ink to the substrate.

Based on the previous discussion, the focus was made on the properties of the fumaric rosin (UCH150H) and Surkopak 5323 in the next part of this study to evaluate the main reasons behind the better adhesion of fumaric rosin (UCH150H) against Surkopak 5323.

5.3 Thermal analysis studies

5.3.1 Differential scanning calorimetry (DSC)

Thermal analysis is a useful tool for characterisation of physical properties and the thermal behaviour of the polyurethane and fumaric rosin samples were characterised using DSC. Figures 5.11 and 5.12 depict the thermograms resulting from the analysis of samples heated from 0°C to 500°C, at a rate of 10 K min^{-1} with nitrogen purging through the system. The glass transition temperature was taken to

be the midpoint between the pre-transitional and post-transitional baselines and the glass transition temperature (T_g) of the fumaric rosin (UCH150H) is 87°C, and for Surkopak 5323 is -12°C. Both samples displayed a significant difference in T_g value, thus fumaric rosin (UCH150H) is a brittle polymer at room temperature and Surkopak 5323 is a thermoplastic one and appears in liquid form at room temperature.
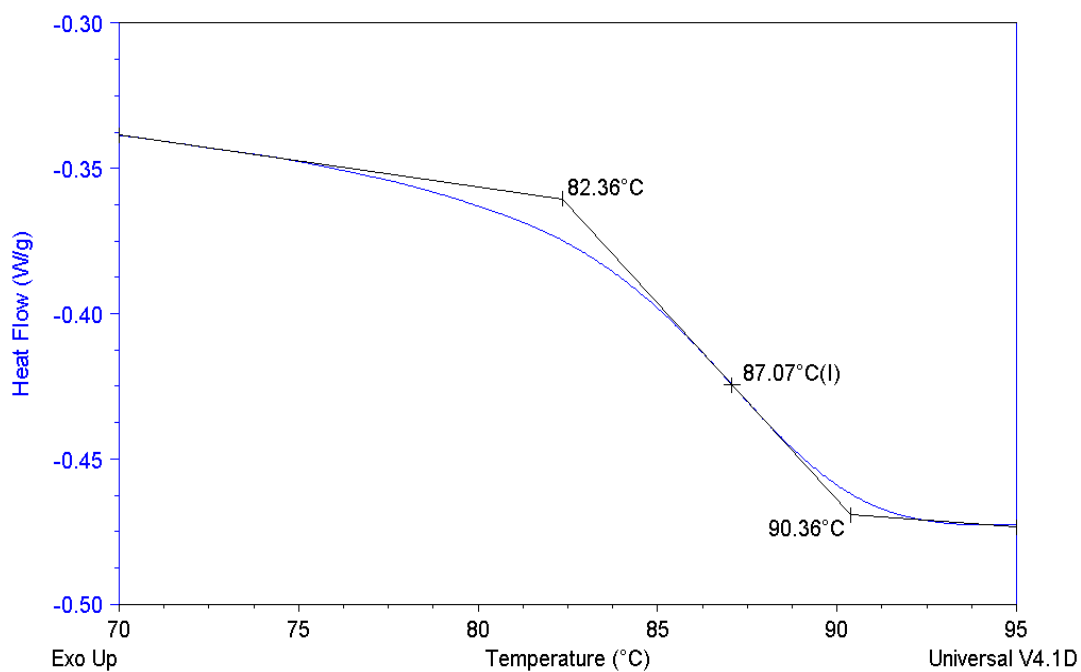
Figure 5.11 Glass transition temperature of the fumaric rosin (UCH150H)
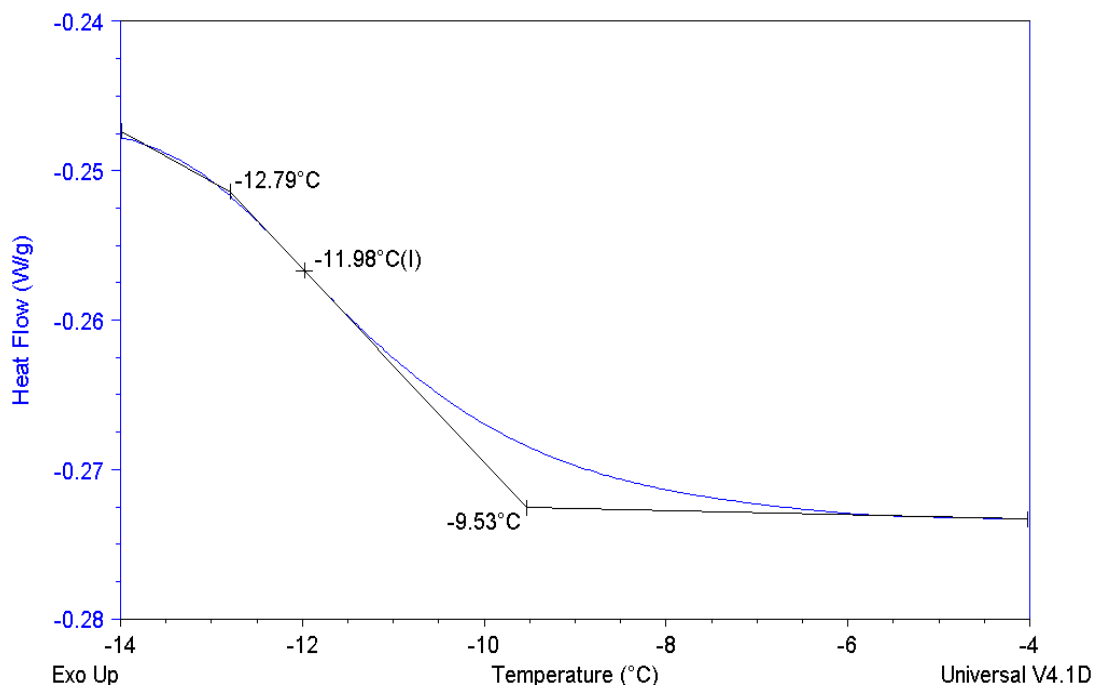
Figure 5.12 Glass transition temperature of the polyurethane Surkopak 5323

5.3.2 Thermogravimetric analysis (TGA)

Thermogravimetric analysis is a useful method to determine the thermal stability of polymers. TGA analysis was carried out on both the polyurethane and the fumaric rosin and the relevant results are discussed below.

A plot of weight percentage against temperature was obtained, showing the weight loss of the fumaric rosin (UCH150H) and Surkopak 5323 as the temperature was increased. It was determined from TGA, Figure 5.13, that the degradation temperature of the fumaric rosin (UCH150H) was around 200°C, also the decomposition occurs in a single step with a very large mass loss of approximately 99.5%, The sample was initially stable with a major weight loss occurring between 200-350°C.
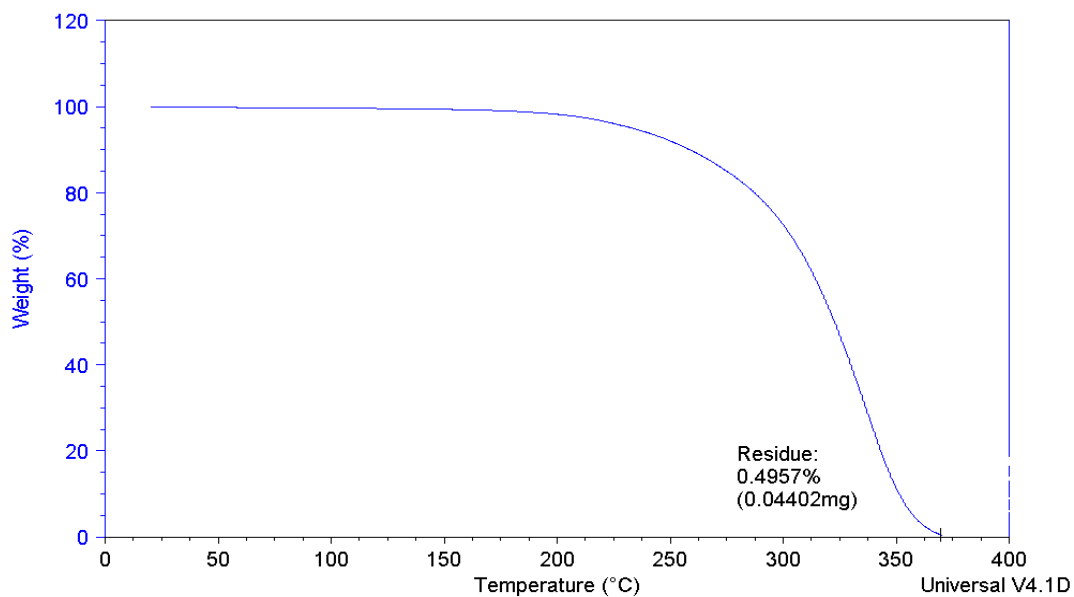
Figure 5.13 Thermogram for TGA analysis of fumaric rosin

Figure 5.14 shows that the initial weight loss occurs around 130°C which could be related to solvent volatilization from Surkopak sample, then it is stable until about 270°C and then starts to decompose. The mass loss at the end of the experimentation period (500°C) was approximately 93% and the residue of about 7% is carbon residue.
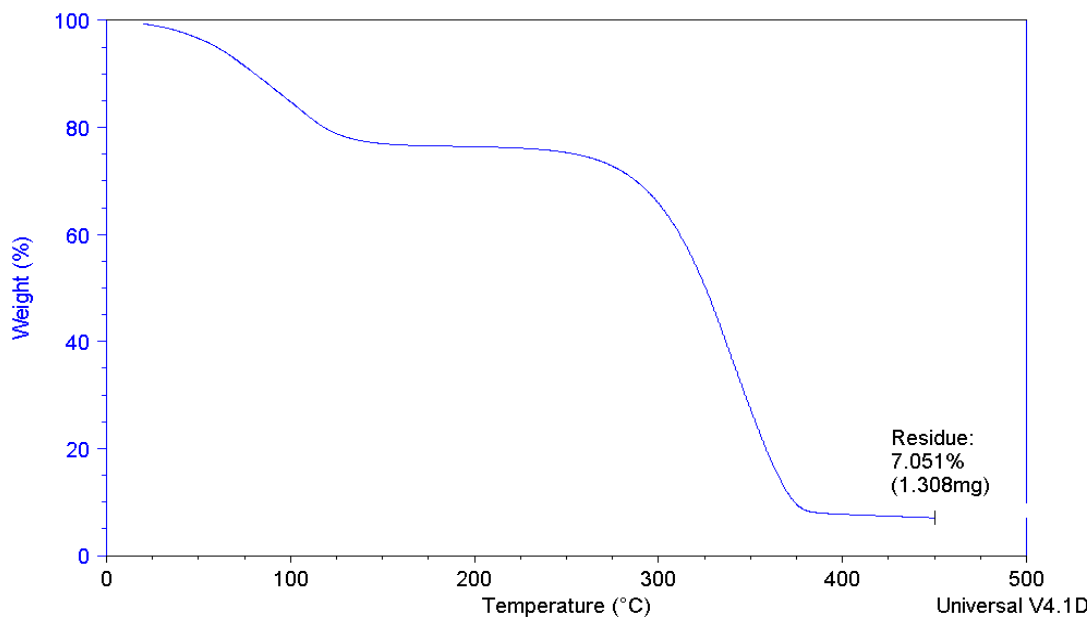
Figure 5.14. Thermogram for TGA analysis of the polyurethane

The interpretation of which was that there was a difference in the thermal behaviour of the two samples, but the starting decomposition temperature is higher in case of Surkopak 5323 than the fumaric rosin (UCH150H).

As the residue of decomposition in case of Surkopak 5323 is 7.051% while it is 0.4957% in case of the fumaric rosin (UCH150H), then a significant difference in the molecular weight is suggested.

5.4 Microstructure of the printed ink films

5.4.1 Optical microscopy

From Figures 5.15 to 5.18, it can be seen that the ink remaining on the substrate after applying the tape test was the best in the case of printing inks No. 01 and No. 02, which confirms that inks containing the fumaric rosin (UCH150H) exhibit better adhesion when printed on BOPP.
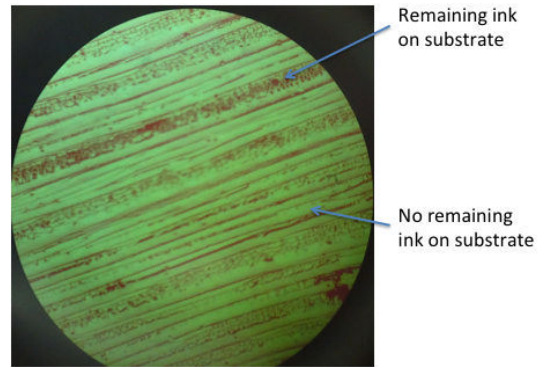
Figure 5.15 Optical micrograph of BOPP substrate printed with ink No. 01 after

applying the tape test at 100X magnification.
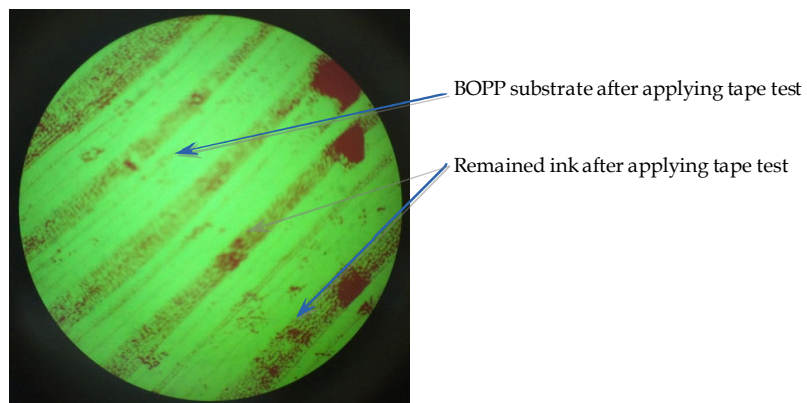
Figure 5.16 Optical micrograph of BOPP substrate printed with ink No.02 after

applying the tape test at 100X magnification.
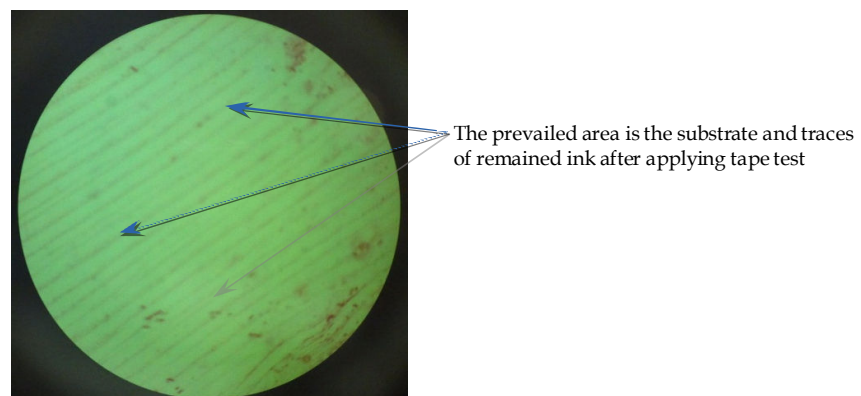
Figure 5.17 Optical micrograph of BOPP substrate printed with ink No.03 after

applying the tape test at 100X magnification.

Wide area of substrate after applying peel test

Wide area of remained ink after applying tape test
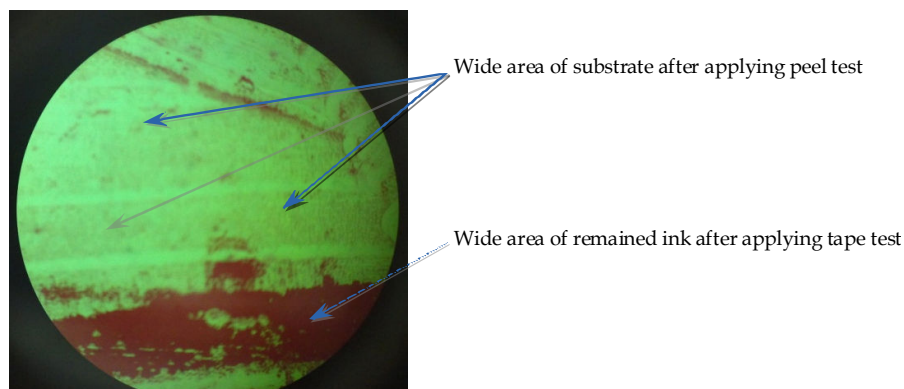
Figure 5.18 Optical micrograph of BOPP substrate printed with ink No.04 after applying the tape test at 100X magnification.

The optical magnification used for all figures 5.15 to 5.18 was applied at 100X magnification.

Moreover, adhesion test result of ink No.02 was better than ink No.04, which confirms that the fumaric rosin (UCH150H) could be used in combination with Surkopak 5323 for formulating flexographic NC inks instead of using adhesion promoter TAA75 with Surkopak 5323. In this way it is possible to reduce the negative effects of using the adhesion promoter in flexographic NC inks mentioned in section 1.3.4.

5.4.2   Scanning electron microscopy (SEM) and electron diffractive X-ray (EDX) studies

Based on Figures 5.19 and 5.20, it can be seen that the Surkopak 5323 extender shows a lack of interfacial adhesion after applying the tape test for adhesion compared to that of the fumaric rosin (UCH150H) extender.
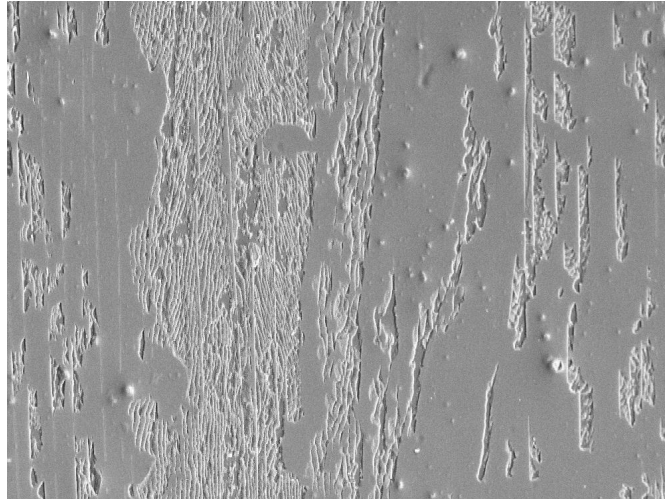
Figure 5.19 SEM image of BOPP printed with the fumaric rosin extender and a

peeling with transparent Scotch tape was applied at 500 X magnification
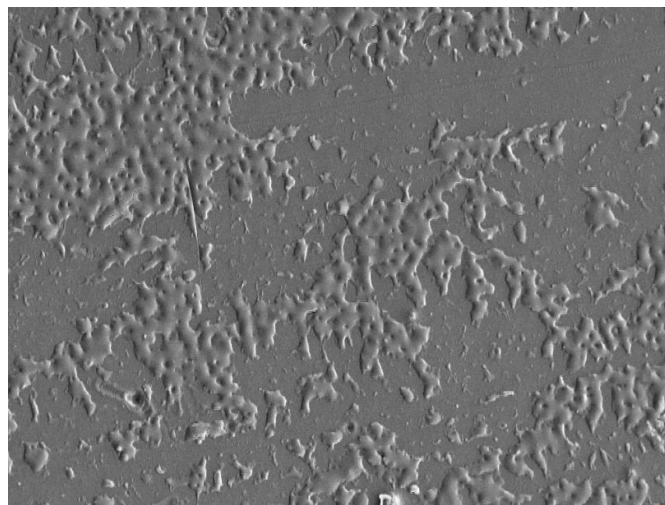
Figure 5.20 SEM image of BOPP printed with the polyurethane extender and a

peeling with transparent Scotch tape was applied at 500 X magnification

In Figure 5.20, it can be seen that the Surkopak extender appears as spheres on the

BOPP substrate which means the Surkopak has a good cohesion and bad adhesion to

the BOPP substrate, while the fumaric rosin (UCH150H) extender exhibits better

adhesion to the BOPP substrate, where the light colour areas in Figure 5.19

represents the fumaric rosin (UCH150H) that remains on the BOPP surface after applying the tape test. From Figure 5.19, the image shows the remaining fumaric UCH150H in white covering a wider area.
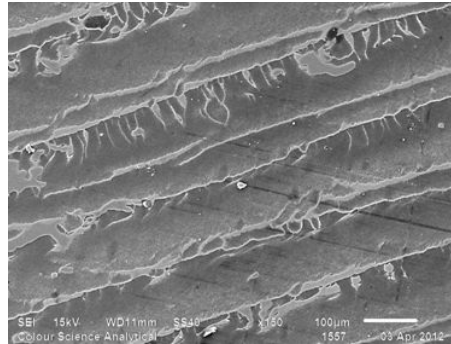
Figure 5.21 SEM of BOPP printed with ink No.01 after applying the tape test
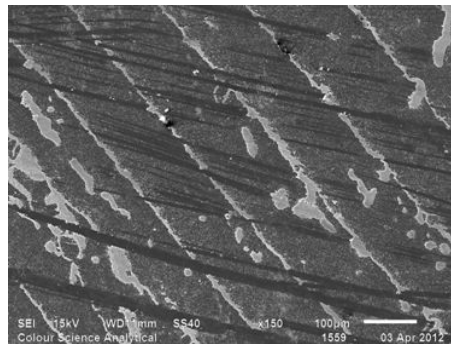
Figure 5.22 SEM of BOPP printed with ink No.02 after applying the tape test
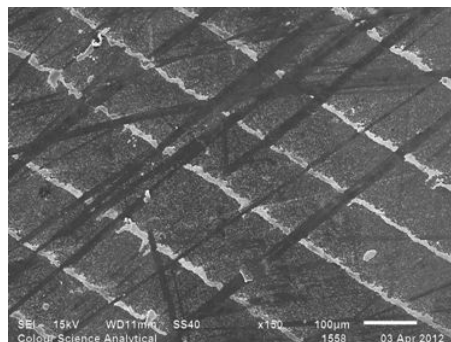
Figure 5.23 SEM of BOPP printed with ink No.03 after applying the tape test
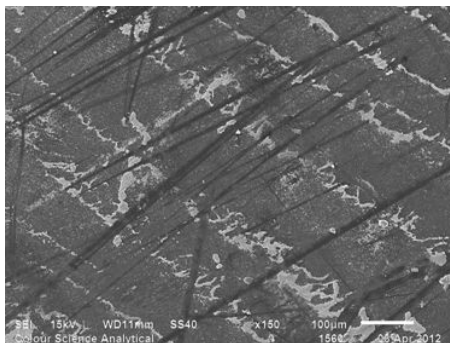
Figure 5.24 SEM of BOPP printed with ink No.04 after applying the tape test

According to Figure 5.21, the ink containing only the fumaric rosin (UCH150H) at about 3.75% in combination with NC exhibits very good adhesion, but the remaining ink layer in white displays a high level of ink residue and cracks are noted on the residual ink surface due to the hardness of the fumaric rosin (UCH150H). Figure 5.22 represents the ink remaining (lighter areas) after applying the tape test, the quantity of the residual ink in Figure 5.22 is higher than that in Figures 5.23 and 5.24.

The residual ink layers in Figures 5.22, 5.23 and 5.24 are smooth and no cracks are observed, which is due to the presence of Surkopak 5323 in inks No.02, No.03 and No.04. The dark lines in Figures 5.21, 5.22, 5.23 and 5.24 are the residual adhesive from the tape after applying the tape test for adhesion.
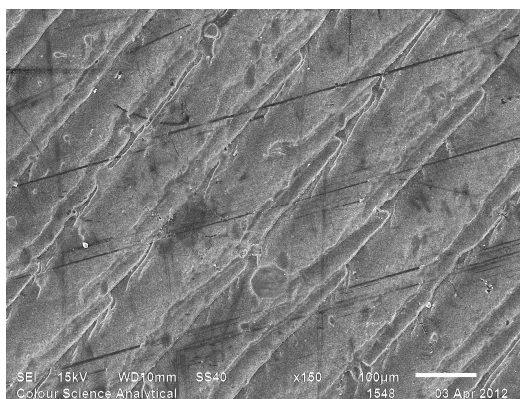
Figure 5.25 SEM of BOPP printed with 0% UCH150H and 0% Surkopak 5323
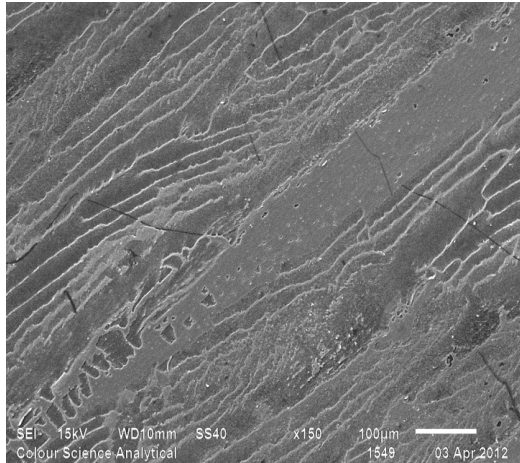
Figure 5.26 SEM of BOPP printed with

ink containing 0.4% Surkopak 5323,

Table 4.4
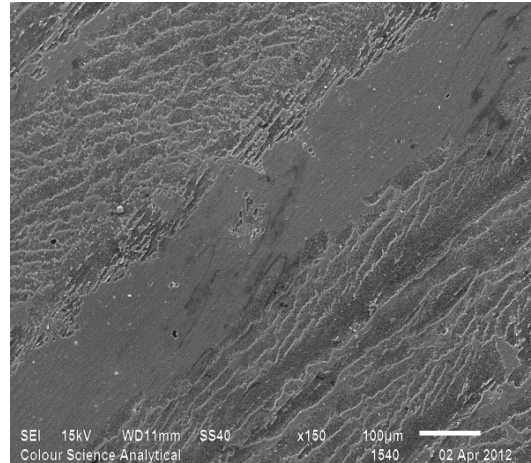
Figure 5.27 SEM of BOPP printed with

ink containing 0.4% fumaric UCH150H,

Table 4.3
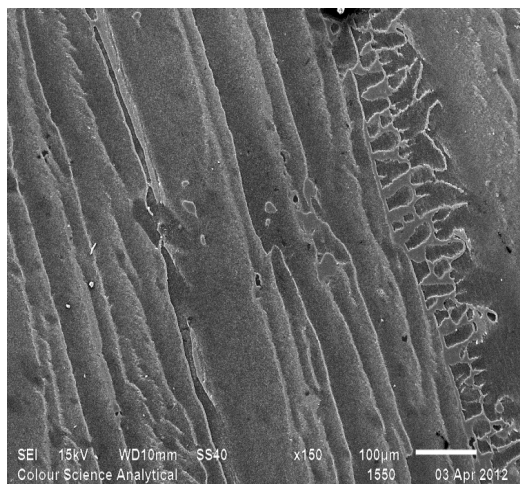
Figure 5.28 SEM of BOPP printed with

ink contains 0.83% Surkopak 5323,

Table 4.4
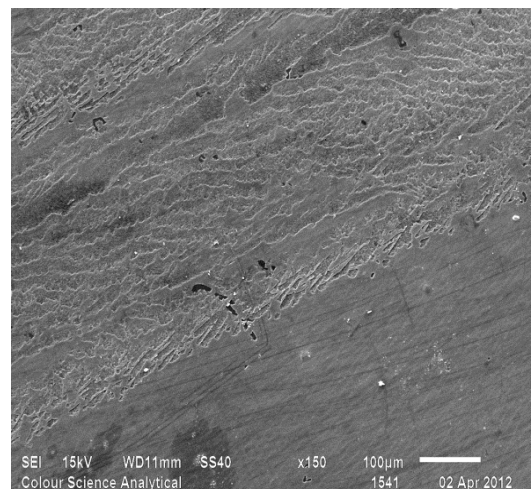
Figure 5.29 SEM of BOPP printed with

ink contains 0.83% fumaric UCH150H,
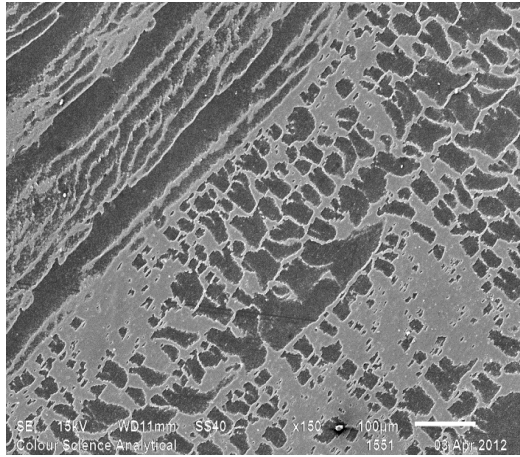
Table 4.3

Figure 5.30 SEM of BOPP printed with

ink contains 1.25% Surkopak 5323,

Table 4.4
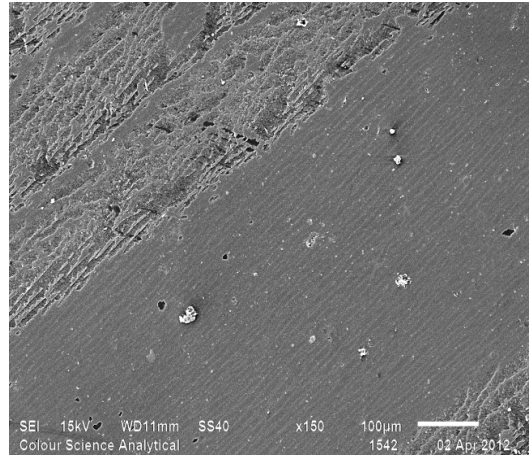
Figure 5.31 SEM of BOPP printed with

ink contains 1.25% fumaric UCH150H,
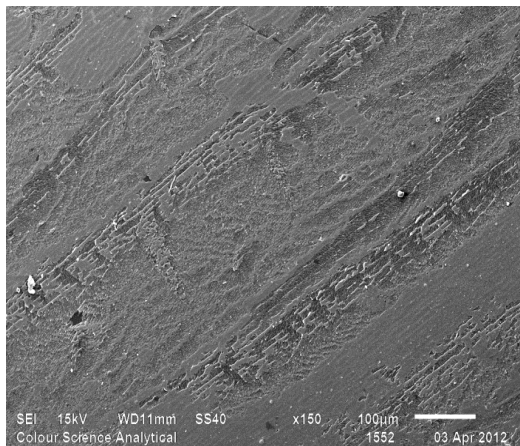
Table 4.3

Figure 5.32 SEM of BOPP printed with

ink contains 1.66% Surkopak 5323,

Table 4.4
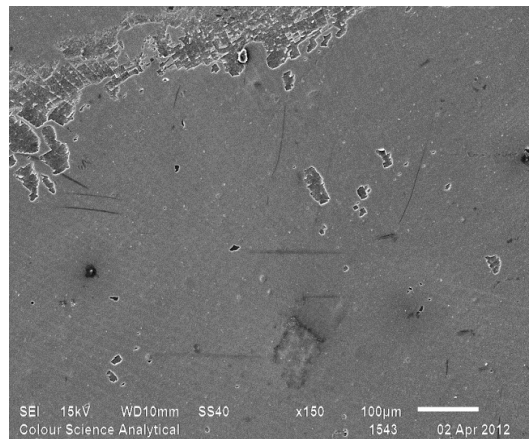
Figure 5.33 SEM of BOPP printed with

ink contains 1.66% fumaric UCH150H,
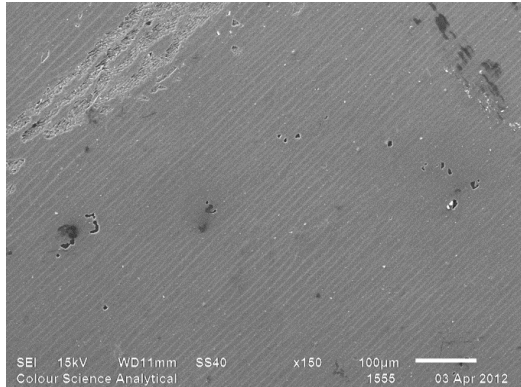
Table 4.3

Figure 5.34 SEM of BOPP printed with

ink contains 3.33% Surkopak 5323,

Table 4.4
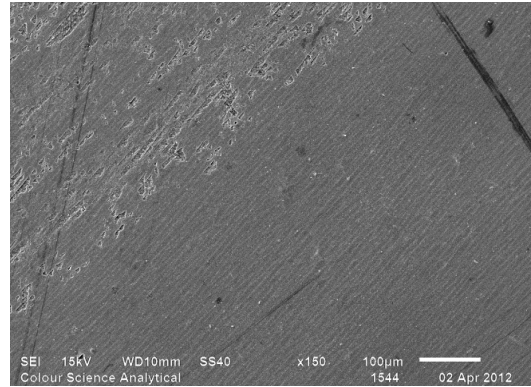
Figure 5.35 SEM of BOPP printed with

ink contains 3.33% fumaric UCH150H,
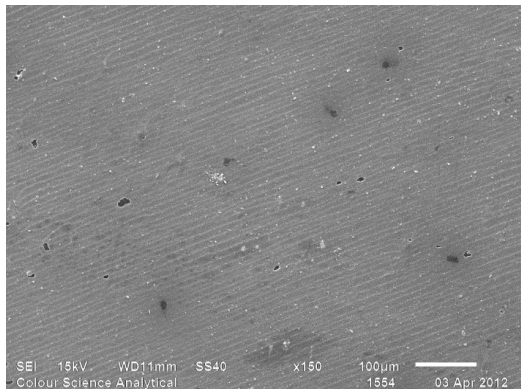
Table 4.3

Figure 5.36 SEM of BOPP printed with

ink contains 5% Surkopak 5323,

Table 4.4
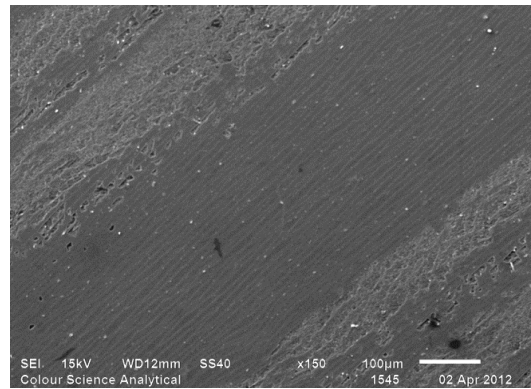
Figure 5.37 SEM of BOPP printed with

ink contains 5% fumaric UCH150H,
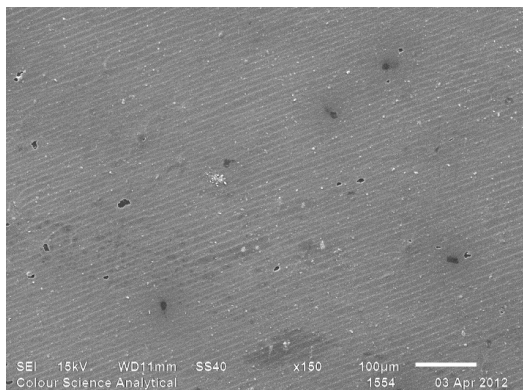
Table 4.3

Figure 5.38 SEM of BOPP printed with

ink contains 6.66% Surkopak 5323,

Table 4.4
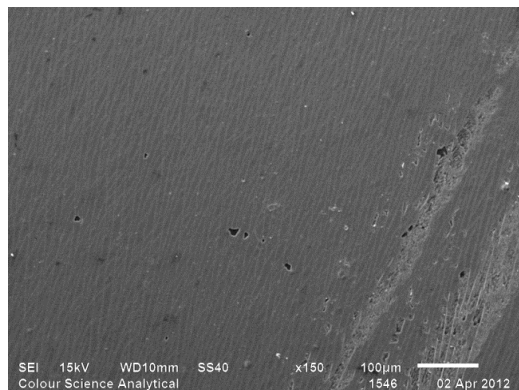
Figure 5.39 SEM of BOPP printed with

ink contains 6.66% fumaric UCH150H,
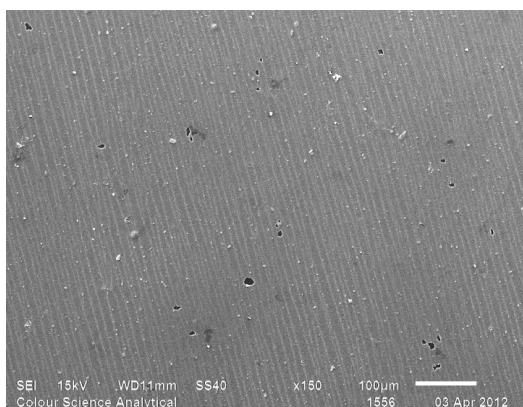
Table 4.3

Figure 5.40 SEM of BOPP printed with

ink contains 8.33% Surkopak 5323,

Table 4.4
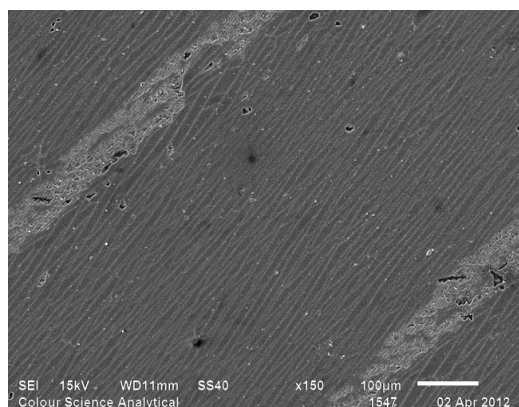
Figure 5.41 SEM of BOPP printed with

ink contains 8.33% fumaric UCH150H,

Table 4.3
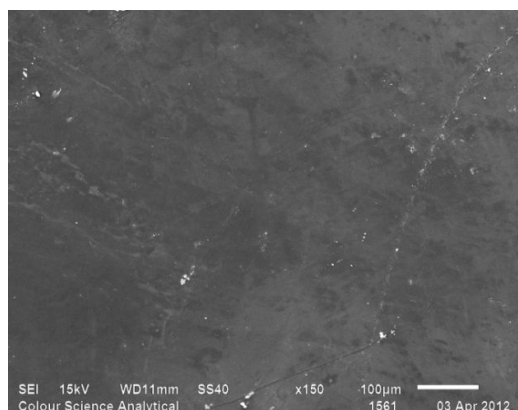
Figure 5.42 SEM of BOPP substrate without printing

It should be remembered that adhesion is the attraction of two different materials, while cohesion is the attraction of molecules of the same substance, thus good adhesion can be achieved if the adhesive wets the substrate (Carrino *et al.*, 2002). Initially the degradation of the fumaric rosin (UCH150H) and Surkopak 5323 was carried out to check at which percentage of each studied polymer the adhesion will be the best.

In the first image in Figure 5.25, one can see that the ink peels off and the residual layer is a rough area with cracks, the latter are the result of film hardness, which results from the presence of nitrocellulose alone in the ink composition. The residual ink in Figure 5.25 is represented by the darker area in the image. By comparing the different concentrations of Surkopak 5323 in the left column to the equivalent concentrations of fumaric rosin (UCH150H) in the right column one can see the following.

At 0.4%, the Surkopak 5323 sample shows small dark black areas related to the residual ink layer, while the fumaric rosin (UCH150H) exposes a larger dark black area. Both images in Figures 5.26 and 5.27 represent clear cracks because of the low percentage of polymers incorporated with the nitrocellulose in the ink formulation,

and the hardness of the applied ink layer is the reason for the cracking on the surface after applying the tape test.

By increasing the concentration to 0.83% it can be seen in Figure 5.29 that there is a considerable dark area relating to the residual ink after applying the tape test, while in Figure 5.28 the ink has peeled in large parts leaving less ink on the surface. This confirms that the adhesion seen in the case of the fumaric rosin (UCH150H) in low concentrations is still better than Surkopak 5323, although the latter exposes better cohesion.

By turning to Figures 5.30 and 5.31 one can see that the dark area in Figure 5.31 is dominant, while only small dark parts of residual ink could be seen in Figure 5.30. Moreover, the ink was peeled to a greater degree in Figure 5.30 than in Figures 5.27, 5.29 and 5.31.

In Figures 5.32 and 5.33 a noticeable change in the tape test result can be observed, the way that the ink peels in Figure 5.32 (for 1.66% Surkopak 5323) is quite different than in previous concentrations, where the adhesion is improved but is still worse than that exhibited in Figure 5.33; the cohesion became worse in Figure 5.32 as the residual ink layer is smoother than in previous concentrations.

Figures 5.35, 5.37, 5.39 and 5.41 are almost identical where a smooth dark black area, relating to the residual ink layer after applying the tape test, is dominant. In Figure 5.34, the residual ink layer is more homogenous and covers the greater area of the image, while Figures 5.36, 5.38 and 5.40 are almost identical (the ink layer is dominant and small, with only a thin layer of ink peeled off in a homogenous way,

and the residual ink layer is flat), but the darkness of images in Figures 5.36, 5.38 and 5.40 is less than in Figures 5.37, 5.39, and 5.41.

These observations confirm that in different concentrations the fumaric rosin (UCH150H) demonstrates better adhesion than Surkopak 5323 after incorporation in flexographic NC inks.   Moreover, at lower concentrations the fumaric rosin (UCH150H) displays remarkably better adhesion than Surkopak 5323 at the same concentration.

The combination of SEM with X-ray detection offers excellent elemental analysis at the sub-micrometre scale. Most SEMs are normally equipped with EDX equipment, and this has proved to be a very valuable technique, it gives only elemental information, making the analysis of complicated compounds particularly challenging (Worobiec *et al.*, 2010).   XPS yields information about very shallow layers (≈ 10 Å). While EDX penetrates more deeply and offers information of bulk composition (Velásquez *et al.*, 2001). The EDX results of samples studied by SEM in Section 4.2.7.5 are displayed in Table 5.5.

Table 5.5 EDX results of samples presented in Section 4.2.7.5

Sample reference	Carbon	Oxygen	Calcium	Titanium
UCH150H, Surkopak 5323 0%	85.47	9.58	0.00	4.96
UCH150H 0.4%	66.56	26.50	1.63	5.32
UCH150H 0.83%	64.89	29.48	1.80	3.83
UCH150H 1.25%	62.11	32.02	2.38	3.49
UCH150H 1.66%	59.52	33.38	2.21	4.48
UCH150H 3.33%	56.93	35.71	2.97	4.38
UCH150H 5%	57.82	34.53	2.68	4.97
UCH150H 6.66%	59.15	34.26	2.68	3.91
UCH150H 8.33%	57.08	35.97	2.80	4.15
Surkopak 5323 0.4%	82.03	11.83	0.00	6.14
Surkopak 5323 0.83%	76.58	17.93	0.80	4.68
Surkopak 5323 1.25%	74.56	19.79	0.94	4.71
Surkopak 5323 1.66%	68.96	25.48	1.11	4.45
Surkopak 5323 3.33%	61.03	33.16	2.14	3.68
Surkopak 5323 5%	56.76	36.54	2.47	4.23
Surkopak 5323 6.66%	58.35	36.19	2.15	3.31
Surkopak 5323 8.33%	58.10	36.27	2.43	3.19
Ink NO.01	84.92	8.97	0.00	6.11
Ink NO.02	85.44	7.69	0.00	6.87
Ink NO.03	86.13	7.29	0.00	6.58
Ink NO.04	86.40	7.48	0.00	6.12
Control sample / unprinted region	97.83	1.56	0.00	0.61

In the interpretation of EDX results, the percentage oxygen content was the main element under consideration and it can be seen that oxygen content increases with increasing polymer percentage. It should be remembered that the SEM data showed that the fumaric rosin (UCH150H) displayed remarkably better adhesion at low concentrations rather than Surkopak 5323 and this could be contributed to the high oxygen content for, when the fumaric rosin UCH 150H concentration was 0.4%, the oxygen percentage was 26.5%, while at the same concentration of Surkopak 5323 the oxygen percentage was only 11.83% and the adhesion of ink sample contains 0.4%

The adhesion improved incrementally by increasing the concentration of fumaric rosin (UCH150H) until a plateau was reached at 3.33%, where the optimum adhesion was obtained, and no further improvements in adhesion were achieved thereafter. This result is in agreement with the observed oxygen composition, which is approximately the same between 3.33% and 8.33%. On the other hand, Surkopak 5323 displayed poor adhesion results below a concentration of 5%, whereupon the adhesion improved significantly and maintained performance until 8.33%. This result is also in agreement with the SEM data and the oxygen composition, which remained approximately constant from 5-8.33% Surkopak 5323.

A comparison was made using EDX of the oxygen composition of the ink samples prepared in Section 4.2.1.3. and the data are presented in Table 5.5. The highest oxygen composition was found for ink No.01, containing only the fumaric rosin (UCH150H) in combination with nitrocellulose, followed by ink No.02 (the next ink to display good adhesion and containing fumaric rosin (UCH150H) along with Surkopak 5323 incorporated with nitrocellulose). In comparison with these materials, the remaining Inks No.03 and No.04 (the latter contains only Surkopak

5323) displayed poor adhesion. The addition of TAA75 to ink No.04 in order to improve the adhesion, yielded results that were no better than ink No.02, indicating that the use of fumaric rosin (UCH150H) as an additive in Flexographic inks is preferred. Furthermore, the analysis of the oxygen content of the BOPP sample (the treated side) revealed a content of 1.56%.

5.4.3   Transform infrared (FTIR) spectroscopy

Vibrational spectra were obtained in transmission for selected samples and these are presented below (Figures 5.43 - 5.49) and the relevance of the spectral assignments are discussed with reference to Section 4.2.7.3.3. From Figure 5.43 the FTIR spectrum of the fumaric rosin (UCH150H), a peak is observed at 1692 cm^{-1} which is attributed to the C=O stretching band of the carboxylic acid, while another band at 1779 cm^{-1} is related to the C=O stretching vibration of the ester (confirming that the fumaric rosin (UCH150H) is an ester that contains an amount of un-reacted carboxylic acid).
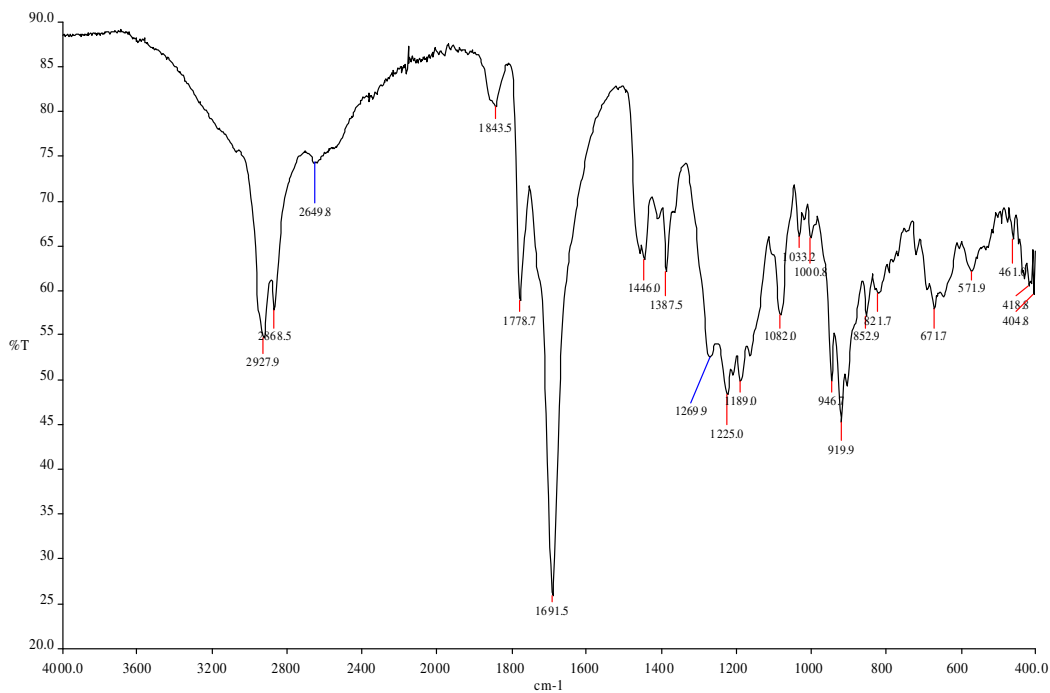
Figure 5.43 FTIR spectrum of the fumaric rosin (UCH150H)

Figure 5.44 shows the FTIR spectrum of Surkopak 5323, which contains a weak band at 3308 cm^{-1} (attributed to NH stretching), another broad band at 1726 cm^{-1} is related to the C=O stretching vibration of the ester associated with Surkopak 5323 which could be ethyl acetate as mentioned in Section 4.1.2.3.
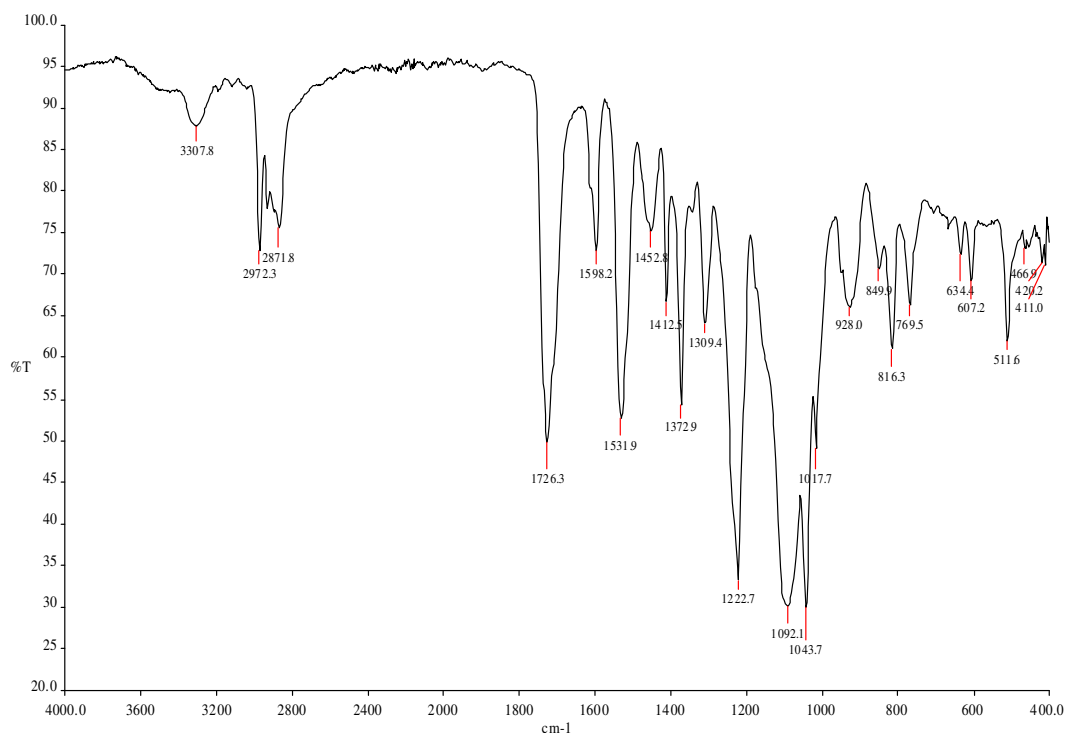
Figure 5.44 FTIR spectrum of the Surkopak 5323

Considering Figure 5.45, the absorbances at 840, 1000 and 1170 cm^{-1} are characteristic of isotactic PP (as explained in Section 1.7) and confirming the tacticity of the BOPP used in this study. The spectrum in Figure 5.46 also shows a weak band at 1102 cm^{-1} which can be attributed to the (coupled) C $-$ O stretching vibration of an ether group, confirming the presence of oxygen in this functional group on the surface of the BOPP sample.
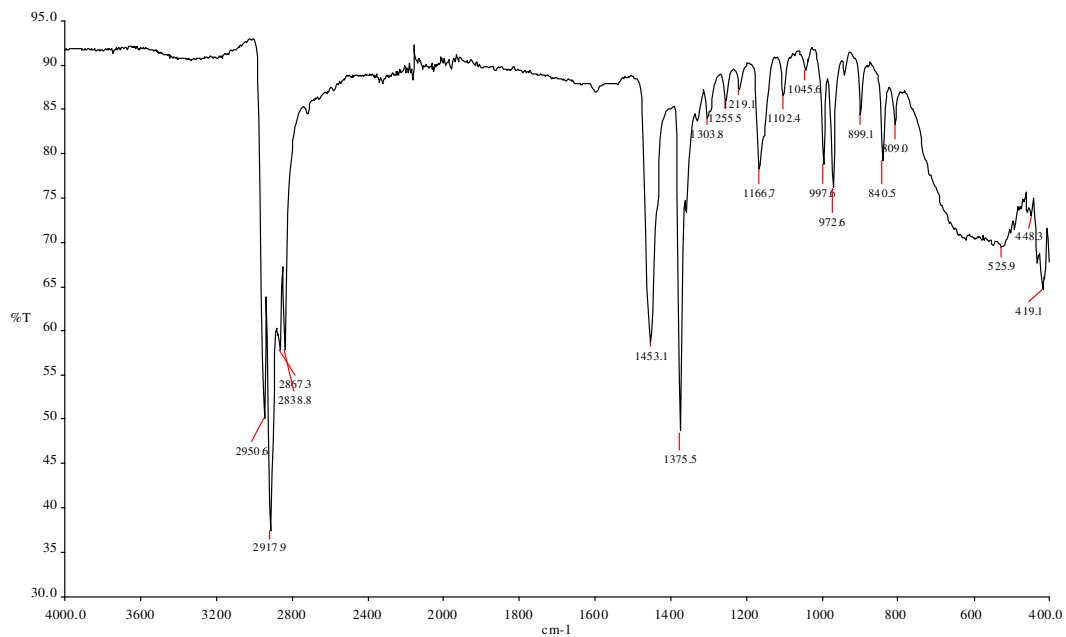
Figure 5.45 FTIR spectrum of White BOPP

Figure 5.46 and 5.47represent the FTIR spectra of the BOPP substrate coated with the fumaric rosin (UCH150H) and Surkopak 5323 respectively, from which it can be seen that the spectra are the same as those of UCH150H and Surkopak 5323 before printing on the BOPP substrate.
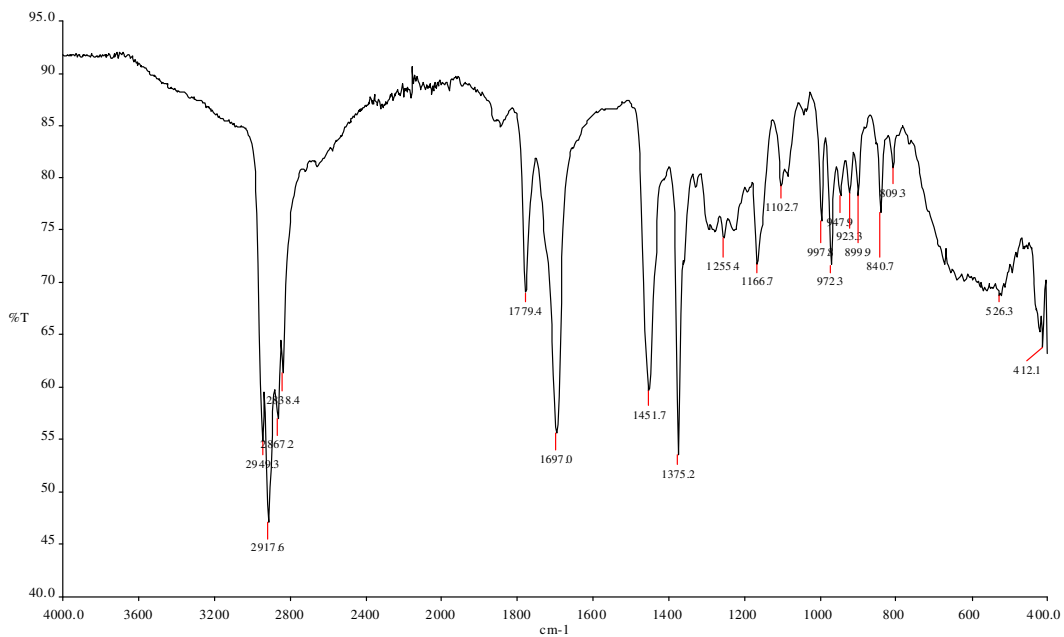
Figure 5.46 FTIR spectrum of White BOPP printed with the fumaric rosin
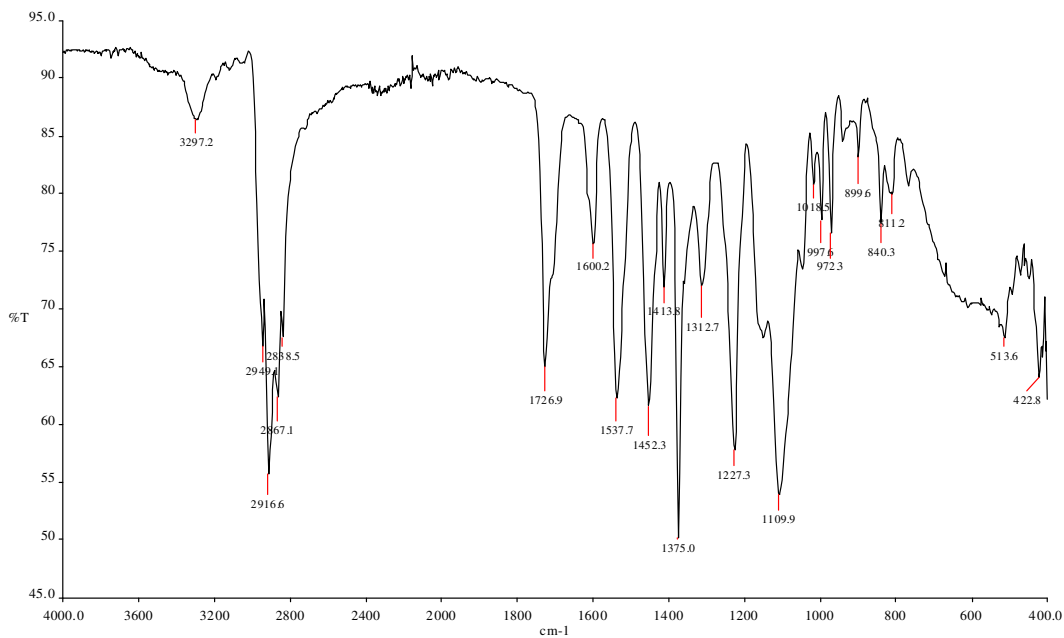
(UCH150H) extender

Figure 5.47 FTIR spectrum of White BOPP printed with the Surkopak 5323 extender

The spectra in Figure 5.48. and 5.49 confirm that the FTIR spectrum of BOPP was not

observed after printing the fumaric rosin (UCH150H) and Surkopak 5323.
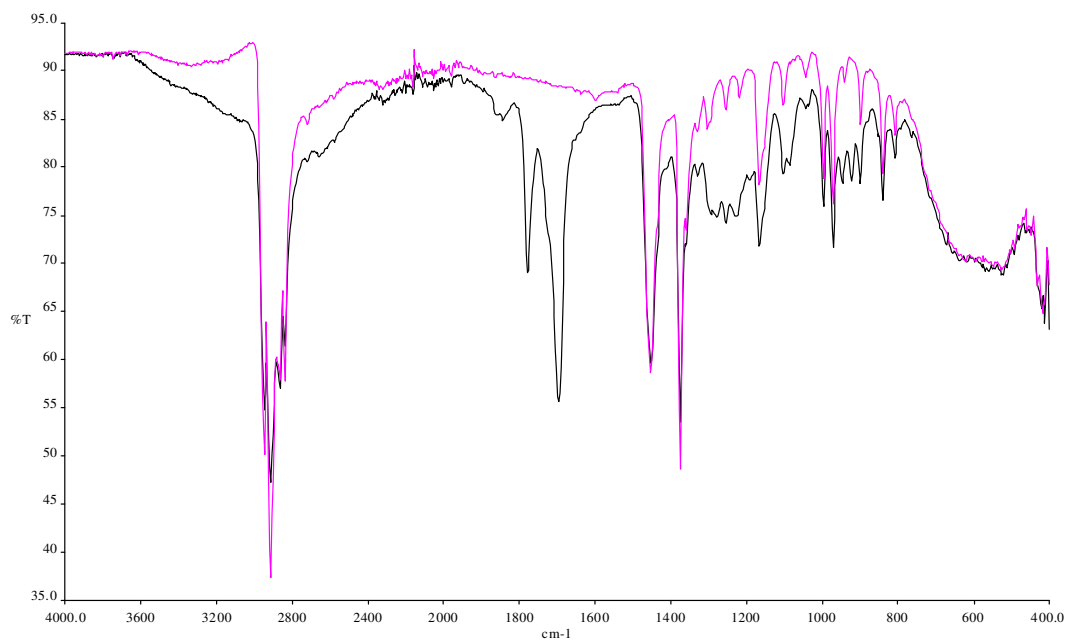
Figure 5.48 FTIR spectra of white BOPP printed with fumaric rosin (UCH150H)

extender (black) and BOPP (red)
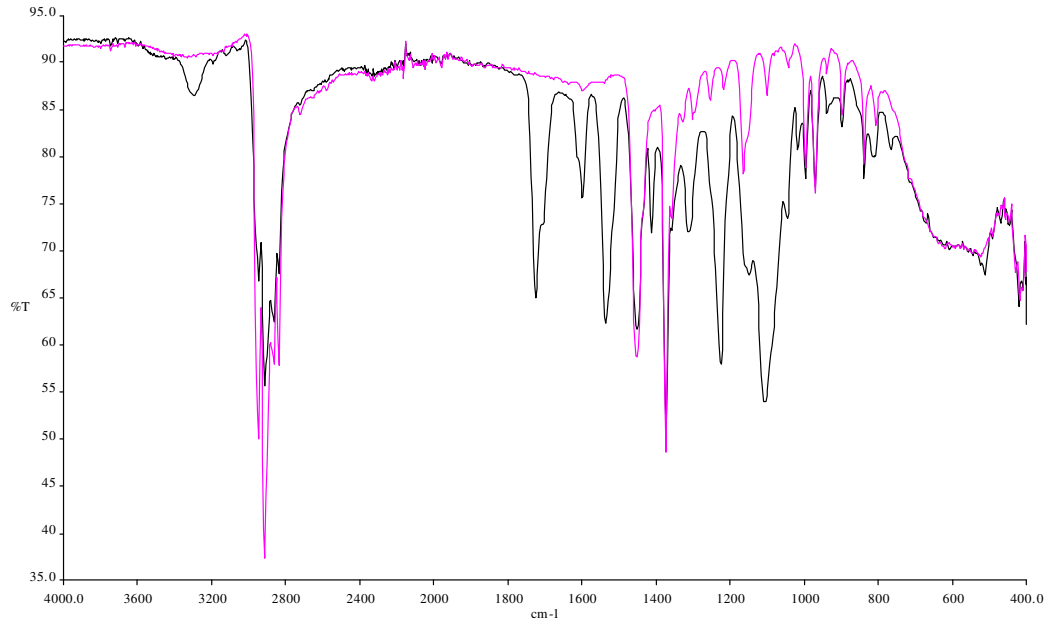
Figure 5.49 FTIR spectra of white BOPP printed with Surkopak 5323 extender

(black) and BOPP (red)

5.4.4   Atomic force microscopy (AFM)

1- BOPP sample

Figure 5.50. exhibits the morphology of a BOPP film, the surface morphology of the

BOPP film is a fibre like network structure.
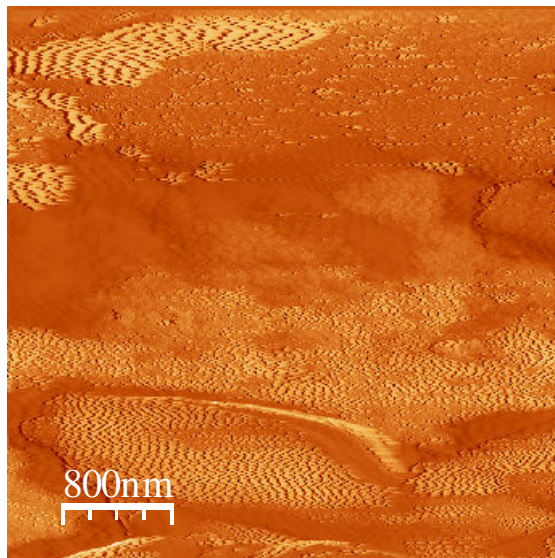
Figure 5.50 AFM image of BOPP surface

The force curve for the uncoated treated BOPP is shown in Figure 5.51 and this will

be used as the baseline against which the coated substrates will be compared.
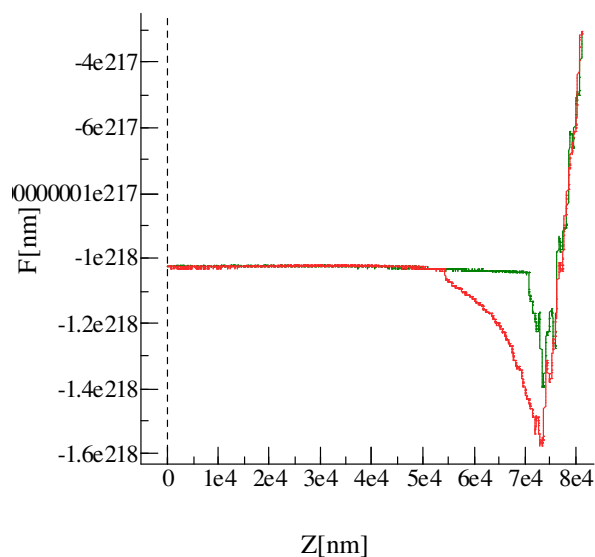
Figure 5.51 Force curve of BOPP

2- BOPP coated with fumaric rosin (UCH150H) extender

Figure 5.52 shows the morphology of BOPP coated with the fumaric rosin
(UCH150H) extender, as prepared according to the procedure mentioned in Section
4.2.7.4. However, it is not possible to conclude anything regarding the morphology
of BOPP after applying the polymeric extender from this data. This could be related
to the sticky layer of printed polymers extender, which restrains the tip movement,
and consequently no topographical images of sample's surface could be obtained.
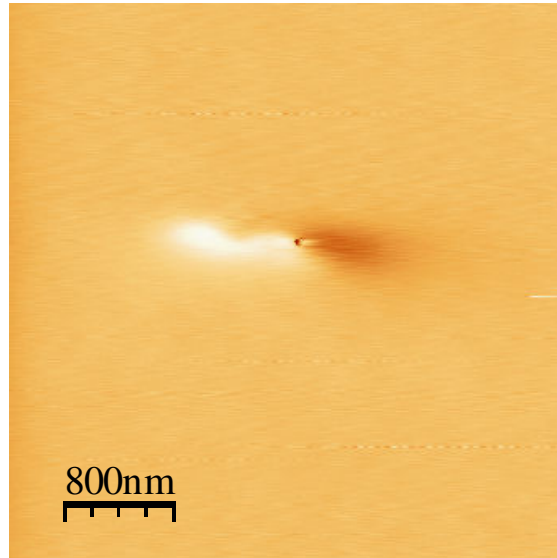
Figure 5.52 AFM image of BOPP coated with fumaric rosin extender

From the force curves in Figure 5.53, one can see that the adhesion force of BOPP coated with the fumaric UCH150H extender is significantly higher than that of BOPP. The adhesion of the tip to BOPP surface is the result of Van der Waals forces, but in case of BOPP coated with fumaric rosin (UCH150H) the better adhesion is the result of attractive forces which means that coated sample's surface is positively charged attracting the negatively charged tip.
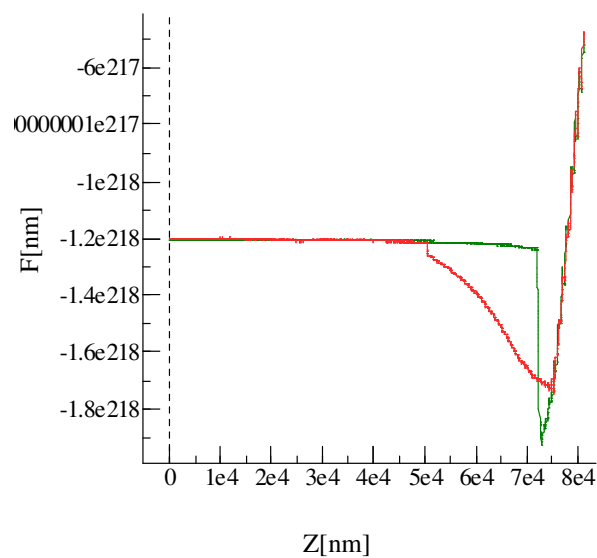
Figure 5.53 Force curve of BOPP coated with Fumaric rosin extender

3- BOPP printed with Surkopak 5323 extender

Figures 5.54 shows the morphology of BOPP coated with the Surkopak 5323 extenders (prepared according to the procedure mentioned in Section 4.2.7.4). Once again it is not possible to conclude anything regarding the morphology of BOPP after applying the polymeric extender. From the force curves in Figure 5.55, one can see that the adhesion force of BOPP coated with the Surkopak 5323 extender is significantly lower than that recorded for the fumaric UCH150H extender.

400nm
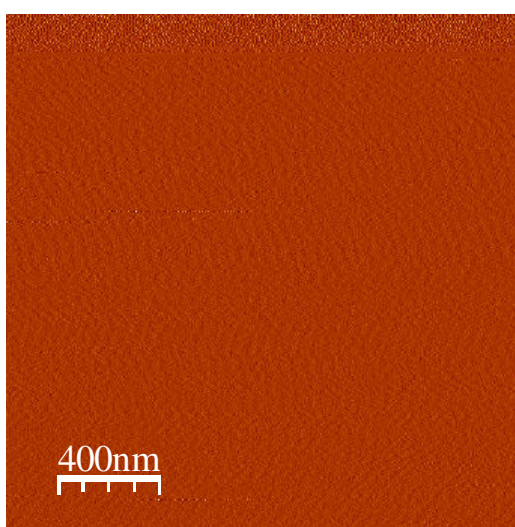
Figure 5.54 AFM image of BOPP coated with PU extender
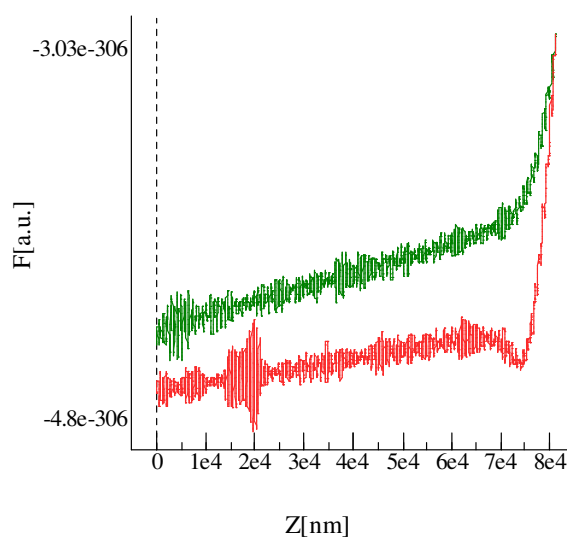
Figure 5.55 Force curve of BOPP coated with PU extender

5.4.5 Nuclear magnetic resonance (NMR) spectroscopy

NMR spectra are beneficial in polymer characterization and enable the researcher to have a good understanding of polymer chain structure (Jena *et al.*, 2007). Two samples (the fumaric rosin UCH 150H and Surkopak 5323) were studied by ^{1}H-NMR in (DMSO-d6) solution by using a Brucker 400 spectrometer available in Homs University, Syria. The study was undertaken to confirm the chemical structures suggested by the supplier. Relying on figure 4.14 in Section 4.2.7.5. and on the data presented in Figure 5.56 the ^{1}H NMR spectrum of Surkopak 5323, δ 7.7-7.43 corresponds to *para*-disubstituted aryl ring, δ 3-4 relates to many protons (perhaps arising from propylene glycol) and δ 1.98 CH_3 present in ethyl acetate. A shift should be observed at δ 8.45 related to NH, but it is not visible in the spectrum in Figure 5.56 as the proton is labile, thus the protons in the solvent (DMSO-d$_6$) exchange with the amine protons. Furthermore, a small shift is observed at δ 2.49 relating to protons of (DMSO-d$_6$).
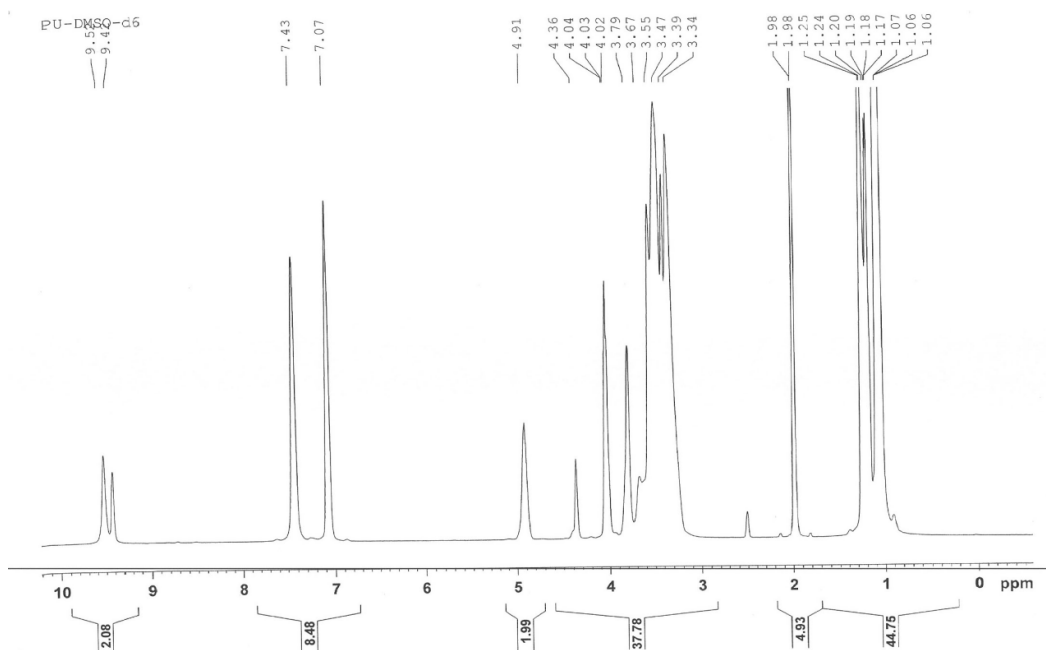
Figure 5.56 Proton magnetic resonance (^{1}H-NMR) spectrum of Surkopak 5323

Figure 5.57 shows the ^{1}H NMR (DMSO-d$_6$) spectrum of the fumaric rosin (UCH150H). Two shifts are observed (δ 5.3-5.48, where δ is the chemical shift scale in NMR spectrum) that are related to the CH attached to OH and this is consistent with the presence of glycerin polymer. The downfield shift at δ 12 is assigned to the OH of the carboxylic acid, which confirms the presence of un-reacted fumaric acid.
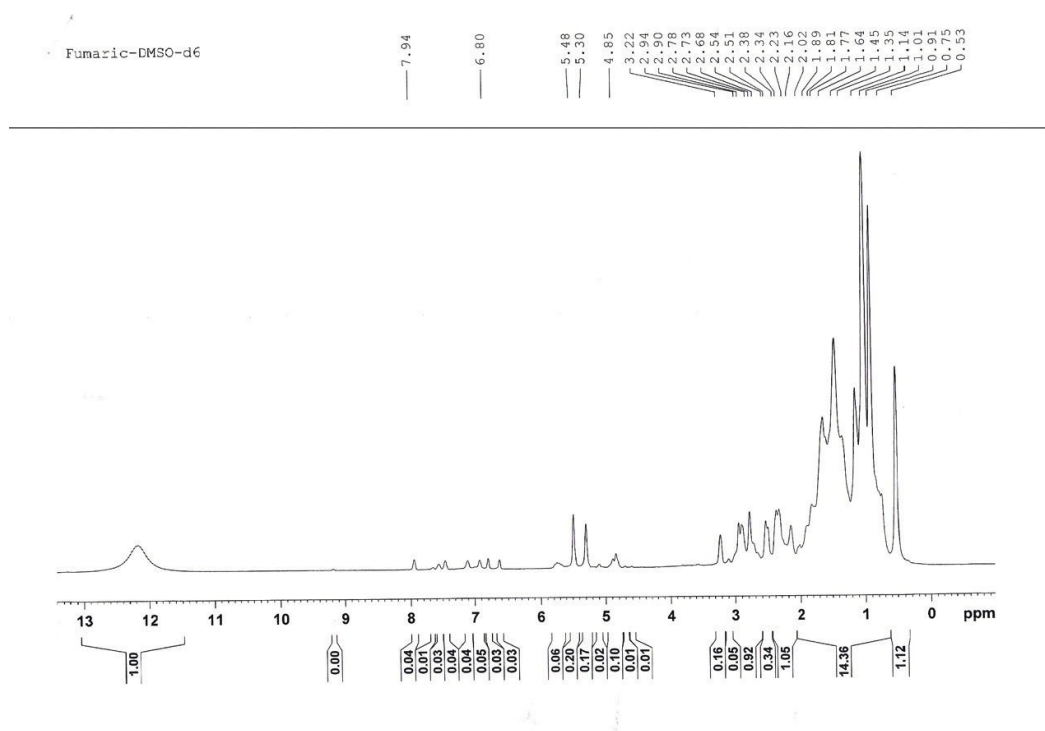
Figure 5.57 Proton magnetic resonance (^{1}H-NMR) spectrum of fumaric rosin (UCH150H)

5.4.6 Electron spectroscopy for chemical analysis (ESCA)

This section presents ESCA and XPS data for selected samples of BOPP both uncoated and coated with the two extenders. Tables 5.6., 5.8., and 5.10. list the key elemental (ESCA) peak binding energies and line widths identified for BOPP, BOPP coated with fumaric rosin (UCH150H) extender and BOPP coated with Surkopak 5323 extender respectively. As the ESCA sensitivity is high and only thin layer of around 100 Angström is utilized for the analysis (Carlson, 1978), then the investigated layer is the coated polymer on the BOPP surface as the deposited layer is about 6 μm.

5.4.6.1 BOPP sample

The ESCA data for the BOPP sample are presented in Table 5.6 and graphically in Figure 5.58.

Table 5.6 ESCA data for BOPP

Name	Start BE	Peak BE	End BE	Height Counts	FWHM eV	Area (P) CPS.eV	Area (N)	At. %
O1s	543.02	532.05	510.32	11010.38	4.33	53534.58	0	0
C1s	295.29	285.16	264.57	82439.19	3.83	322767.1	0	0
C1s	289.4	284.58	281.5	12056.44	1.43	18088.35	0.42	91.96
O1s	537.2	531.8	527.8	1000.41	2.48	2608	0.02	4.66
N1s	405.2	399.51	395.4	126.63	1.59	215	0	0.61
C1s A	289.4	286.82	281.5	332.22	1.43	498.43	0.01	2.53
N1s A	405.2	401.87	395.4	47.71	1.59	81.01	0	0.23
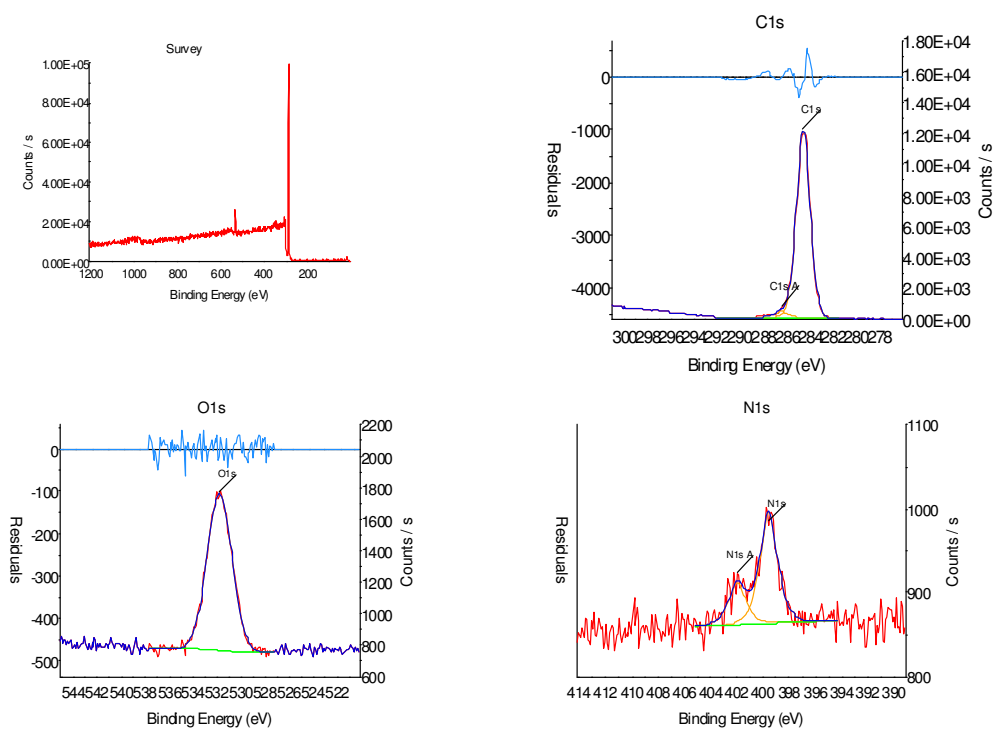
Figure 5.58 Carbon, oxygen and nitrogen ESCA spectra of BOPP substrate corona

treated

The ESCA investigation of the BOPP confirms the presence of oxygen on the surface

(Table 5.7).

Table 5.7 X-ray photoelectron data of BOPP surface

	C_{1S}		O_{1S}	N_{1S}
	1	**2**		
BE (ev)	284.58	286.82	531.8	399.51
FWHM (ev)	1.43	1.43	2.48	1.59
Area %	0.042	0.01	0.02	0
	C-C	**CH₂-O**	**C-O- C**	**weak**

5.4.6.2 BOPP coated with fumaric rosin extender (10% fumaric rosin + 90% ethanol)

The ESCA data for the BOPP sample coated with the fumaric rosin are presented in Table 5.8 and graphically in Figure 5.59.

Table 5.8 ESCA data for BOPP coated with fumaric rosin extender

Name	Start BE	Peak BE	End BE	Height Counts	FWHM eV	Area (P) CPS.eV	Area (N)	At. %
C1s	293.8	284.52	281.3	5280.08	1.84	10217.19	0.24	49.57
N1s	409.3	401.94	396.1	92.33	2.88	327.8	0	0.89
O1s	539.3	532.53	528	2181.29	3.08	7140.82	0.06	12.18
C1s A	293.8	286.26	281.3	2531.48	1.84	4898.53	0.11	23.77
C1s B	293.8	289.64	281.3	378.53	1.84	732.48	0.02	3.56
C1s C	293.8	288.16	281.3	812.08	1.84	1571.42	0.04	7.63
O1s A	539.3	534.7	528	430.1	3.08	1407.99	0.01	2.4
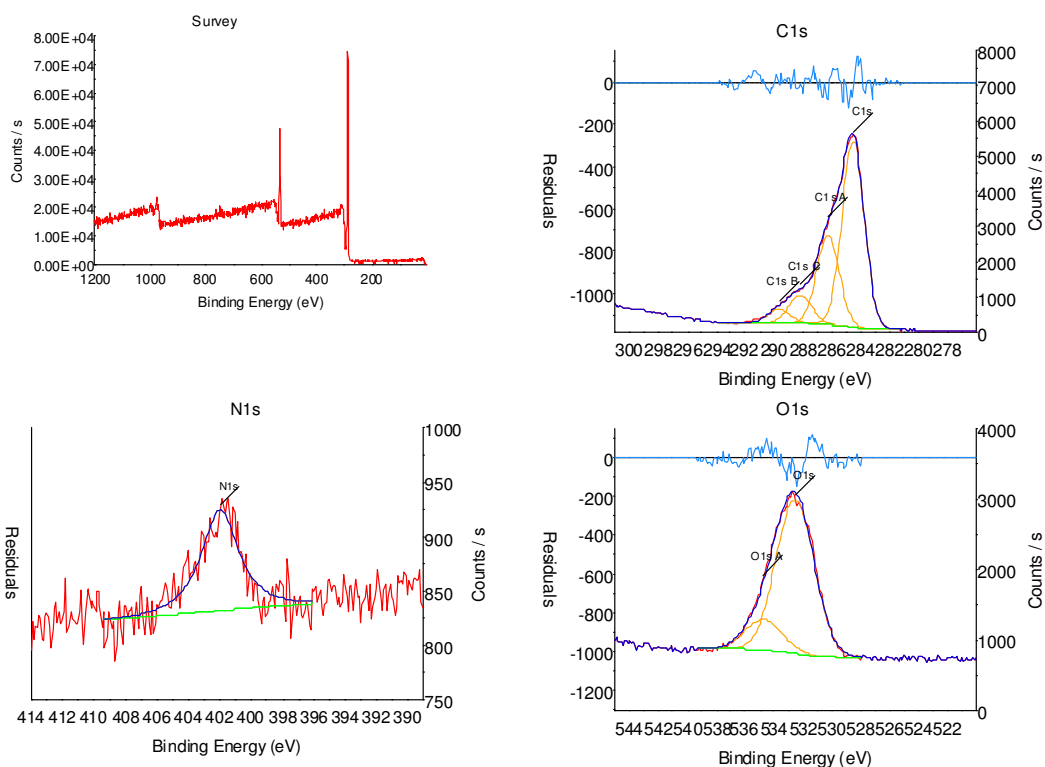
Figure 5.59 Carbon, oxygen and nitrogen ESCA spectra of BOPP substrate coated

with fumaric rosin (UCH150H) extender

The ESCA spectra of the fumaric rosin (UCH150H) show that binding energies of the

carbons and oxygen associated with the various functional groups and are assigned

according to Table 5.9. which confirms to a great extent the suggested structure of

fumaric rosin (UCH150H) in Section 4.1.2.2.

Table 5.9 X-ray photoelectron data of BOPP coated with fumaric rosin (UCH150H)

extender

	C_{1S}				O_{1S}		N_{1S}
	1	2	3	4	1	2	
BE (ev)	284.52	286.26	289.64	288.16	532.53	534.7	401.94
FWHM (ev)	1.84	1.84	1.84	1.84	3.08	3.08	2.88
Area %	0.24	0.11	0.02	0.04	0.06	0.01	0
	C-C	C-O	C=O	C=O O	C-OH	C=O O	Weak

5.4.6.3 BOPP coated with polyurethane extender (10% Surkopak 5323 + 90% ethanol)

The ESCA data for the BOPP sample coated with the polyurethane are presented in Table 5.10 and graphically in Figure 5.60.

Table 5.10 ESCA data for BOPP coated with the polyurethane extender

Name	Start BE	Peak BE	End BE	Height Counts	FWHM eV	Area (P) CPS.eV	Area (N)	At. %
C1s	292.32	284.38	274.48	79206.96	3.95	336748.8	0	0
N1s	440.96	399.45	370.6	3140.18	6.33	9024.62	0	0
O1s	579.69	531.16	519.24	26910.1	4.07	173844.2	0	0
OKL1	1012.72	975.72	959.21	4817.07	7.82	74595.98	0	0
C1s	292.3	284.6	281	7113.77	1.4	10509.99	0.24	58.73
O1s	536.6	532.11	527.2	3073.53	1.69	5525.78	0.04	10.85
N1s	405.3	399.68	396	343.17	1.55	557.45	0.01	1.75
C1s A	292.3	284.6	281	1030.81	1.4	1522.94	0.04	8.51
C1s B	292.3	286.14	281	2256.5	1.4	3333.78	0.08	18.63
O1s A	536.6	530.72	527.2	347.6	1.69	624.94	0.01	1.23
N1s A	405.3	401.59	396	58.34	1.55	94.76	0	0.3
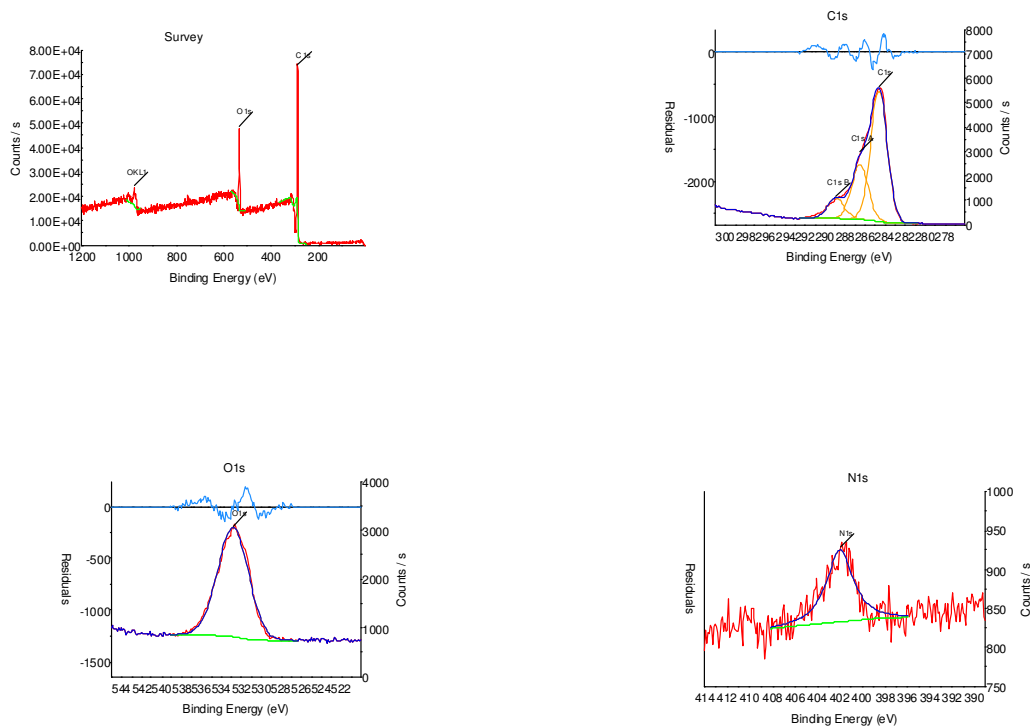
Figure 5.60 Carbon, oxygen and nitrogen ESCA spectra of BOPP substrate coated

with Surkopak 5323 extender

Table 5.11 X-ray photoelectron data of BOPP coated with Surkopak 5323 extender

	C_{1S}		O_{1S}		N_{1S}
	1	2	1	2	
BE (ev)	284.6	286.14	532.11	530.72	399.68
FWHM (ev)	1.4	1.4	1.69	1.69	1.55
Area %	0.04	0.08	0.04	0.01	0.01
	CH_2-CH_2	CH_2-O	C-O-C	NH-C=O	NHC=O

Finally the ESCA spectra of Surkopak 5323 confirms that it is aromatic in nature

based on the data presented in Figures 4.15, 4.16 in Section 4.2.7.6.

5.5   Surface studies

5.5.1   Wetting

Contact angles were measured according to the procedure outlined in Section 4.2.8.1.

and the results were as follows.

Table 5.12 Contact angle results determined for selected liquids

	Contact angle ⏹
Solution 50% Surkopak 5323 + 50% ethanol	40.7
Solution 50% fumaric UCH150H + 50% ethanol	40.0
Ink No.01	50.0
Ink No.03	54.6

Similarly, the schematic diagrams of the obtained results in Table 5.12. are represented in Figure 5.61.
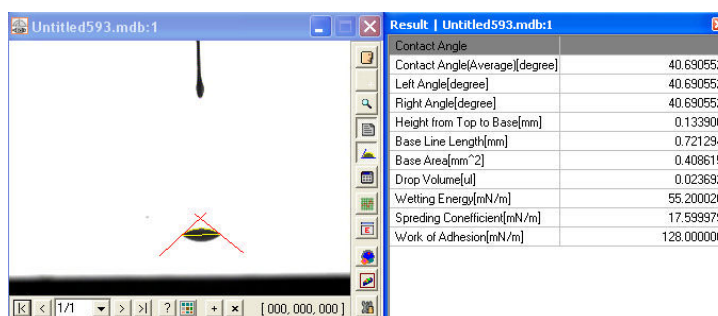
Figure 5.61 Contact angle of 50% Surkopak 5323 + 50% ethanol
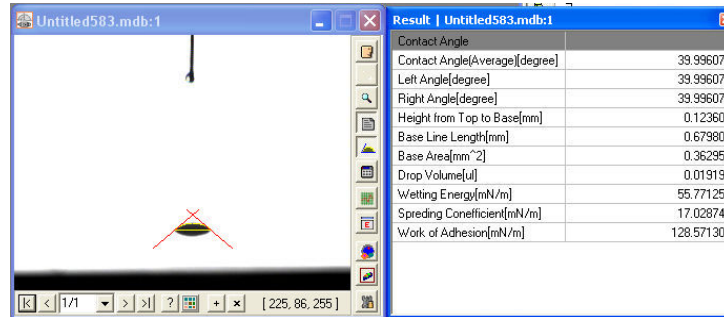
Figure 5.62 Contact angle of 50% fumaric UCH150H + 50% ethanol
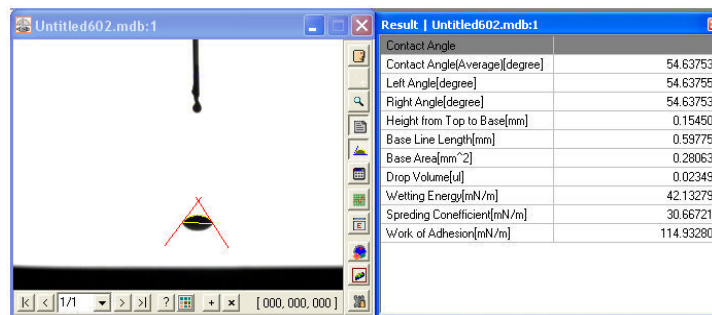
Figure 5.63 Contact angle of Ink No.03
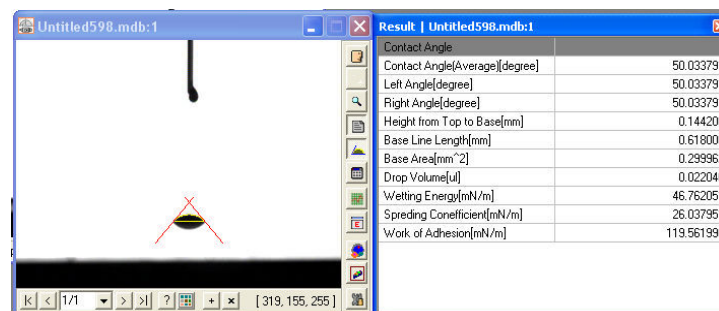
Figure 5.64 Contact angle of Ink No.01

By comparing the contact angle results it can be seen that the solutions of fumaric rosin (UCH150H) and Ink No.01, which is based on fumaric rosin (UCH150H), display smaller contact angles than those containing Surkopak 5323. This, in turn, confirms the better adhesion observed for inks containing fumaric rosin (UCH150H).

On the other hand, from the contact angle results of the two polymer solutions, it is confirmed that the polymer used in any flexographic ink composition plays the main role in determining the strength of adhesion.

5.5.2   Inverse gas chromatography (IGC)

IGC studies at infinite dilution were conducted on the polyurethane polymer (PU), the fumaric rosin polymer, BOPP that was coated with the polyurethane and BOPP that was coated with the fumaric rosin to obtain information concerning the surface polarity and acid-base nature of the particles. Although the polymers and the BOPP that was coated with the polymers were analysed separately, common probes were used so that both qualitative and quantitative associations between the polymers and the probes could be concluded from the analysis.   This information was important as it was thought that it could provide a basis for determining the potential chemical interactions between the polymer used in flexographic ink compositions and a coated BOPP surface.

The retention times of apolar probe molecules and polar probe molecules, each on the polymer surface, were determined at specific temperatures. These retention values were used to enable the calculation of the retention volume, energy of adsorption, enthalpy of adsorption of the probes as well as, the acidic and basic character of the surface of the material.   Background theory and experimental details have been provided in sections 2.1 and 4.2.8.2, respectively.

Evaluation of the column containing the polyurethane

Determination of the dispersive component of surface free energy

The Fowkes approach considered in section 2.1 was used to determine the dispersive component of the surface free energy of the polymer over a range of temperatures. Figure 2.1 illustrates the determination of the dispersive component of the surface.

For each temperature studied, the value of RTln(V_n) was plotted against $a\sqrt{(\gamma_l^d)}$. These graphs are shown in Figures 5.65 - 5.68 Data obtained from studies of polar probes are also included in these graphs.

Table 5.13 Retention time tr, specific retention volume V_g, Gibbs free energy

of adsorption RTLn(V_n), for the n-alkanes on Surkopak 5323 at T = 313.15 K, F = 50

cm³min⁻¹, CH₄ = 29.4 s J = 0.66, C = 0.90, P_i = 196 kPa, P_o = 101 kPa, m=0.93 gr

Probe Molecule	t_r (s)	V_n (cm³/g)	ln V_n (cm³/g)	RTln(V_n) (kJ/mol)	V_g	RTln(V_g) (kJ/mol)
Pentane	55.80	784.08	6.66	17.35	843.10	17.54
Hexane	102.00	2156.22	7.68	19.98	2318.52	20.17
Heptane	219.00	5631.12	8.64	22.48	6054.97	22.67
Octane	513.00	14362.92	9.57	24.92	15444.00	25.11
THF	573.00	16144.92	9.69	25.23	17360.13	25.42
DCM	307.92	8272.04	9.02	23.49	8894.67	23.67
EtAc	481.50	13427.37	9.51	24.75	14438.03	24.94
Acetone	258.42	6801.89	8.82	22.98	7313.86	23.16

Surkopak 5323, T=40ºC
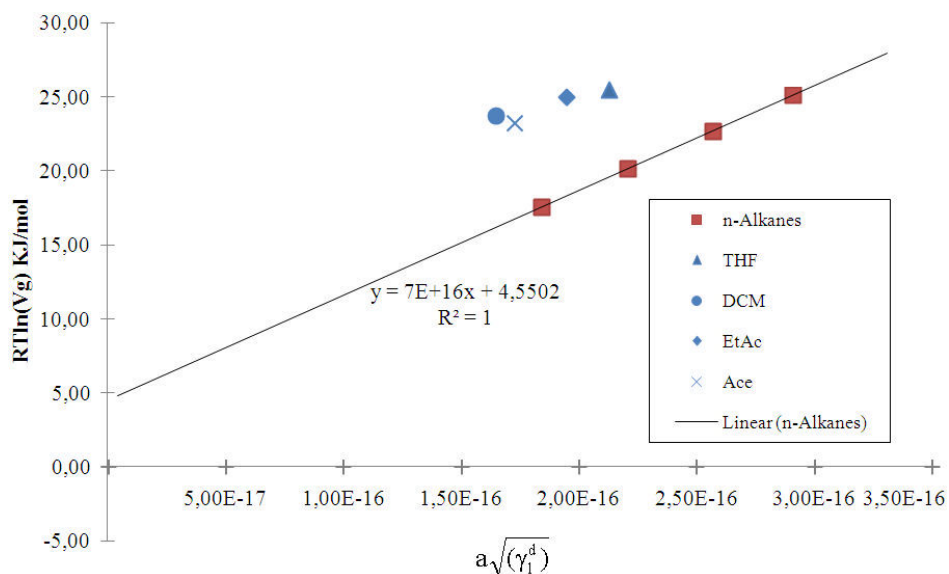
Figure 5.65 A plot of RTLn(V$_g$) *versus* $a\sqrt{(\gamma_1^d)}$ of n-alkane and polar probes on the

surface of Surkopak 5323, at 313.15K

Table 5.14 Retention time tr, specific retention volume V$_g$, Gibbs free energy

of adsorption RTLn(V$_n$), for the n-alkanes on Surkopak 5323 at T = 323.15 K,

F = 50 cm³min⁻¹, CH$_4$ = 29.4 s J = 0.66, C = 0.90, P$_i$ = 196 kPa, P$_o$ = 101 kPa, m=0.93 gr

Probe Molecule	t$_r$ (s)	V$_n$ (cm³/g)	ln V$_n$ (cm³/g)	RTln(V$_n$) (kJ/mol)	V$_g$	RTln(V$_g$) (kJ/mol)
Pentane	53.40	712.80	6.57	17.65	766.45	17.29
Hexane	87.00	1710.72	7.44	20.00	1839.48	19.57
Heptane	170.40	4187.70	8.34	22.41	4502.90	21.90
Octane	365.10	9970.29	9.21	24.74	10720.74	24.16
THF	367.20	10032.66	9.21	24.76	10787.81	24.18
DCM	232.20	6023.16	8.70	23.38	6476.52	22.85
EtAc	349.20	9498.06	9.16	24.61	10212.97	24.03
Acetone	258.42	5034.15	8.52	22.90	5413.06	22.38

Surkopak 5323, T=50°C
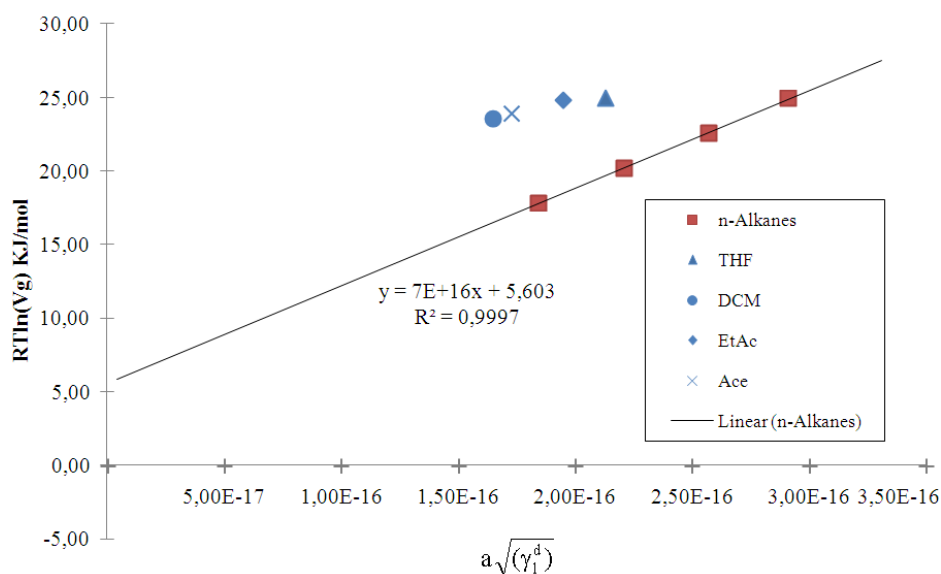
Figure 5.66 A plot of RTLn(V_g) *versus* $a\sqrt{(\gamma_l^d)}$ of n-alkane and polar probes on the

surface of Surkopak 5323 at 323.15K

Table 5.15 Retention time tr, specific retention volume V_g, Gibbs free energy

of adsorption RTLn(V_n), for the n-alkanes on Surkopak 5323 at T = 333.15 K,

F = 50 cm3min-1, CH$_4$ = 29.4 s, J = 0.66, C = 0.90, P_i = 196 kPa, P_o = 101 kPa, m=0.93 gr

Probe Molecule	t_r (s)	V_n (cm³/g)	ln V_n (cm³/g)	RTln(V_n) (kJ/mol)	V_g	RTln(V_g) (kJ/mol)
Pentane	49.20	588.06	6.38	17.66	632.32	17.86
Hexane	75.18	1359.67	7.21	19.99	1462.01	20.19
Heptane	135.60	3154.14	8.06	22.32	3391.55	22.52
Octane	268.80	7110.18	8.87	24.57	7645.35	24.77
THF	313.20	8428.86	9.04	25.04	9063.29	25.24
DCM	177.60	4401.54	8.39	23.24	4732.84	23.44
EtAc	257.40	6771.60	8.82	24.43	7281.29	24.63
Acetone	198.90	5034.15	8.52	23.61	5413.06	23.81

Surkopak 5323, T=60°C
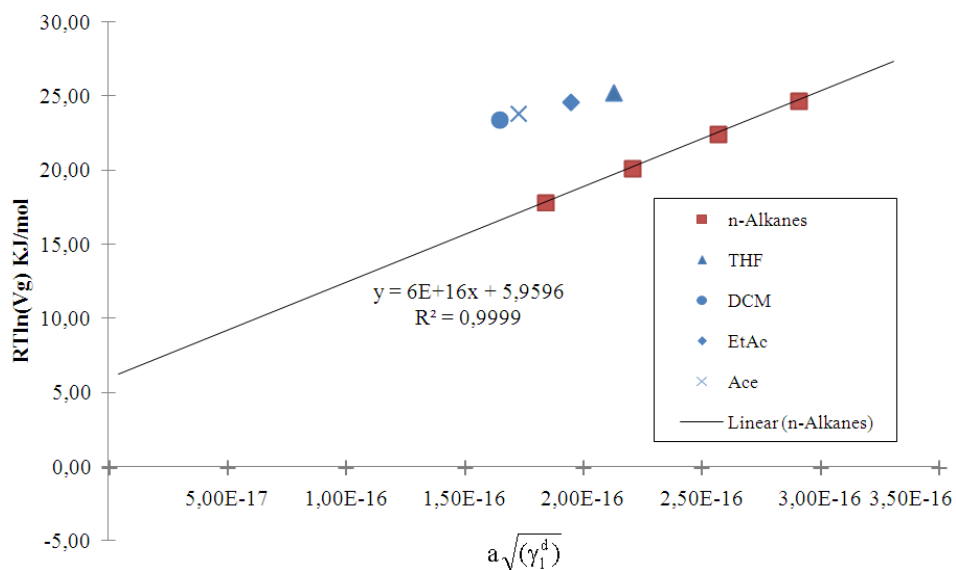
Figure 5.67 A plot of RTLn(V_g) *versus* $a\sqrt{(\gamma_l^d)}$ of n-alkane and polar probes on the

surface of Surkopak 5323, at 333.15K

Table 5.16 Retention time tr, specific retention volume V_g, Gibbs free energy

of adsorption RTLn(V_n), for the n-alkanes on Surkopak 5323, at T = 343.5 K,

F = 50 cm³min-1, CH₄ = 29.4 s, J = 0.66, C = 0.90, P_i = 196 kPa, P_o = 101 kPa, m=0.93 gr

Probe Molecule	t_r (s)	V_n (cm³/g)	ln V_n (cm³/g)	RTln(V_n) (kJ/mol)	V_g	RTln(V_g) (kJ/mol)
Pentane	44.40	445.50	6.10	17.40	479.03	17.61
Hexane	65.94	1085.24	6.99	19.94	1166.92	20.15
Heptane	108.60	2352.24	7.76	22.15	2529.29	22.35
Octane	201.00	5096.52	8.54	24.36	5480.13	24.56
THF	239.40	6237.00	8.74	24.93	6706.45	25.14
DCM	143.82	3398.27	8.13	23.20	3654.05	23.40
EtAc	191.40	4811.40	8.48	24.19	5173.33	24.40
Acetone	154.20	3706.56	8.22	23.45	3985.55	23.65

Surkopak 5323, T=70°C
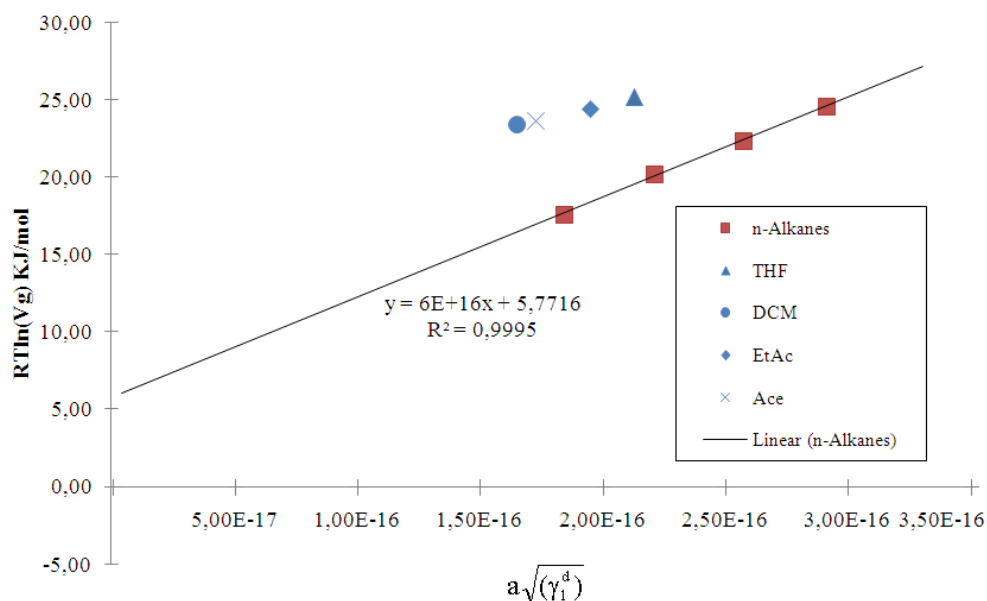
Figure 5.68 A plot of RTLn(V$_g$) *versus* $a\sqrt{(\gamma_l^d)}$ of n-alkane and polar probes on the

surface of Surkopak 5323, at 333.15K

A good correlation coefficient was obtained from each of the linear fits. The slope for

the linear fit obtained for each n-alkane plot gives the dispersive component of the

surface free energy, γ_s^d, at that temperature. The dispersive component of the surface

free energy was found to be between 33.64 - 24.80 mJ/m². This follows a trend that with

increases in temperature, the dispersive interaction becomes weaker, suggesting that it

would be easier to remove the molecules from the surface.

Determination of the specific component of the surface free energy

The behaviour of a range of polar probes was used to determine the specific

component of the surface free energy. The acidic probe used was dichloromethane,

basic probe tetrahydrofuran (THF) and amphoteric probes acetone (Ace) and ethyl

acetate (EtAc).

Plots shown in Figures 5.65 to 5.68 give the polar probe values also at the relevant temperature. The specific component of free energy was calculated using the difference between the calculated value of RTln(V_n) and that which was derived using the equation of the linear fit for the n-alkane reference line.

The values of $\Delta G_a^s/T$ against $1/T$ were plotted, allowing determination of the enthalpy and entropy of adsorption, illustrated in Figure 5.69.

Polar Probes Surkopak 5323

y = 27,188x - 0,006
R² = 0,9726

y = 30,547x - 0,0177
R² = 0,9996

y = 26,677x - 0,0095
R² = 0,9987

y = 18,876x + 0,0146
R² = 0,8734
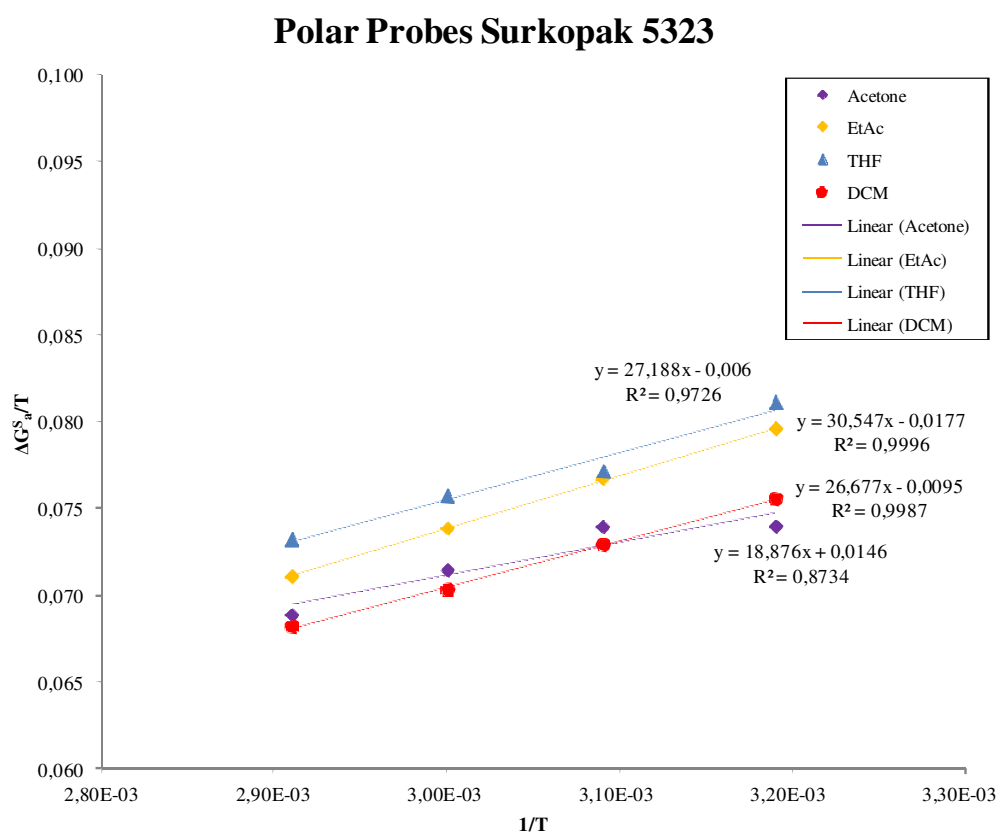
Figure 5.69 Determination of the specific component of the enthalpy of adsorption and the entropy of adsorption of polar probes, on the surface of Surkopak 5323

The values of enthalpy and entropy of adsorption for polar probes were determined from the slope and intercept as shown in Table 5.17.

Table 5.17 Specific components of the enthalpy of adsorption and the entropy of adsorption, ΔH_a^s and ΔS_a^s, respectively, of polar probes on the surface of Surkopak 5323

Probe	ΔH_a [kJ/mol]	ΔS_a [kJ/mol]
THF	27.1880	- 0.0060
DCM	26.6770	- 0.0095
Acetone	18.8760	- 0.0146
EtAc	30.5470	- 0.0177

The value of ΔH_a indicates the strength of the interaction between the probe and the surface of the pigment. Thus, the strength of interaction increases in the order: Ace<DCM<THF<EtAc. This order suggests that the polyurethane was amphoteric in nature, But the enthalpic value does not take into account the relative strengths of the basic and acidic probe molecules (*i.e.* THF is a stronger base than DCM is an acid).

Surkopak 5323 Column
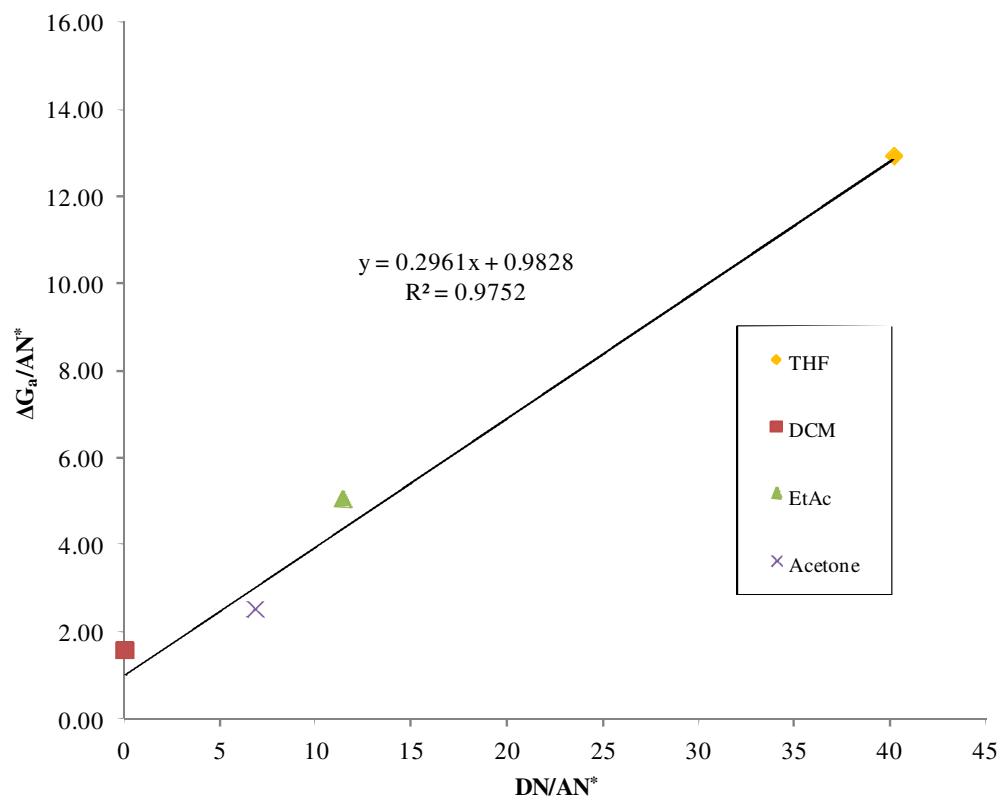
Figure 5.70 Determination of K_a and K_b for Surkopak 5323

Calculation of the K_a and K_b values allows the determination of the Lewis acidity and the Lewis basicity of the polymer. K_a and K_b are obtained from the plot of ΔH_a /AN^* against DN/AN^*, with K_a as the slope and K_b as the intercept. From the plot illustrated in Figure (5.70), it can be seen that K_a is 0.2961, and K_b is 0.9828. Thus, it can be suggested that polyurethane is predominantly Lewis basic in nature.

Evaluation of the fumaric rosin-based column

A similar approach was adopted for the second extender.

Determination of the dispersive component of surface free energy

Table 5.18 Retention time tr, specific retention volume V_g, Gibbs free energy of

adsorption RTLn(V_n), for the n-alkanes on the fumaric rosin, UCH150H at

T = 313.5 K, F = 20 cm^{3}min^{-1}, CH$_4$ = 65.82 s, J = 0.66, C = 0.61, P$_i$ = 196 kPa

P$_o$ = 101 kPa, m=1.04g

Probe Molecule	tr (s)	V_n (cm³/g)	ln V_n (cm³/g)	RTln(V_n) (kJ/mol)	V_g	RTln(V_g) (kJ/mol)
Pentane	75.90	10.08	81.16	11.45	78.04	11.34
Hexane	79.32	13.50	108.70	12.21	104.52	12.10
Heptane	85.98	20.16	162.33	13.25	156.08	13.15
Octane	102.75	36.93	297.36	14.83	285.92	14.72
THF	82.50	16.68	134.31	12.76	129.14	12.66
DCM	87.42	21.60	173.92	13.43	167.23	13.33
EtAc	83.88	18.06	145.42	12.96	139.83	12.86
Acetone	81.30	15.48	124.64	12.56	119.85	12.46

Fumaric Rosin UCH150H, T=40ºC
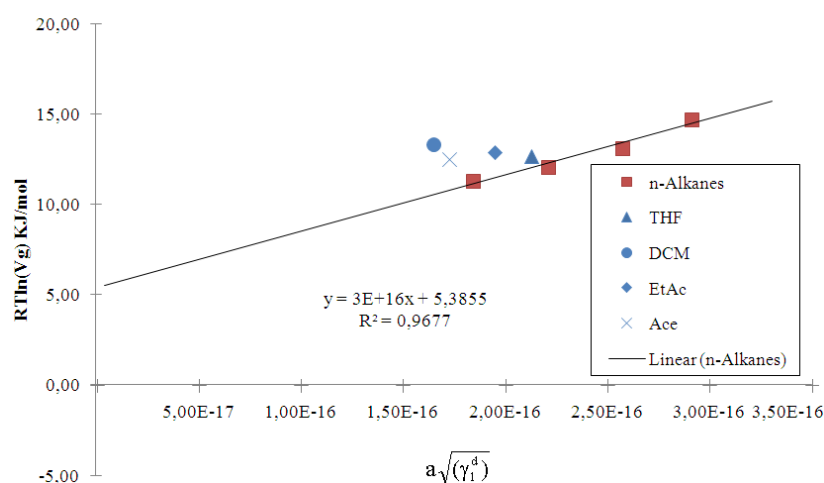
Figure 5.71 A plot of RTln(V_g) *versus* $a\sqrt{(\gamma_l^d)}$ for the n-alkane and polar probes on

the surface of the fumaric rosin (UCH150H), at 313.15K

Table 5.19 Retention time tr, specific retention volume V_g, Gibbs free energy

of adsorption RTLn(V_n), for the n-alkanes on fumaric rosin (UCH150H)

at T = 323.5 K, F = 20 cm³min⁻¹, CH₄ = 65.82 s, J = 0.66, C = 0.61, P_i = 196 kPa,

P_o = 101 kPa, m=1.04g

Probe Molecule	tr (s)	V_n (cm³/g)	ln V_n (cm³/g)	RTln(V_n) (kJ/mol)	V_g	RTln(V_g) (kJ/mol)
Pentane	73.20	7.38	59.42	10.97	57.14	10.87
Hexane	75.78	9.96	80.20	11.78	77.11	11.67
Heptane	80.52	14.70	118.36	12.83	113.81	12.72
Octane	91.20	25.38	204.36	14.29	196.50	14.19
THF	79.20	13.38	107.74	12.57	103.59	12.47
DCM	85.32	19.50	157.01	13.58	150.98	13.48
EtAc	79.32	13.50	108.70	12.60	104.52	12.49
Acetone	76.92	11.10	89.38	12.07	85.94	11.97
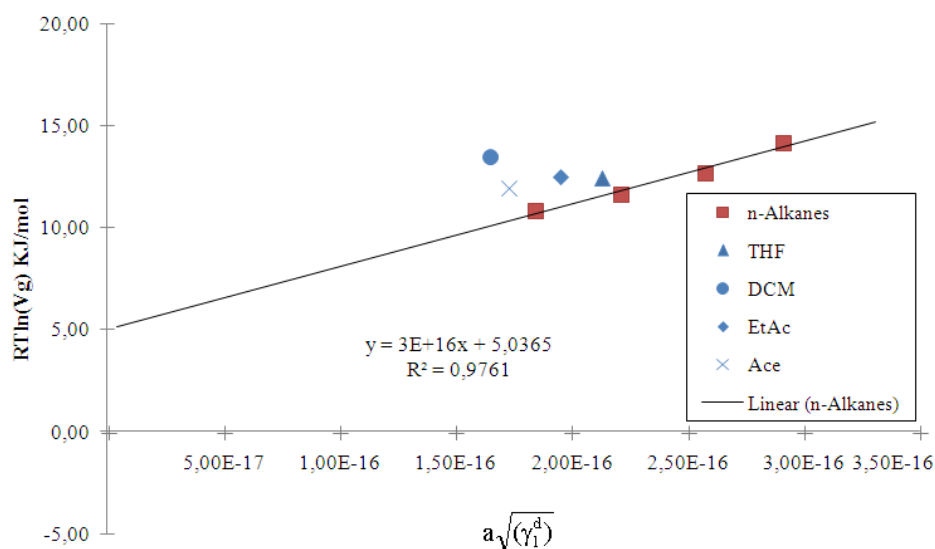
Figure 5.72 A plot of RTLn(V_g) *versus* $a\sqrt{(\gamma_l^d)}$ for n-alkane and polar probes on the

surface of the fumaric rosin (UCH150H), at 323.15K

Table 5.20 Retention time tr, specific retention volume V_g, Gibbs free energy of

adsorption RTLn(V_n), for the n-alkanes on the fumaric rosin (UCH150H),

at T = 333.5 K, F = 20 cm³min⁻¹, CH₄ = 65.82 s, J = 0.66, C = 0.61, P_i = 196 kPa,

P_o = 101 kPa, m=1.04gr

Probe Molecule	tr (s)	V_n (cm³/g)	ln V_n (cm³/g)	RTln(V_n) (kJ/mol)	V_g	RTln(V_g) (kJ/mol)
Pentane	70.80	4.98	40.10	10.22	38.56	10.12
Hexane	73.08	7.26	58.46	11.27	56.21	11.16
Heptane	76.38	10.56	85.03	12.31	81.76	12.20
Octane	83.82	18.00	144.94	13.78	139.36	13.67
THF	75.72	9.90	79.71	12.13	76.65	12.02
DCM	82.50	16.68	134.31	13.57	129.14	13.46
EtAc	76.32	10.50	84.55	12.29	81.29	12.18
Acetone	74.28	8.46	68.12	11.69	65.50	11.58
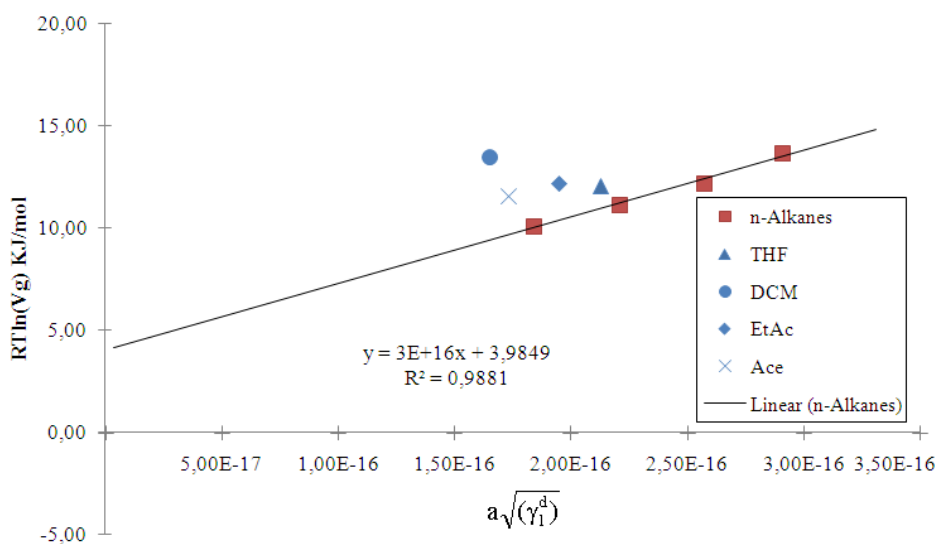
Figure 5.73 A plot of RTLn(V_g) *versus* $a\sqrt{(\gamma_l^d)}$ of n-alkane and polar probes on the

surface of the fumaric rosin (UCH150H), at 333.15K

Table 5.21 Retention time tr, specific retention volume V_g, Gibbs free energy of

adsorption RTLn(V_n), for the n-alkanes on Fumaric rosin (UCH150H)

at T = 343.5 K, F = 20 cm³min⁻¹, CH₄ = 65.82 s, P_{H2O}=0.4, J = 0.66, C = 0.61,

P_i = 196 kPa, P_o = 101 kPa, m=1.04g

Probe Molecule	tr (s)	V_n (cm³/g)	ln V_n (cm³/g)	RTln(V_n) (kJ/mol)	V_g	RTln(V_g) (kJ/mol)
Pentane	69.42	3.60	28.99	9.61	27.87	9.49
Hexane	70.80	4.98	40.10	10.53	38.56	10.42
Heptane	73.08	7.26	58.46	11.61	56.21	11.49
Octane	78.30	12.48	100.49	13.15	96.62	13.04
THF	73.20	7.38	59.42	11.65	57.14	11.54
DCM	79.50	13.68	110.15	13.41	105.91	13.30
EtAc	73.08	7.26	58.46	11.61	56.21	11.49
Acetone	73.20	7.38	59.42	11.65	57.14	11.54
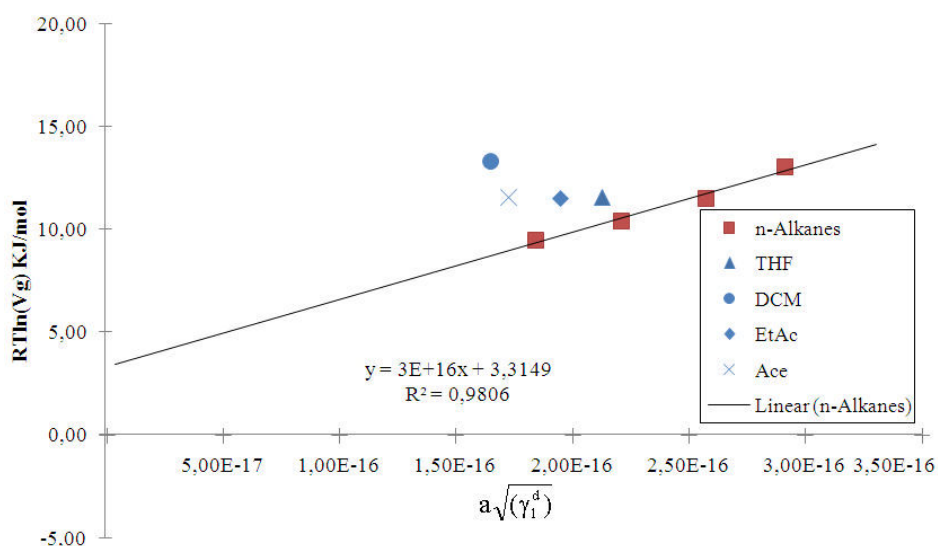
Figure 5.74 A plot of RTLn(V_g) *versus* $a\sqrt{(\gamma_l^d)}$ of n-alkane and polar probes on the

surface of the fumaric rosin (UCH150H), at 343.15K

Table 5.22 Retention time tr, specific retention volume V_g, Gibbs free energy of

adsorption $RTLn(V_n)$, for the n-alkanes on the fumaric rosin (UCH150H),

at T = 353.5 K, F = 20 cm³min⁻¹, CH_4 = 65.82 s, P_{H2O}=0.4, J = 0.66, C = 0.61,

P_i = 196 kPa, P_o = 101 kPa, m=1.04g

Probe Molecule	tr (s)	V_n (cm³/g)	ln V_n (cm³/g)	$RTln(V_n)$ (kJ/mol)	V_g	$RTln(V_g)$ (kJ/mol)
Pentane	67.32	1.50	12.08	7.31	11.61	7.20
Hexane	68.88	3.06	24.64	9.41	23.69	9.29
Heptane	70.8	4.98	40.10	10.84	38.56	10.72
Octane	75.18	9.36	75.37	12.69	72.47	12.58
THF	71.52	5.70	45.90	11.23	44.13	11.12
DCM	76.38	10.56	85.03	13.05	81.76	12.93
EtAc	71.58	5.76	46.38	11.27	44.60	11.15
Acetone	72.18	6.36	51.21	11.56	49.24	11.44
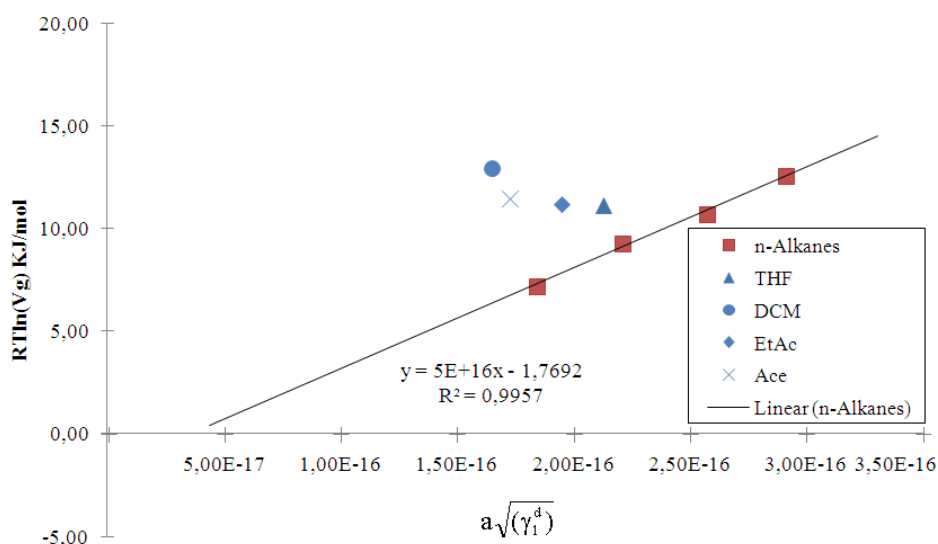
Figure 5.75 A plot of $RTLn(V_g)$ *versus* $a\sqrt{(\gamma_l^d)}$ of n-alkane and polar probes on the

surface of the fumaric rosin (UCH150H), at 353.15K

The dispersive component of the surface free energy was found to lie between 49.9 – 64.4 mJ/m^2. This finding does not follow the expected trend that, with an increase in the temperature of the system, the dispersive interaction becomes weaker. This implies that the composition is not as straightforward or simple as is usually depicted.

Determination of the specific component of the surface free energy

Polar Probes Fumaric Rosin UCH150H

Figure 5.76 Determination of the specific component of the enthalpy

of adsorption and the entropy of adsorption of the polar probes on the surface of the

fumaric rosin (UCH150H)

Table 5.23 Specific components of the enthalpy of adsorption and the entropy

of adsorption, ΔH_a^s and ΔS_a^s, respectively, of polar probes on the surface of the

fumaric rosin (UCH150H)

Probe	ΔH_a[kJ/mol]	ΔS_a [kJ/mol]
THF	25.22	- 0.0398
DCM	13.834	- 0.0014
Acetone	26.659	- 0.0439
EtAc	20.254	- 0.0254

The value of ΔH_a indicates the strength of the interaction between the probe and the surface of the pigment. Thus, the strength of interaction increases in the order: DCM<EtAc<THF<Acetone. This order suggests that the fumaric rosin is amphoteric in nature.

From the plot illustrated in Figure 5.77, it can be seen that K_a is 0.2731, and K_b is 0.7435. Thus, it can be suggested that the fumaric rosin was predominantly basic in nature. However, this basicity is lower than that of the polyurethane considered earlier.
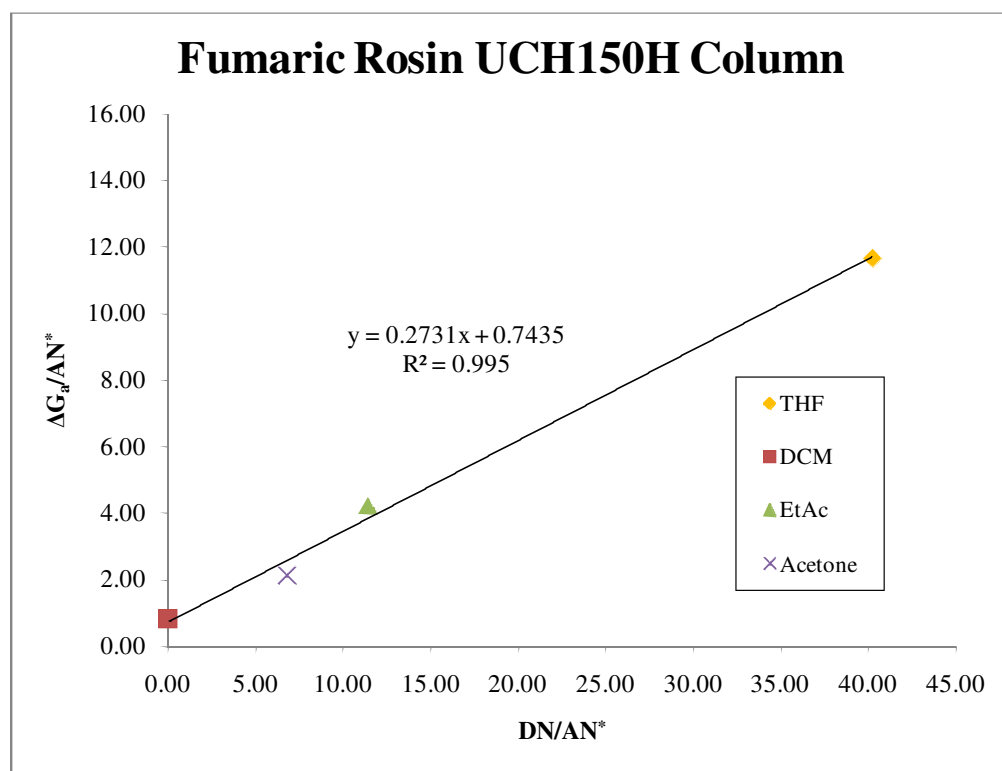
Figure 5.77 Determination of K_a and K_b for the fumaric rosin (UCH150H)

Evaluation of column containing BOPP-PU

Determination of the dispersive component of the surface free energy

The relevant information is given for the BOPP-PU system.

Table 5.24 Retention time tr, specific retention volume V_g, Gibbs free energy

of adsorption RTLn(V_n), for the n-alkanes on BOPP-Surkopak 5323,

at T = 313.15 K, F = 20 cm³min-1, CH_4 = 67.62 s, P_{H2O}=0.4, J = 0.66, C = 0.61,

P_i = 196 kPa, P_o = 101 kPa, m=0.54 gr

Probe Molecule	tr (s)	V_n (cm³/g)	ln V_n (cm³/g)	RTln(V_n) (kJ/mol)	V_g	RTln(V_g) (kJ/mol)
Pentane	79.50	95.66	4.56	11.87	177.14	13.48
Hexane	90.48	184.07	5.22	13.58	340.87	15.18
Heptane	128.52	490.37	6.20	16.13	908.09	17.73
Octane	243.12	1413.13	7.25	18.88	2,616.90	20.49
THF	98.82	251.22	5.53	14.39	465.23	15.99
DCM	83.58	128.51	4.86	12.64	237.98	14.25
EtAc	93.90	211.61	5.35	13.94	391.86	15.55
Acetone	79.80	98.07	4.59	11.94	181.62	13.54
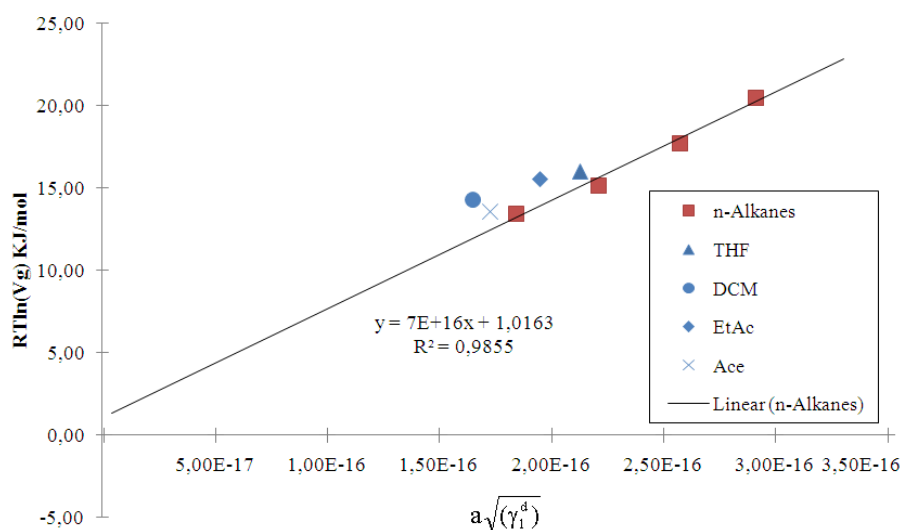
Figure 5.78 A plot of RTLn(V_g) *versus* $a\sqrt{(\gamma_l^d)}$ for the n-alkanes and the polar probes

on the surface of BOPP-Surkopak 5323, at 313.15K

Table 5.25 Retention time tr, specific retention volume V_g, Gibbs free energy

of adsorption RTLn(V_n), for the n-alkanes on BOPP-Surkopak 5323, at T = 323.15

K, F = 20 cm³min⁻¹, CH₄ = 67.62 s, P_{H2O}=0.4, J = 0.66, C = 0.61, P_i = 196 kPa,

P_o = 101 kPa, m=0.54 g

Probe	tr	V_n	ln V_n	RTln(V_n)	V_g	RTln(V_g)
Molecule	(s)	(cm³/g)	(cm³/g)	(kJ/mol)		(kJ/mol)
Pentane	76.98	75.37	4.32	11.61	139.57	13.27
Hexane	85.50	143.97	4.97	13.35	266.61	15.01
Heptane	113.82	372.00	5.92	15.90	688.89	17.56
Octane	196.68	1,039.19	6.95	18.66	1,924.43	20.32
THF	91.68	193.73	5.27	14.15	358.76	15.80
DCM	79.68	97.11	4.58	12.29	179.83	13.95
EtAc	86.52	152.18	5.03	13.50	281.82	15.16
Acetone	76.08	68.12	4.22	11.34	126.15	13.00
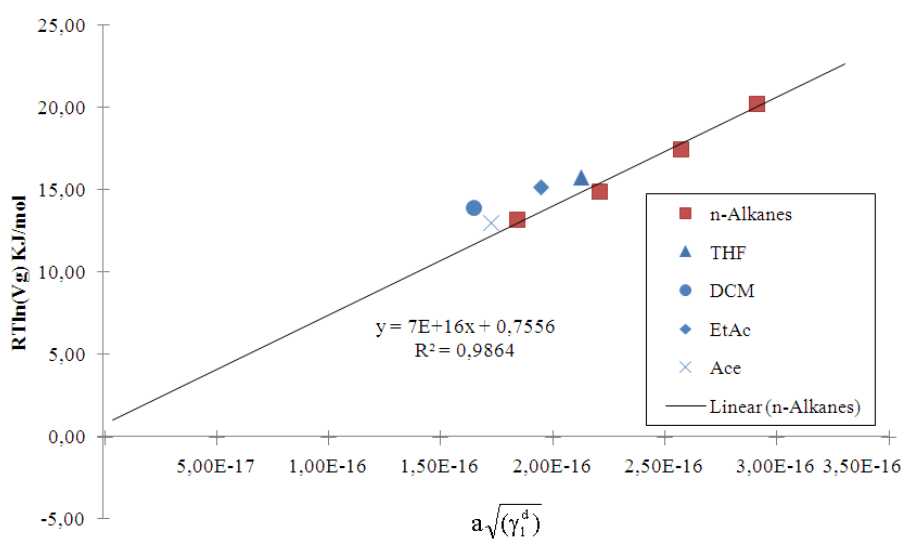
Figure 5.79 A plot of RTLn(V_g) *versus* $a\sqrt{(\gamma_l^d)}$ of n-alkanes and polar probes on the

surface of BOPP-Surkopak 5323, at 323.15K

Table 5.26 Retention time tr, specific retention volume V_g, Gibbs free energy of

adsorption RTLn(V_n), for the n-alkanes on BOPP-Surkopak 5323, at T = 333.15 K,

F = 20 cm³min⁻¹, CH_4 = 67.62 s, P_{H2O}=0.4, J = 0.66, C = 0.61, P_i = 196 kPa,

P_o = 101 kPa, m=0.54 g

Probe Molecule	tr (s)	V_n (cm³/g)	ln V_n (cm³/g)	RTln(V_n) (kJ/mol)	V_g	RTln(V_g) (kJ/mol)
Pentane	73.92	50.73	3.93	10.88	93.94	12.58
Hexane	82.38	118.85	4.78	13.23	220.09	14.94
Heptane	104.52	297.12	5.69	15.77	550.22	17.48
Octane	168.18	809.71	6.70	18.55	1,499.46	20.26
THF	88.32	166.68	5.12	14.17	308.66	15.88
DCM	77.28	77.78	4.35	12.06	144.04	13.77
EtAc	82.98	123.68	4.82	13.34	229.03	15.05
Acetone	74.52	55.56	4.02	11.13	102.89	12.83

BOPP-Surkopak 5323, T=60°C

$y = 7E+16x - 0,7234$
$R^2 = 0,9969$
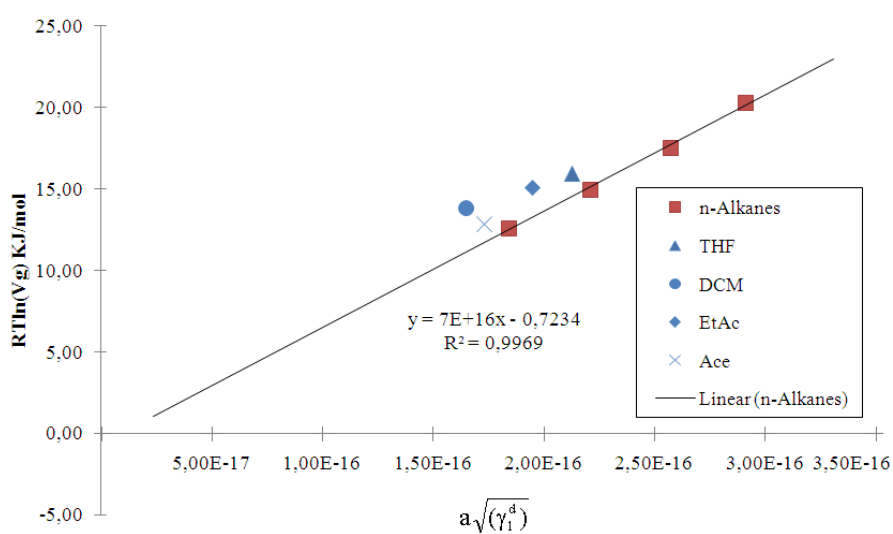
Figure 5.80 A plot of RTLn(V_g) *versus* $a\sqrt{(\gamma_l^d)}$ of the n-alkanes and the polar probes

on the surface of BOPP-Surkopak 5323, at 333.15K

Table 5.27 Retention time tr, specific retention volume V_g, Gibbs free energy of

adsorption RTLn(V_n), for the n-alkanes on BOPP-Surkopak 5323, at T = 343.15 K,

F = 20 cm^{3}min^{-1}, CH$_4$ = 67.62 s, P_{H2O}=0.4, J = 0.66, C = 0.61, P_i = 196 kPa,

P_o = 101 kPa, m=0.54 g

Probe Molecule	tr (s)	V_n (cm³/g)	ln V_n (cm³/g)	RTln(V_n) (kJ/mol)	V_g	RTln(V_g) (kJ/mol)
Pentane	72.30	37.68	3.63	10.35	69.78	12.11
Hexane	79.02	91.79	4.52	12.89	169.99	14.65
Heptane	97.68	242.04	5.49	15.66	448.23	17.42
Octane	151.8	677.82	6.52	18.60	1,255.22	20.36
THF	84.00	131.89	4.88	13.93	244.24	15.69
DCM	75.90	66.67	4.20	11.98	123.46	13.74
EtAc	79.50	95.66	4.56	13.01	177.14	14.77
Acetone	71.7	32.85	3.49	9.96	60.84	11.72
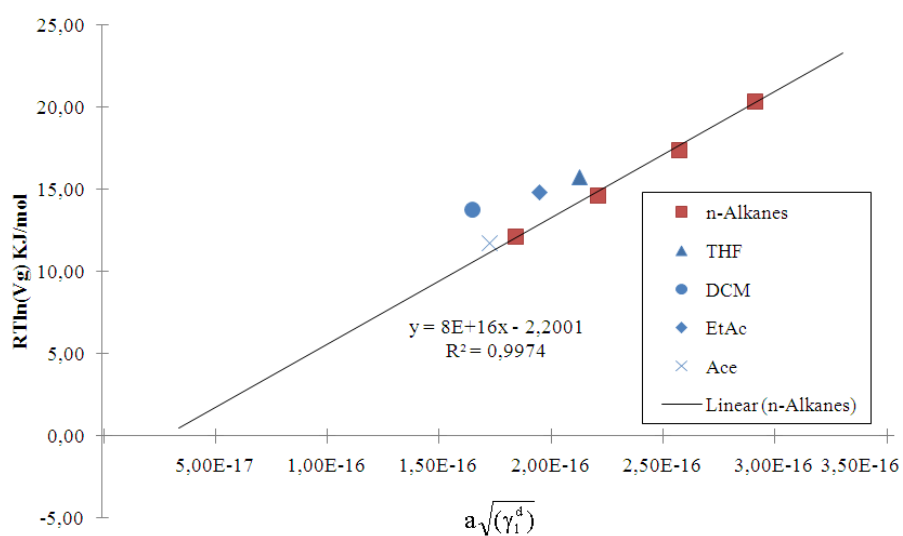
Figure 5.81 A plot of RTLn(V_g) *versus* $a\sqrt{(\gamma_l^d)}$ for the n-alkanes and the polar probes

on the surface of BOPP-Surkopak 5323, at 343.15K

The dispersive component of the surface free energy was found to be between 33.64 – 81.5 mJ/m². which does not conform to the previously observed trend that with increasing in temperature, the dispersive interaction becomes weaker. This raises the possibility of chemical interventions arising during measurement.

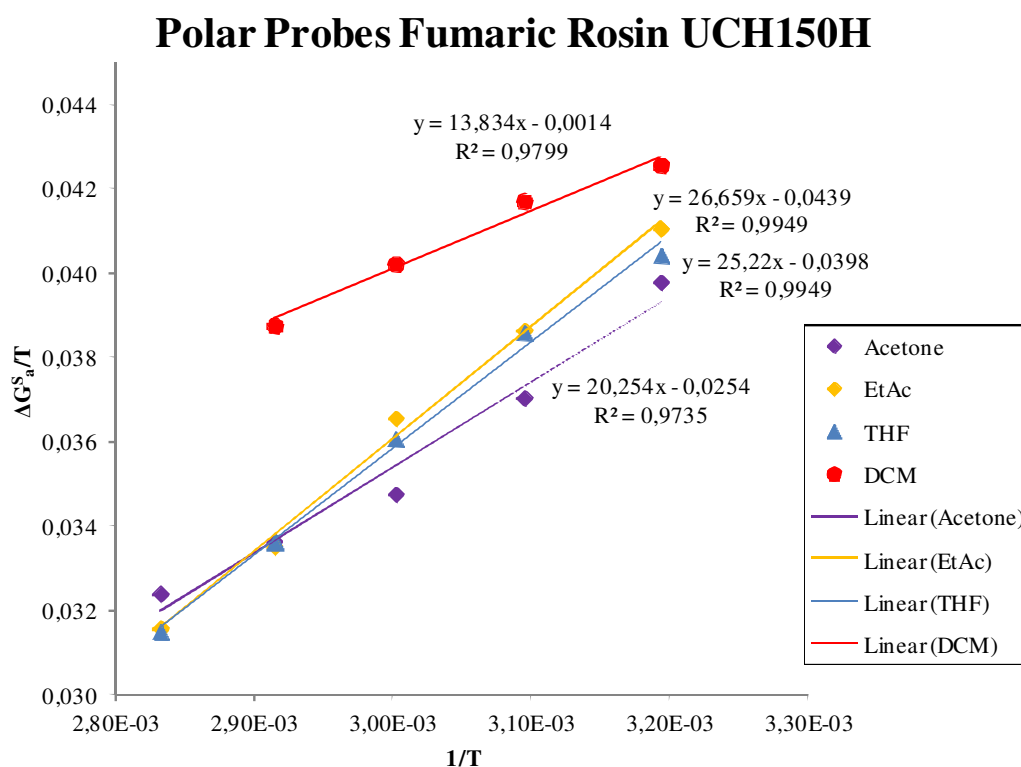**Determination of the specific component of the surface free energy**
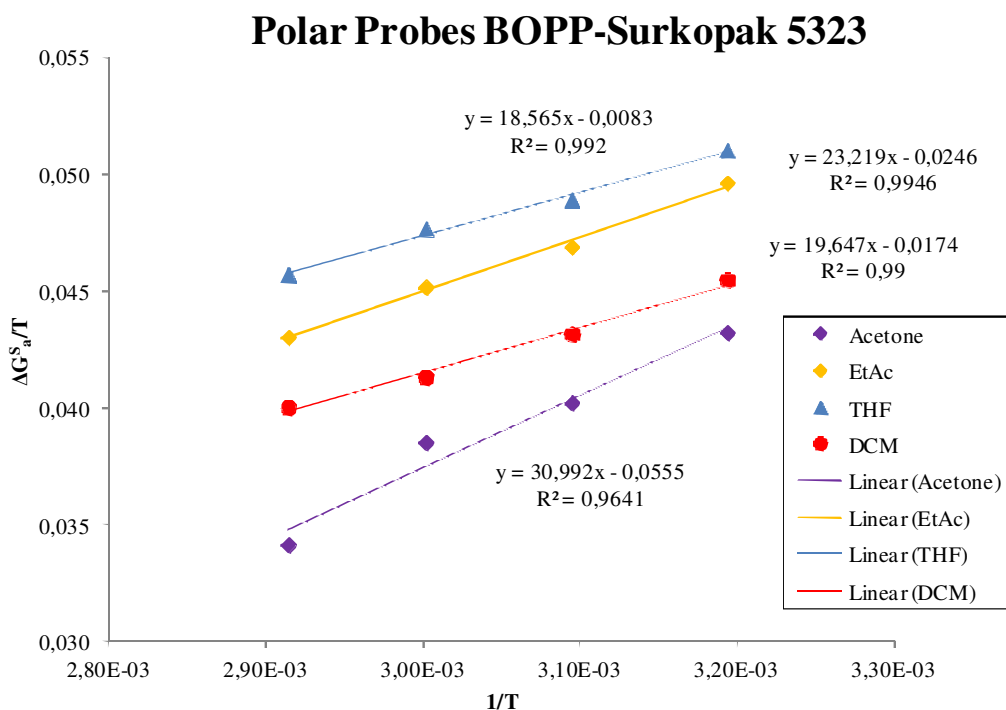
Figure 5.82. Determination of the specific component of the enthalpy

of adsorption and the entropy of adsorption of polar probes on the surface

of BOPP-Surkopak 5323

Table 5.28 Specific components of the enthalpy of adsorption and the entropy

of adsorption, ΔH_a^s and ΔS_a^s, respectively, of polar probes on the surface

of BOPP-Surkopak 5323

Probe	ΔH_a[kJ/mol]	ΔS_a [kJ/mol]
THF	18.56	- 0.0083
DCM	19.647	- 0.0174
Acetone	30.992	- 0.0555
EtAc	23.219	- 0.0246

The value of ΔH_a indicates the strength of the interaction between the probe and the

surface of the BOPP-Surkopak 5323. Thus, the strength of interaction increases in

the order: THF<DCM<ETAC<Acetone. This order suggests that the BOPP-Surkopak

5323 is amphoteric in nature, the properties being dominated by the Surkopak 5323

component of the composite system.

BOPP-Surkopak 5323 Column

y = 0.1852x + 1.4653
R² = 0.9957
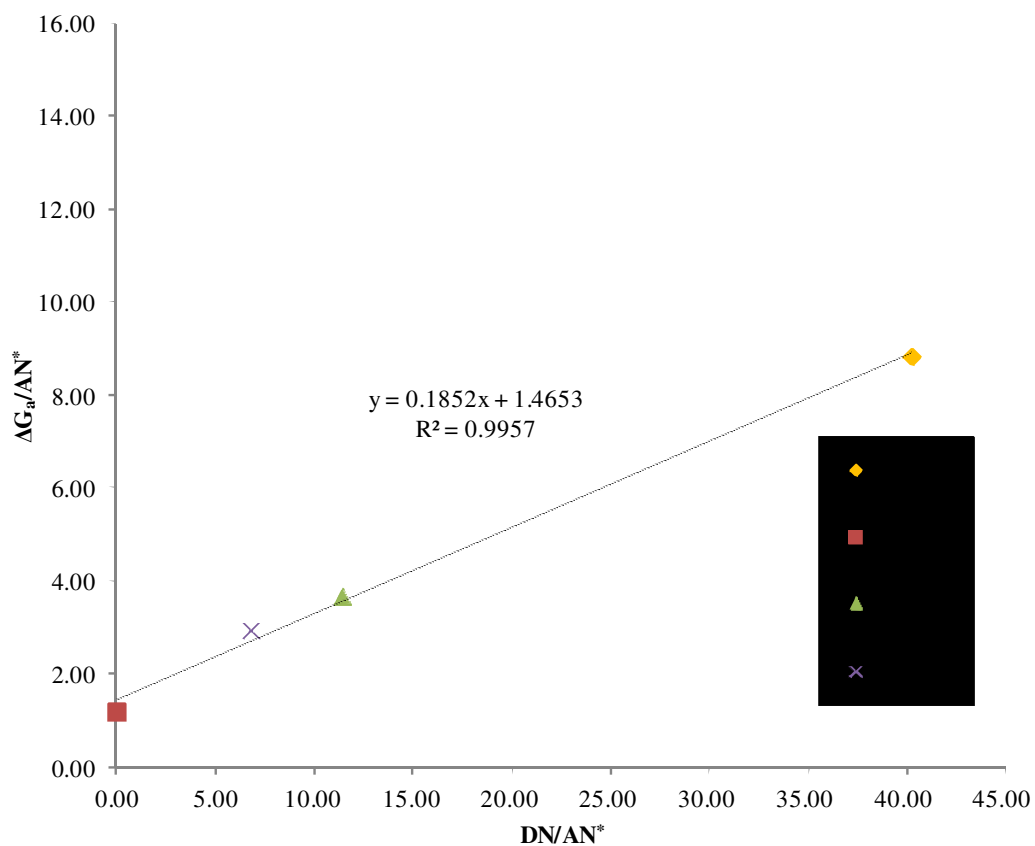
Figure 5.83 Determination of K_a and K_b for BOPP-Surkopak 5323

From calculation of the K_a and K_b values allow one to determine the Lewis acidity and the Lewis basicity of the polymer. From the plot illustrated in Figure (5.83), it can be seen that K_a is 0.1852, and K_b is 1.4653. Thus, it can be suggested that BOPP-PU is remarkably basic in nature. This pronounced basicity is greater than that of "pure" polyurethane.

Evaluation of BOPP-fumaric rosin (UCH150H) column

Determination of the dispersive component of surface free energy

Table 5.29 Retention time tr, specific retention volume V_g, Gibbs free energy

of adsorption $RTLn(V_n)$, for the n-alkanes on BOPP-fumaric rosin (UCH150H)

at T = 373.15 K, F = 20 cm³min⁻¹, CH_4 = 101.4 s, P_{H2O}=0.4, J = 0.66, C = 0.61,

P_i = 196 kPa, P_o = 101 kPa, m=0.68 g

| Probe Molecule	tr (s)	V_n (cm³/g)	ln V_n (cm³/g)	$RTln(V_n)$ (kJ/mol)	V_g	$RTln(V_g)$ (kJ/mol)
Pentane	127.50	209.67	16.58	308.34	5.73	17.78
Hexane	151.02	399.06	18.58	586.85	6.37	19.78
Heptane	208.98	865.75	20.98	1273.16	7.15	22.18
Octane	329.88	1,839.24	23.32	2704.76	7.90	24.52
THF	169.98	551.72	19.59	811.36	6.70	20.78
DCM	138.48	298.09	17.68	438.36	6.08	18.87
EtAc	145.68	356.06	18.23	523.62	6.26	19.42
Acetone	124.98	189.38	16.27	278.50	5.63	17.46

BOPP-Fumaric Rosin UCH150H, T=100ºC
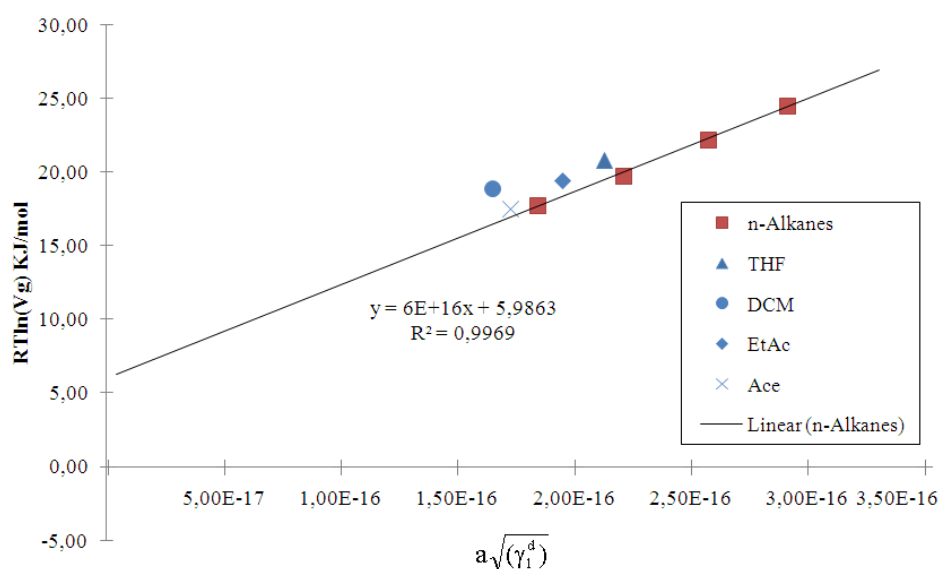
Figure 5.84 A plot of $RTLn(V_g)$ *versus* $a\sqrt{(\gamma_l^d)}$ of the n-alkanes and the polar probes

on the surface of the BOPP-fumaric rosin (UCH150H), at 373.15K

Table 5.30 Retention time tr, specific retention volume V_g, Gibbs free energy of

adsorption RTLn(V_n), for the n-alkanes on the OPP-fumaric rosin (UCH150H) at

T = 378.15 K, F = 20 cm³min⁻¹, CH₄ = 101.46 s, P_{H2O}=0.4, J = 0.66, C = 0.61,

P_i = 196 kPa, P_o = 101 kPa, m=0.68 g

| Probe Molecule	tr (s)	V_n (cm³/g)	ln V_n (cm³/g)	RTln(V_n) (kJ/mol)	V_g	RTln(V_g) (kJ/mol)
Pentane	126.92	205.00	16.74	301.48	5.71	17.95
Hexane	150.48	394.71	18.79	580.45	6.36	20.01
Heptane	203.28	819.85	21.09	1,205.67	7.09	22.31
Octane	311.40	1,690.44	23.37	2,485.94	7.82	24.58
THF	165.90	518.87	19.65	763.05	6.64	20.87
DCM	136.68	283.59	17.76	417.05	6.03	18.97
EtAc	143.52	338.67	18.31	498.04	6.21	19.53
Acetone	123.78	179.72	16.32	264.30	5.58	17.53
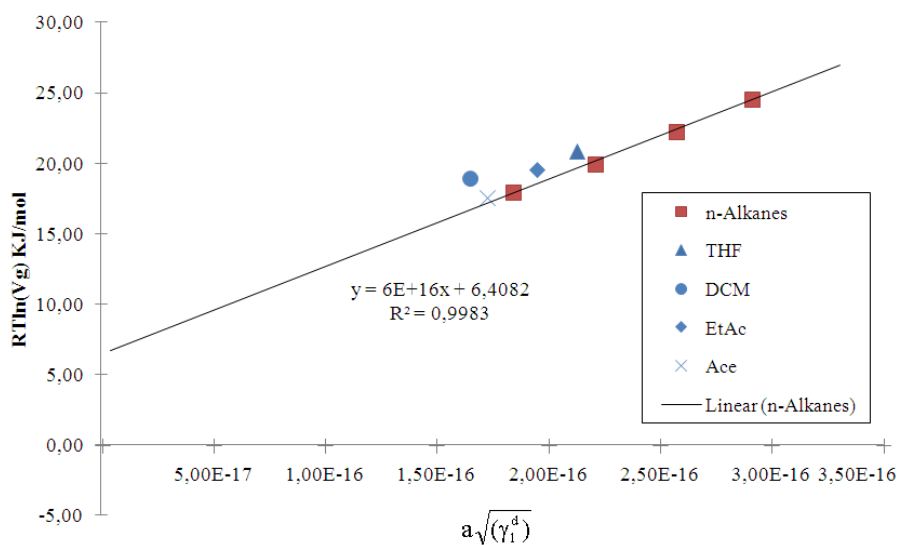
Figure 5.85 A plot of RTLn(V_g) *versus* $a\sqrt{(\gamma_i^d)}$ of the n-alkanes and the polar probes

on the surface of BOPP-fumaric rosin (UCH150H), at 378.15K

Table 5.31 Retention time tr, specific retention volume V_g, Gibbs free energy

of adsorption RTLn(V_n), for the n-alkanes on the BOPP-fumaric rosin (UCH150H) at

T = 383.15 K, F = 20 cm³min⁻¹, CH$_4$ = 101.46 s, P$_{H2O}$=0.4, J = 0.66, C = 0.61,

P$_i$ = 196 kPa, P$_o$ = 101 kPa, m=0.68 g

Probe Molecule	tr (s)	V_n (cm³/g)	ln V_n (cm³/g)	RTln(V_n) (kJ/mol)	V_g	RTln(V_g) (kJ/mol)
Pentane	126.48	201.46	16.90	2.96	1.09	3.46
Hexane	148.98	382.63	18.94	5.63	1.73	5.50
Heptane	196.92	768.64	21.17	11.30	2.43	7.73
Octane	290.52	1,522.31	23.34	22.39	3.11	9.90
THF	161.88	486.50	19.71	7.15	1.97	6.27
DCM	134.52	266.20	17.79	3.91	1.36	4.35
EtAc	139.98	310.16	18.28	4.56	1.52	4.83
Acetone	122.52	169.58	16.35	2.49	0.91	2.91

BOPP-Fumaric Rosin UCH150H, T=110°C
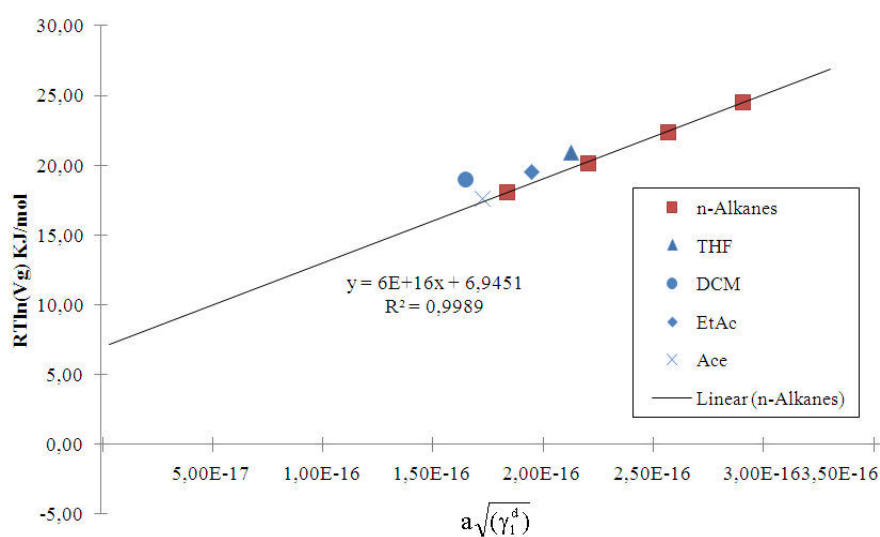
Figure 5.86 A plot of RTLn(V_g) *versus* $a\sqrt{(\gamma_l^d)}$ of the n-alkanes and the polar probes

on the surface of the BOPP-fumaric rosin (UCH150H), at 383.15K

Table 5.32 Retention time tr, specific retention volume V_g, Gibbs free energy

of adsorption RTLn(V_n), for the n-alkanes on the BOPP-fumaric rosin (UCH150H)

at T = 388.15 K, F = 20 cm³min⁻¹, CH₄ = 101.46 s, P_{H2O}=0.4, J = 0.66, C = 0.61,

P_i = 196 kPa, P_o = 101 kPa, m=0.68 gr

Probe Molecule	tr (s)	V_n (cm³/g)	ln V_n (cm³/g)	RTln(V_n) (kJ/mol)	V_g	RTln(V_g) (kJ/mol)
Pentane	126.35	200.41	17.10	294.73	5.69	18.35
Hexane	147.18	368.14	19.07	541.38	6.29	20.31
Heptane	189.48	708.74	21.18	1,042.26	6.95	22.43
Octane	272.52	1,377.38	23.33	2,025.55	7.61	24.57
THF	158.52	459.45	19.78	675.66	6.52	21.03
DCM	132.18	247.36	17.78	363.76	5.90	19.03
EtAc	136.92	285.52	18.25	419.89	6.04	19.49
Acetone	120.60	154.12	16.26	226.64	5.42	17.50

BOPP-Fumaric Rosin UCH150H, T=115°C
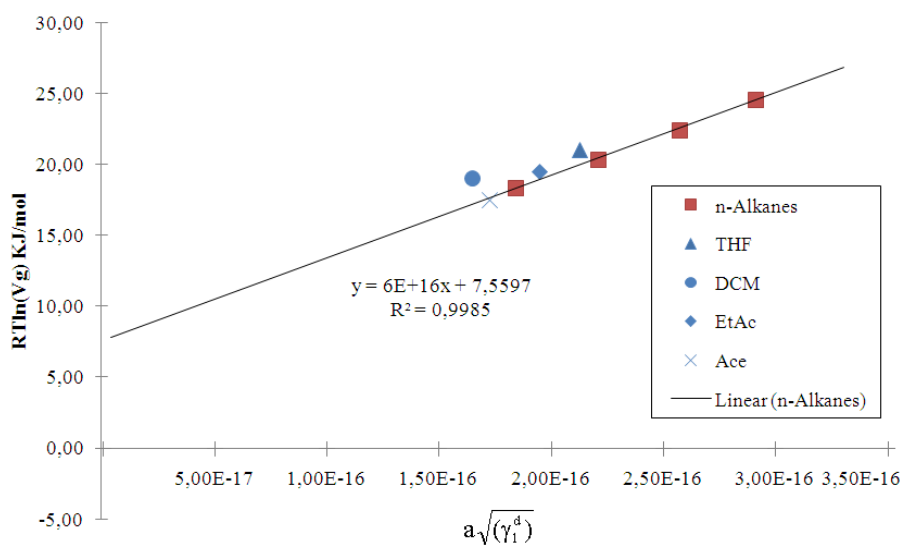
Figure 5.87 A plot of RTLn(V_g) *versus* $a\sqrt{(\gamma_i^d)}$ of the n-alkanes and the polar probes

on the surface of the BOPP-fumaric rosin (UCH150H), at 388.15K

The dispersive component of the surface free energy was between 49.8 mJ/m² at all the studied temperatures, which as before, not consistent with the trend that with increasing temperature, the dispersive interaction becomes weaker.

But is unlikely to be the fumaric rosin UCH150H that is changing, as the thermal analysis results suggest that it is stable at these temperatures.

Determination of the specific component of the surface free energy
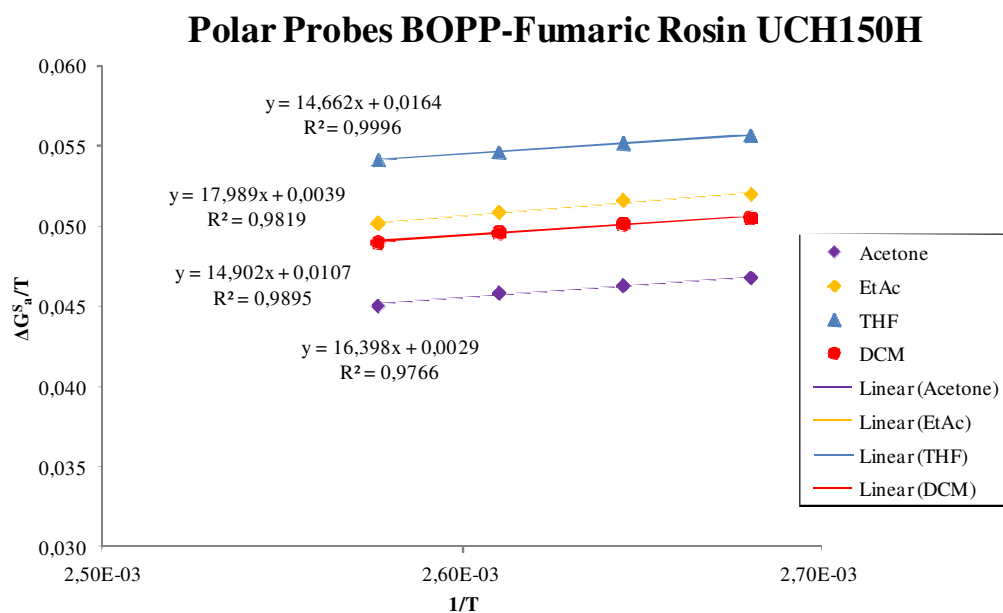
Figure 5.88 Determination of the specific component of the enthalpy

of adsorption and the entropy of adsorption of polar probes on the surface of BOPP-

fumaric rosin (UCH150H)

Table 5.33 Specific components of the enthalpy of adsorption and the entropy of

adsorption, ΔH_a^s and ΔS_a^s, respectively, of polar probes on the surface of BOPP-

fumaric rosin (UCH150H)

Probe	ΔH_a[kJ/mol]	ΔS_a [kJ/mol]
THF	14.662	0.0164
DCM	14.902	0.0107
Acetone	17.989	0.0039
EtAc	16.398	0.0029

The value of ΔH_a indicates the strength of the interaction between the probe and the surface of the pigment. Thus, the strength of interaction increases in the order: THF<DCM<ETAC<Acetone. This order suggests that the BOPP-fumaric rosin combination is amphoteric in nature, which is the same conclusion as that drawn up for the BOPP-PU column.

BOPP-Fumaric Rosin UCH150H Column

$$y = 0{,}1535x + 0{,}837$$
$$R^2 = 0{,}9919$$
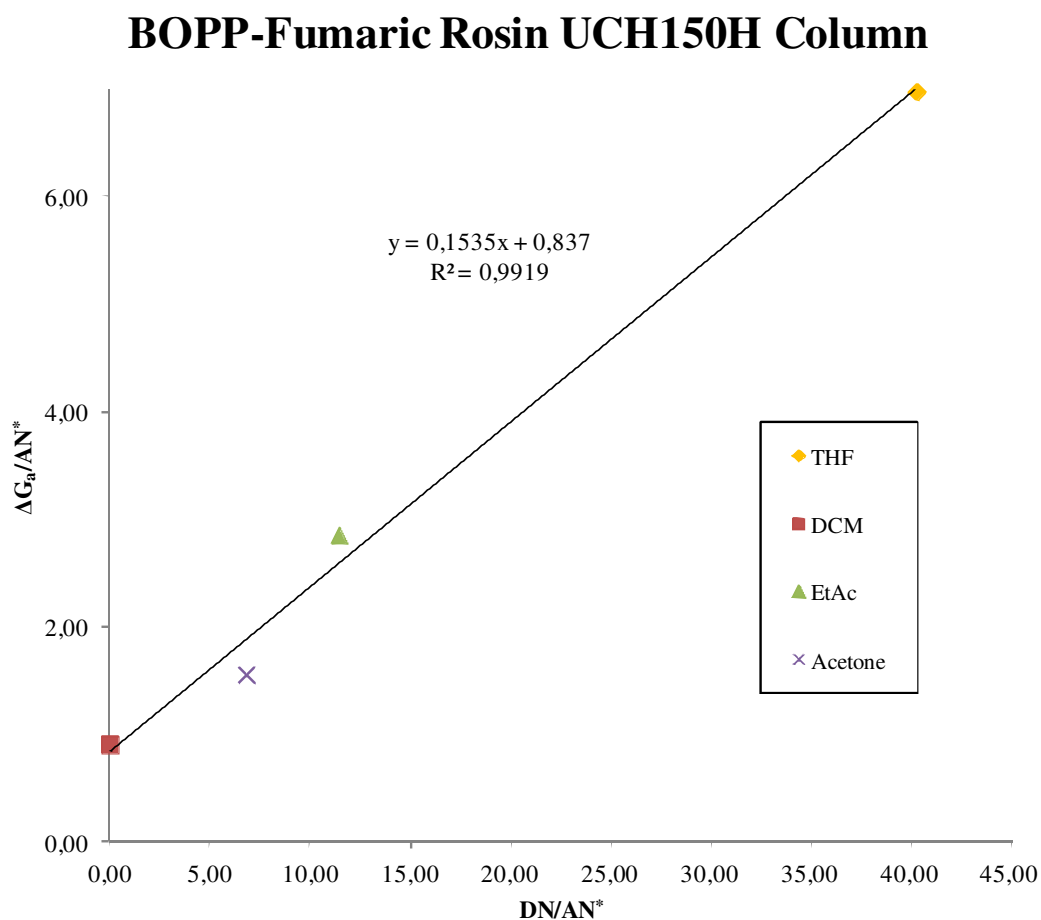
Figure 5.89 Determination of K_a and K_b for BOPP-fumaric rosin (UCH150H)

Calculation of K_a and K_b values allows one to determine the Lewis acidity and the Lewis basicity of the polymer concerned. From the plot illustrated in Figure (5.89), it can be seen that K_a is 0.1535, and K_b is 0.837. Thus, it can be suggested that the

BOPP-fumaric rosin combination is remarkably basic in nature, this basicity being greater than that of the polyurethane.

Table 5.34 Dispersive component of the surface free energy mJ/m² of the studied columns

	Dispersive component of the Surface free energy mJ/m²	Temperature scale of this study ºC
Fumaric rosin UCH150H	49.90 - 64.4	40 – 80
Surkopak 5323	24.80 - 33.64	40 - 80
BOPP-Surkopak 5323	33.64 - 81.50	40 - 70
BOPP-fumaric rosin	49.80	100 - 115

The dispersive component of the free energy of the fumaric rosin, and of the BOPP-fumaric rosin combination was calculated at 49.8 mJ m⁻² for both samples. Also, the dispersive component of the free energy of PU and of BOPP-PU was calculated at 33.64 mJ m⁻² for both samples. Hence, applying the polymer onto the BOPP did not affect the values of the Gibbs free energy of adsorption.

Table 5.35 The order of change in entropy in studied columns

	Strength of interaction
Fumaric rosin (UCH150H)	DCM<EtAc<THF<Ace
Surkopak 5323	Ace<DCM<THF<EtAc
BOPP-Surkopak 5323	THF<DCM<EtAc<Ace
BOPP-fumaric rosin (UCH150H)	THF<DCM<EtAc<Ace

Table 5.36 Specific components of the enthalpy of adsorption and the entropy

of adsorption, ΔH_a^s and ΔS_a^s, respectively, for the polar probes on the surface of the

Surkopak 5323, UCH150H, the BOPP-Surkopak 5323 and the BOPP-fumaric rosin

(UCH150H)

	Surkopak 5323		Fumaric rosin UCH150H		BOPP-Surkopak 5323		BOPP-fumaric rosin UCH150H	
Probe Molecule	ΔH_a^s (kJmol^{-1})	ΔS_a^s (Jmol^{-1}K^{-1})	ΔH_a^s (kJmol^{-1})	ΔS_a^s (Jmol^{-1}K^{-1})	ΔH_a^s (kJmol^{-1})	ΔS_a^s (Jmol^{-1}K^{-1})	ΔH_a^s (kJmol^{-1})	ΔS_a^s (Jmol^{-1}K^{-1})
THF	27.19	-6.00	25.22	-39.80	18.56	-8.30	14.66	16.40
DCM	26.68	-9.50	13.830	-1.40	19.647	-17.40	14.90	10.70
ACE	18.88	-14.60	26.66	-43.90	30.99	-5.55	17.99	3.90
EAA	30.55	-17.70	20.25	-25.40	23.22	-2.46	16.40	2.90

The ΔH_a^s values obtained suggest that the four studied samples exhibit similar

interaction profiles with the strongest interactions occurring with the amphoteric

probe molecules ACE and EAA.

The ΔH_a^s values obtained for UCH150H and Surkopak 5323 are greater for

amphoteric molecules ACE and EAA, and for the basic molecules (THF) than for the

acidic molecule (DCM).

However, it is clear that the ΔH_a^s value of UCH150H with DCM is the lowest value.

Thus, the surface of UCH150H is Lewis amphoteric with greater Lewis acidity than

that possessed by Surkopak 5323.

After printing the BOPP surface with the fumaric rosin (UCH150H) and the Surkopak 5323, it is still amphoteric but with strong Lewis-basic character. The Lewis acidity of UCH150H and Surkopak 5323 was reduced.

If the value of ΔH_a^s can be considered to indicate the strength of the interaction between the probe and the surface of studied system, (Fagelman and Guthrie, 2005), then the strength of interaction in the systems under study here increases in the orders mentioned in table 5.35. These orders suggest that all of the studied columns were amphoteric in nature.

An increase of the system's entropy implies an increase in the number of degrees of freedom and a considerable increase in the disorder of the system. This may be the case, if the entropy of the adsorbent increases sufficiently owing to adsorption (Santos et al, 2002) or to chemical interactions having occurred, resulting in chemical changes in the adsorbent species. Thus, the remarkable increase in values given by BOPP-fumaric UCH150H in comparison with to fumaric UCH150H and BOPP-Surkopak 5323 shows the better adsorption of polar molecules in case of BOPP-fumaric UCH150H system rather than other studied systems.

Table 5.37 Comparison of K_a and K_b of studied columns by IGC

	K_a	K_b
Fumaric rosin UCH150H	0.2837	0.6116
Surkopak 5323	0.2961	0.9828
BOPP-Surkopak 5323	0.1852	1.4653
BOPP-UCH150H	0.1535	0.8370

According to the previous results of K_a and K_b, we can see the following:

The results indicate a minor decrease in the Lewis acidity and an increase in the Lewis basicity of the BOPP that was coated with the fumaric rosin and the PU compared to the normal nature of these polymers. The results indicate that the Lewis basicity increases after applying the polymer onto the substrate surface (BOPP).

In comparing Surkopak 5323 with the fumaric rosin (UCH150H), it was observed that the latter is less Lewis basic than the Surkopak 5323.

Chapter 6   Conclusions

- Flexographic printing continues to grow in popularity due to its low cost and environmentally friendly nature. Ink adhesion of the printed substrate is one of the more important features.

  BOPP film has become the most rapidly implemented film product across the world, especially in printing field because of its superior printability.

  Thus, the adhesion of flexographic inks on BOPP film is of vital importance, and consequently, the investigation of flexographic ink adhesion onto BOPP substrate formed the basis of this study.

- Various formulations of flexographic ink nitro cellulose based were provided, and the preparation of flexographic NC based inks was introduced.

  It was found that the grinding process, can yield fine particle sizes of ground pigments by combining 23% pigment with 22.5% NC and the balance is alcohol solvent, where alcohols are the best used solvents in flexographic inks. Depending on this percentages, the particle size of ground pigment was less than 0.5 micron for cyan and yellow and about 1.6 micron for magenta. Moreover, the obtained pigment concentrate was stable by time, no precipitation of pigment was noticed neither a decrease in colour density.

- Once the concentrated pigment is obtained, then many kinds of extenders can be prepared and incorporated in the final flexographic ink formulation.

When the pigment concentration in flexographic inks is about 13%, then it was suggested to use 60% of pigment concentrate in the final Flexographic ink formulation and the 40% is the extender.

The suggested extenders are based mainly on two polymers, Surkopak 5323 and fumaric rosin (UCH150H), these two polymers exhibited a remarkable difference in adhesion result when incorporated in flexographic NC inks.

- The ultimate aim of this study was to illustrate the good adhesion of flexographic ink contains fumaric rosin (UCH150H) when applied to the BOPP surface in comparison with flexographic ink contains Surkopak 5323.

- Four flexographic inks were prepared, the first one contained fumaric rosin (UCH150H), the second one contained fumaric rosin (UCH150H) and Surkopak 5323, the third one contained only Surkopak 5323 and the final one contained Surkopak 5323 with Tyzor AA75 as an additive to improve the adhesion of flexographic ink NC based when applied to the BOPP surface.

- The adhesion of the four prepared flexographic inks when applied to BOPP surface were compared, the inks contained fumaric rosin (UCH150H) exhibited better adhesion than the inks contained Surkopak 5323.

Also, the viscosity of prepared inks were compared, the viscosity of inks contain Surkopak 5323 were stable by time, while the viscosity of   ink

contained fumaric rosin (UCH150H) increased by time, but this   increase   was about 10 seconds, which is still acceptable.

Moreover, the colour densities of the four inks were compared, and they showed almost identical results.

- According to previous results, it can be seen that all the prepared inks were identical and the only difference was the adhesion result, which is related to polymer difference that incorporated in the flexographic ink formulation.

- Thermal analysis was carried out to compare the physical properties of fumaric rosin (UCH150H) and Surkopak 5323 which showed that the latter started to decompose arround 270 °C with a residue of decomposition of about 7.051% and the T_g value was -12 °C, while fumaric rosin (UCH150H) decomposed at about 200 °C with a residual percentage of 0.4957% and T_g value of 87 °C , These data confirms that Surkopak 5323 has a higher molecular weight and the fumaric is solid at room temperature while Surkopak 5323 is liquid and could be as plasticizing agent in flexographic inks altering the rigidity of flexographic inks.

- Through optical microscopy, it can be seen that inks containing fumaric rosin (UCH150H) exhibited better adhesion than inks contained Surkopak 5323, suggesting that the fumaric rosin (UCH150H) can be used in combination with Surkopak 5323 instead of using adhesion promoter TAA75 as an additive in flexographic NC-PU inks, to avoid the negative effects resulting from the use TAA75.

- Different concentrations of fumaric rosin (UCH150H) and Surkopak 5323 were incorporated in flexographic NC inks and then applied to the BOPP

substrate to compare the adhesion result by SEM, which confirmed that inks contained fumaric rosin (UCH150H) contributed to better adhesion results even at low concentrations of UCH150H, while Surkopak 5323 resulted in good adhesion at higher concentration, this result was certified by EDX where the oxygen content was investigated to find that the percentages of oxygen within fumaric rosin (UCH150H) inks were higher than inks prepared with Surkopak 5323 at low concentrations. The oxygen content increased with polymer concentration in both cases, but the oxygen percentage reached its highest level at 3.33% in case of fumaric rosin (UCH150H) then it became nearly stable, while the oxygen percentage reached its highest value in case of Surkopak 5323 at 5% and then it became stable. The results of the tape test in case of fumaric rosin (UCH150H) was better at lower concentration rather than Surkopak 5323 at higher concentrations.

- Moreover, it was noticed by SEM that the cohesion of Surkopak 5323 was much better than fumaric rosin (UCH150H), while the adhesion of fumaric rosin (UCH150H) was much better than Surkopak 5323.

- According to microscopy studies, no change in the fumaric rosin (UCH150H) and the Surkopak 5323 chemistry was observed after these had been applied to the BOPP surface. This observation suggests that no chemical reactions were involved. However, the more sensitive IGC techniques suggest otherwise.

- By FTIR it was confirmed the presence of un-reacted carboxylic acid in fumaric rosin UCH150, and this result was certified by NMR and ESCA, moreover, it was noticed that applying the polymers to the BOPP surface did

not make any change in chemical structure of applied polymer, which means that no chemical reaction happened.

- By FTIR and ESCA it was confirmed that BOPP surface contained -ether groups, and EDX confirmed the presence of oxygen (1.56%).

- The application of AFM did not offer the intended results, due to the strength of adhesion forces between the probe and the surface under study. The desired result, indicating improved adhesion between the applied polymer film and the BOPP surface was not confirmed, as the topographic image of the surface was not clear in case of BOPP coated with fumaric rosin (UCH150H) and Surkopak 5323 because the probe became stuck to the surface, so the surface imaging was very difficult to achieve and no information was obtained.

- From the contact angle measurements it was confirmed that flexographic inks containing fumaric rosin (UCH150H) when measured over BOPP substrate have lower contact angles than flexographic inks containing Surkopak 5323.

  - To confirm the importance of incorporated polymer in flexographic inks in adhesion result, contact angle measurements of separate ethanolic solutions of fumaric rosin (UCH150H) and Surkopak 5323 were obtained, and the results were in line with those obtained for the inks containing these polymers. This confirms that the polymer incorporated into the flexographic ink formulation plays an important role on the magnitude of adhesion.

- The IGC study was carried out on four samples: fumaric rosin (UCH150H), Surkopak 5323, BOPP coated with fumaric rosin (UCH150H) and BOPP

coated with Surkopak 5323, to compare the physical properties of fumaric rosin (UCH150H) and Surkopak 5323 before and after coating.

- After applying the polymer to the BOPP surface, it was noted that Lewis basicity increased in case of the BOPP-Surkopak 5323 system more than it did in the case of the BOPP-Fumaric rosin (UCH150H). This suggests that when fumaric rosin (UCH150H) and Surkopak 5323 were applied to the BOPP surface, the adhesion of these polymers was as a result of Lewis acidic contribution of the moieties present in both polymers.

- Surkopak 5323 could interact preferentially with itself, because of its relatively strong Lewis basic character and the localized presence of Lewis acid functionalities. Fumaric rosin (UCH150H) has more Lewis acidic character than Surkopak 5323, thus, the fumaric rosin (UCH150H) is prone to form a hydrogen bonds with the BOPP surface.

- As stated previously, the strong interactions are a result of the strong intermolecular hydrogen bonding that exists between the C=O groups and the -OH groups of un-reacted carboxylic acid groups in the fumaric rosin (UCH150H). The -OH groups present in the chemical structure of fumaric rosin (UCH150H) could also participate in forming hydrogen bonds. However, but when the number of -OH groups is greater in UCH150H then there could be a considerable number of -OH groups that did not form hydrogen bonds and compromised the basic nature of the BOPP-fumaric rosin (UCH150H) system.

- Bearing in mind that the oxygen atom on the surface of BOPP (amount determined by SEM-EDX) was from the -CO grouping only, and that the oxygen percentage on BOPP corona treated was 1.56% only, which is very low in comparison with the oxygen percentage after coating with the fumaric rosin (UCH150H) and the Surkopak 5323, on the surface of the BOPP.

- In case of Surkopak 5323, there is also the formation of hydrogen bonds between the -CO, C=O, and NH groups present in Surkopak 5323 and -CO groups at the surface of the BOPP substrate. However, at low concentrations of Surkopak 5323, the hydrogen bonds are formed between the Surkopak 5323 molecules. This could be the reason for the good cohesion that is achieved at low loadings of Surkopak 5323 and the consequential bad adhesion result, as confirmed by SEM.

- When the Surkopak 5323 loading was increased to about 5%, then hydrogen bonds between the polymer molecules and BOPP are formed providing a basis for the acceptable adhesion of the Surkopak 5323 to the BOPP substrate.

- However, at lower loadings of the fumaric rosin (UCH150H) of about 0.4% good adhesion occurs in comparison with that achieved with Surkopak 5323, reaching an optimum adhesion result at a loading of 3.33% of the fumaric rosin (UCH150H).

- Figures 6.1 and 6.2 clarify the supposed mechanism of hydrogen bonds formation in case of Surkopak 5323 and the fumaric rosin (UCH150H) respectively, with the BOPP surface, by the presence of isopropanol traces, coming from the polymers extender (10% polymer+90% isopropanol) that was applied to the BOPP surface.

- In figure 6.1, it can be seen that the –NH group contributes to the hydrogen bonding and that the Lewis basicity of the BOPP-Surkopak 5323 combination is greater than that of Surkopak 5323 itself. This is because the –NH group is adjacent to a carbonyl group. This group is an electron- withdrawing group and the electron density becomes lower around the nitrogen atom and the Lewis basicity becomes lower. Thus, when the –NH forms a hydrogen bond, the electron is allocated around the nitrogen atom and the basicity is increased again.
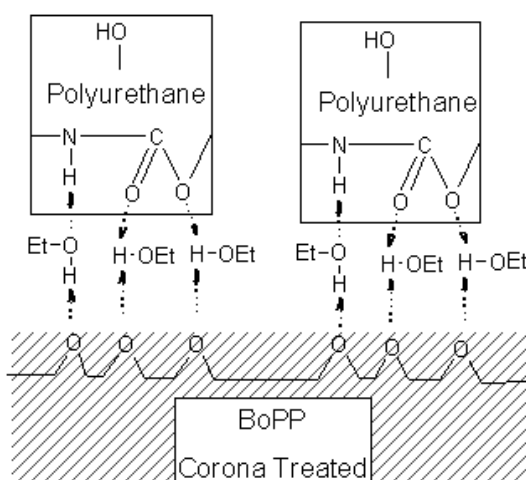
Figure 6.1 A schematic figure clarifying the mechanism of hydrogen bond formation between BOPP and Surkopak 5323
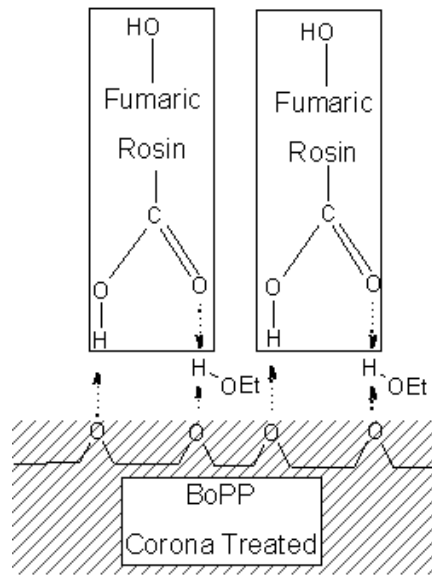
Figure 6.2 A schematic figure clarifying the mechanism of hydrogen bond formation

between the BOPP and the remaining un-reacted carboxylic acid groups in the

fumaric rosin (UCH150H)

Chapter 7   Future Works

For future study, the following is suggested:

- Atomic force microscopy is a very important tool in studying adhesion, it is based on the measurement of atomic forces between a very sharp tip and the sample surface, considerable results can obtained by covering the probe with the studied polymer and imagining the substrate surface by using this new probe, thus the study of the interaction between probe and surface can be done.

- It is very useful to generalise the study to cover many other polymers by using (IGC technique), these polymer should exhibit different adhesion results when incorporated in the flexographic nitro-cellulose ink formulation.

- Preparation of polymers in the laboratory for analysis using the various techniques investigated. The current work was carried out using polymers which were commercially available which had been bulk produced. Thus, there was a lack of absolute purity.

Chapter 8   References

1. Abramovitch, D. Y., Anderson, S. B., Pao, L. Y., and Schitter, G. (2007). A Tutorial on the Mechanisms, Dynamics and Control of Atomic Force Microscopes. *In* "Proceedings of the 2007 American Control Conference", Marriott Marquis Hotel at Times Square.

2. Acklam, B. (2006). "Reactive dye coloration of clay composites," University of Leeds, Department of Colour and Polymer Chemistry.

3. Adams, J. M., & Dolin, P. A. (2002). Printing technology (5th ed.). Albany, NY: Delmar..

4. Al-Saigh, Z. Y., and Munk, P. (1984). Study of polymer - polymer interaction coefficients in polymer blends using inverse gas chromatography. *Macromolecules* **- 17**, 803- 809.

5. Arcurio, R., Rocco, M., Slavinski, J.D., and Schneider, M. (20 April 2004). Solvent soluble poly(urethane/urea) resins. Sun Chemical Corporation.

6. Atkins, P. (1999). "Shriver and Atkins Inorganic Chemistry," 2nd ed. Oxford University Press.

7. Atkins.P.W (1996). "The Elements of Physical Chemistry," 2nd ed. Oxford University Press.

8. Baoli, S., Qianru, Z., Lina, J., Yang, L., and Bin, L. (2007). Surface Lewis acid-base properties of polymers measured by inverse gas chromatography. *Journal of Chromatography A* **1149**, 390-393.

9. Belgacem, M. N., Czeremuszkin, G., Sapieha, S., and Gandini, A. (1995). Surface characterization of cellulose fibers by XPS and inverse gas chromatography. *Cellulose* **- 2**, 145 - 157.

10. Bikerman, J. J. (1967). Causes of poor adhesion: weak boundary layers. *Industrial & Engineering Chemistry* **59**, 40-44.

11. Blais, P., Carlsson, D. J., Csullog, G. W., and Wiles, D. M. (1974). The chromic acid etching of polyolefin surfaces, and adhesive bonding. *Journal of Colloid and Interface Science* **47**, 636-649.

12. Blitshteyn, M. (1995). Wetting tension measurements on corona-treated polymer films. Tappi Journal 78, 138-143.

13. Bovely, F. A., and Mirau, P. A. (1996). "NMR OF Polymers," Academic Press, Inc.

14. Brewis, D. M., and Briggs, D. (1985). "Industrial Adhesion Problems," Orbital Press, Oxford.

15. Briggs, D., Kendall, C. R., Blythe, A. R., and Wootton, A. B. (1983). Electrical discharge treatment of polypropylene film. *Polymer* **24**, 47-52.

16. Burnett, D., Thielmann, F., and Ryntz, R. (2007). Correlating thermodynamic and mechanical adhesion phenomena for thermoplastic polyolefins. *Journal of Coatings Technology and Research* **- 4**, 211 - 215.

17. Calhoun, A. A., Nicholson, P. D., and Barnes, A. B. (2006). The use of inverse gas chromatography to study surface thermal oxidation of polypropylene. *Polymer Degradation and Stability* **91**, 1964-1971.

18. Carlson, T. A. (1978). "X-Ray Photoelectron Spectroscopy," Dowden, Hutchinson & Ross, The University of California.

19. Carlsson, D. J., and Wiles, D. M. (1970). Surface studies by attenuated total reflection spectroscopy. corona treatment of polypropylene. *Canadian Journal of Chemistry* **48**, 2397.

20. Carrino, L., Moroni, G., and Polini, W. (2002). Cold plasma treatment of polypropylene surface: a study on wettability and adhesion. *Journal of Materials Processing Technology* **121**, 373-382.

21. Chehimi, M. M., Abel, M. L., Sahraoui, Z., Fraoua, K., Lascelles, S. F., and Armes, S. P. (1997). Time-dependent variation of the surface energy of conducting polypyrrole. *International Journal of Adhesion and Adhesives* **17**, 1-8.

22. Chen, F. (1988). Study of acceptor-donor interactions at the polymer interface by inverse gas chromatography data analysis. *Macromolecules* **- 21**, 1640- 1643.

23. Christine, S., Dong, Z., and Wadsworth, L. C. (1999). : Corona treatment of polyolefin films - A review. *Advances in Polymer Technology* **18**, 171 - 180.

24. Clark, D. T., and Peeling, J. (1976). Applications of ESCA to polymer chemistry. XII. Structure and bonding in commercially produced fluorographites. *Journal of Polymer Science: Polymer Chemistry Edition* **14**, 2941-2967.

25. Comyn, J. (1997). "Adhesion Science," Royal Society of Chemistry, Cambridge.

26. Comyn, J., and Philippe, C. (2006). Chapter 1 Theories of adhesion. *In* "Handbook of Adhesives and Sealants", Vol. Volume 2, pp. 1-50. Elsevier Science Ltd, Technology and Engineering.

27. Conder, J. R., Young, C. L., Sons, J. W., and Chichester, W. (1979). Physicochemical measurement by gas chromatography. *Chromatographia* **- 13**, - 712.

28. Courval, G. J., and Gray, D. G. (1975). Kinetic effects and gas chromatographic peak shapes near polymer glass transitions. *Macromolecules* **- 8**, 916- 920.

29. Czeremuszkin, G., Mukhopadhyay, P., and Sapieha, S. (1997). Elution behavior of chemically different probes on the evaluation of surface properties of cellulose by inverse gas chromatography. *Journal of Colloid and Interface Science* **194**, 127-137.

30. Deganello, D., Cherry, J. A., Gethin, D. T., and Claypole, T. C. (2012). Impact of metered ink volume on reel-to-reel flexographic printed conductive networks for enhanced thin film conductivity. *Thin Solid Films* **520**, 2233-2237.

31. Di Paola-Baranyi, G., Fletcher, S. J., and Degre, P. (1982). Gas chromatographic investigation of poly(vinylidine fluoride)-poly(methyl methacrylate) blends. *Macromolecules* **- 15**, 885 - 889.

32. Eriksson, P., Reitberger, T. R., and Stenberg, B. (2002). Gas-phase contribution to the spreading of oxidation in polypropylene as studied by imaging chemiluminescence. *Polymer Degradation and Stability* **78**, 183-189.

33. Evonik industries (Personal communication).

34. Fagelman, K. E., and Guthrie, J. T. (2005). Preferential interactions in pigmented, polymer blends - C.I. Pigment Blue 15:4 and C.I. Pigment Red 122 - as used in a

poly(carbonate)-poly(butylene terephthalate) polymer blend. *Journal of Chromatography A* **1095**, 145-155.

35. Fekete, E., Mcz̄, J., and Pukǔnszky, B. (2004). Determination of the surface characteristics of particulate fillers by inverse gas chromatography at infinite dilution: a critical approach. *Journal of Colloid and Interface Science* **269**, 143-152.

36. Fowkes, F. M., and Mittal, K. (1981). "Physiochemical Aspect of Polymer Surfaces," Plenum, New York.

37. Frieden, U.; S. Purohit,; S. Griffioen,; Zeneca Resins,. "New Developments of Solvent-Based Polyurethane Resins for Printing Inks." Ink World. Rodman Publishing Co. 1999. Retrieved June 20, 2011 from HighBeam Research: http://www.highbeam.com/doc/1G1-57294024.html

38. Frank, E., and Rupp, R. (2000). - Printing Inks. Wiley online library.

39. Parfitt, G. D., & Sing, K. S. W. (1976). Characterization of powder surfaces: With special reference to pigments and fillers. London: Academic Press.

40. Goodhew, P.J. (1975). "Electron Microscopy and Analysis," Wykeham Publications (London) Ltd.

41. Gourianova, S., Willenbacher, N., and Kutschera, M. (2005). Chemical force microscopy study of adhesive properties of polypropylene films: influence of surface polarity and medium. *Langmuir* **21**, 5429-5438.

42. Gutierrez, M. C., Rubio, J., Rubio, F., and Oteo, J. L. (1999). Inverse gas chromatography: a new approach to the estimation of specific interactions. *Journal of Chromatography A* **845**, 53-66.

43. Hercules, D.M., and David, M. (1974). Electron spectroscopy for chemical analysis. *Journal of Electron Spectroscopy and Related Phenomena* **5**, 811-826.

44. Haller, W. in: Wolfgang Gerhartz (Ed.), Ullman's Encyclopedia of Industrial Chemistry, vol. A1, VCH Verlagsgesellschaft mbH, Weinheim, FRG, 1988.

45. Instruments, M. (2012). WWW.Malvern.co.uk.

46. Jacquot, C., and Takadoum, J. (2001). A study of adhesion forces by atomic force microscopy. *Journal of Adhesion Science and Technology* **15**, 681-687.

47. Jena, K. K., Chattopadhyay, D. K., and Raju, K. V. S. N. (2007). Synthesis and characterization of hyperbranched polyurethane-urea coatings. *European Polymer Journal* **43**, 1825-1837.

48. Kamdem, D. P., Bose, S. K., and Luner, P. (1993). Inverse gas chromatography characterization of Birch wood meal. *Langmuir* **- 9**, 3039 - 3044.

49. Khulbe, K. C., Feng, C. Y., and Matsuura, T. (2008). Adhesion. *In* "Synthetic Polymeric Membranes", pp. 157-167. Springer, Berlin Heidelberg.

50. Kimya, A. (2003). Pioloform, Vinol and Vinnapas resins for printing inks. WACKER confedential proprietary.

51. Koleske, Joseph V. (1995). Paint and Coating Testing Manual (14th Edition): (MNL 17).. ASTM International. Online version available at: http://www.knovel.com/web/portal/browse/display?_EXT_KNOVEL_DISPL AY_bookid=1739&VerticalID=0

52. Kunjappu, J. T. (2001). "Essays in ink chemistry (For paints and coatings too)," Nova Science publisher, Inc., New York.

53. Laden, P. (1997). "Chemistry and Technology of Water Based Inks," Blackie Academic & professional. The University of Michigan.

54. Lavoie, A., and Guillet, J. E. (1969). Estimation of glass transition on temperatures from gas chromatographic studies on polymers. *Macromolecules* **- 2**, 443- 446.

55. Leach, R.H., and Pierce, R.J. (1999). "The Printing Ink Manual, Flexographic inks," 5th ed. Kluwer Academic Publishers. London.

56. Levine, M., Ilkka, G., and Weiss, P. (1964). Relation of the critical surface tension of polymers to adhesion. *Journal of Polymer Science Part B: Polymer Letters* **2**, 915-919.

57. Lichtenthaler, R. D. N., Liu, D. D., and Prausnitz, J. M. (1974). Polymer-solvent interactions from gas-liquid chromatography with capillary columns. *Macromolecules* **- 7**, 565 - 570.

58. Lin, L., Galton, D., Batting, A., Mumby, R., and Guthrie, J. (2004). Printing ink formulation and application processes. *In* "Module COLO5241", Leeds University.

59. Louey, M. D., Mulvaney, P., and Stewart, P. J. (2001). Characterisation of adhesional properties of lactose carriers using atomic force microscopy. *Journal of Pharmaceutical and Biomedical Analysis* **25**, 559-567.

60. Maier, C.; Calafut, T. (1998). Polypropylene - The Definitive User's Guide and Databook.. William Andrew Publishing/Plastics Design Library. Online version available at:
http://www.knovel.com/web/portal/browse/display?_EXT_KNOVEL_DISPLAY_bookid=54&VerticalID=0

61. Marrion, A. R. (2004). "The Chemistry and Physics of Coatings," Royal Society of Chemistry, Cambridge.

62. Mesic, B., Lestelius, M., and Engström, G. (2006). - Influence of corona treatment decay on print quality in water-borne flexographic printing of low-density polyethylene-coated paperboard. Packaging Technology and Science, Volume 19, issue 2, p. 61 - 70. John Wiley & Sons.

63. Mittal, K. L (2003). Contact Angle, Wettability and Adhesion, Volume 2. pp. 45-71. VSP - An imprint of BRILL, Zeist/NL.

64. Mochizuki, A., Senshu, K., Seita, Y., Yamashita, S., and Koshizaki, N. (2000). Studies on surface structures of poly(ethylene oxide)-segmented nylon films. Journal of Polymer Science Part A: Polymer Chemistry 38, 1045-1056.

65. Mukhopadhyay, P., and Schreiber, H. P. (1993). Inverse gas chromatography for polymer surface characterization above and below Tg. Macromolecules 26, 6391-6396.

66. Munro, H. S., and Till, C. (1984). ESCA studies of metal-containing plasma polymers. Part I. Incorporation of mercury into plasma-polymerized perfluorobenzene. Journal of Polymer Science: Polymer Chemistry Edition 22, 3933-3942.

67. O'Hare, L. A., Leadley, S. R., Parbhoo, B., and Francis, J. G. (2001). Adhesion of silicone coatings to polypropylene films. Polymer Preprints, Volume 42.

68. Olabisi, O., Robeson, L. M., and Shaw, M. T. Polymer-polymer miscibility "., New York : Academic Press, 1997.

69. Oldring, P. K. T., and Editor-in-Chief: Robert, A. M. (2003). Coatings, Colorants, and Paints. In "Encyclopedia of Physical Science and Technology (Third Edition)", pp. 175-190. Academic Press, New York.

70. Overney, R. M., Luthi, R., Haefke, H., Frommer, J., Meyer, E., Guntherodt, H. J., Hild, S., and Fuhrmann, J. (1993). An atomic force microscopy study of corona-treated polypropylene films. Applied Surface Science 64, 197-203.

71. Pascual, M., Sanchis, R., Sánchez, L., Garc, A., D, and Balart, R. (2008). Surface Modification of Low Density Polyethylene (LDPE) Film Using Corona Discharge Plasma for Technological Applications. Journal of Adhesion Science and Technology 22, 1425-1442.

72. Petrie, E. M. (2000). Handbook of Adhesives and Sealants. New York: McGraw-Hill.

73. Planinšek, O., Trojak, A., and Srcic, S. (2001). The dispersive component of the surface free energy of powders assessed using inverse gas chromatography and contact angle measurements. International Journal of Pharmaceutics 221, 211-217.

74. Rajan, G. S., Vu, Y. T., Mark, J. E., and Myers, C. L. (2004). Thermal and mechanical properties of polypropylene in the thermoplastic elastomeric state. European Polymer Journal 40, 63-71.

75. Rentzhog, M. (2004). Characterisation of Water-Based Flexographic inks and their interactions with Polymer-Coated Board, Ytkemiska Institutet, Stockholm.

76. Riddle, F. L., and Fowkes, F. M. (1990). Spectral shifts in acid-base chemistry. 1. van der Waals contributions to acceptor numbers. Journal of the American Chemical Society 112, 3259-3264.

77. Roberts, C. J. (2005). What can we learn from atomic force microscopy adhesion measurements with single drug particles? European Journal of Pharmaceutical Sciences 24, 153-157.

78. Santos, J. M. R. C. A., Fagelman, K., and Guthrie, J. T. (2002). Characterisation of the surface Lewis acid-base properties of the components of pigmented, impact-modified, bisphenol A polycarbonate-poly(butylene terephthalate) blends by inverse gas chromatography-phase separation and phase preferences. Journal of Chromatography A 969, 119-132.

79. Santos, J. M. R. C. A., and Guthrie, J. T. (2005). Study of a core-shell type impact modifier by inverse gas chromatography. Journal of Chromatography A 1070, 147-154.

80. Schreiber Henry, P., and Lloyd Douglas, R. (1989). Overview of inverse gas chromatography. In "Inverse Gas Chromatography", Vol. 391, pp. 1-10. American Chemical Society.

81. Shi, L., Shen, P., Zhang, D., Lin, Q., and Jiang, Q. (2009). Wetting and evaporation behaviors of water–ethanol sessile drops on PTFE surfaces. Surface and Interface Analysis 41, 951-955.

82. Sindel, U., and Zimmermann, I. (2001). Measurement of interaction forces between individual powder particles using an atomic force microscope. Powder Technology 117, 247-254.

83. Stuart, B. (2004). "Infrared Spectroscopy: Fundamentals and applications," John Wiley and Sons Ltd, Chichester.

84. Subedi, D. P. (2011). "Contact Angle Measurement for the Surface Characterization of Solids," Himalayan Physics, Nepal.

85. Thielmann, F., and Levoguer, C. IGC - A new instrumental technique for characterising the physico-chemical properties of pharmaceutical materials. Surface Measurement Systems Ltd., 2001 Application note 301.

86. Thompson, B. (1998). "Printing materials science and technology / Adhesion and Adhesives / Chapter 12," Pira International, Leatherhead, UK.

87. Todd, R. E. (1994). "Printing inks formulation principles, manufacture and quality control testing procedures," Pira International, Leatherhead/GB.

88. Toit, F. J. D., and Sanderson, R. D. (1999). Surface fluorination of polypropylene 2. Adhesion properties. Journal of Fluorine Chemistry 98, 115-119.

89. Velásquez, P., Leinen, D., Pascual, J., Ramos-Barrado, J. R., Cordova, R., Gimez, H., and Schrebler, R. (2001). XPS, SEM, EDX and EIS study of an electrochemically modified electrode surface of natural chalcocite (Cu2S). Journal of Electroanalytical Chemistry 510, 20-28.

90. Wake, W. C. (1978). Theories of adhesion and uses of adhesives: a review. Polymer 19, 291-308.

91. Williams, C. (2001). "Printing Ink Technology," Pira International Ltd, Leatherhead, UK.

92. Worobiec, A., Potgieter-Vermaak, S., Brooker, A., Darchuk, L., Stefaniak, E., and Van Grieken, R. (2010). Interfaced SEM/EDX and micro-Raman spectrometry for characterisation of heterogeneous environmental particles - fundamental and practical challenges. Microchemical Journal 94, 65-72.

93. Yovcheva, T. A., Avramova, I. A., Mekishev, G. A., and Marinova, T. S. (2007). Corona-charged polypropylene electrets analyzed by XPS. Journal of Electrostatics 65, 667-671.

94. www.dupont.com/tyzor, [accessed on 2.11.2011].

95. www.profarb.com.pl/eng/machines.htm, [accessed on 30.08.2010].